

Time-Resolved Observations of Precipitation structure and storm Intensity with a Constellation of SmallSats



Level-1 Radiance Algorithm Theoretical Basis Document

1 January 2022

Revision 2.1



National Aeronautics and Space Administration
Goddard Earth Science Data Information and
Services Center (GES DISC)

DISTRIBUTION STATEMENT A. Approved for public release. Distribution is unlimited.
This material is based upon work supported by the National Aeronautics and Space
Administration under Air Force Contract No. FA8702-15-D-0001. Any opinions, findings,
conclusions or recommendations expressed in this material are those of the author(s) and
do not necessarily reflect the views of the National Aeronautics and Space Administration .
© 2022 Massachusetts Institute of Technology.
Delivered to the U.S. Government with Unlimited Rights, as defined in DFARS Part 252.227-
7013 or 7014 (Feb 2014). Notwithstanding any copyright notice, U.S. Government rights in
this work are defined by DFARS 252.227-7013 or DFARS 252.227-7014 as detailed above. Use
of this work other than as specifically authorized by the U.S. Government may violate any
copyrights that exist in this work.

Prepared by: R. Vincent Leslie & Mike DiLiberto
MIT Lincoln Laboratory

Date: _____

Approved by: _____
William J. Blackwell
TROPICS Principal Investigator
MIT Lincoln Laboratory

Date: _____

Approved by: _____
Scott Braun
TROPICS Project Scientist
NASA Goddard Space Flight Center

Date: _____

Approved by: _____
R. Vincent Leslie
TROPICS Project Manager
MIT Lincoln Laboratory

Date: _____



Revision History

<i>Version</i>	<i>Description</i>	<i>Date</i>	<i>Initiator</i>
0.1	Initial Draft	09/17/2017	Vince Leslie
0.2	Pre-PDR Peer Review Feedback	11/21/2017	Vince Leslie
1.0	TIM version	11/28/2017	Vince Leslie
1.1	PDR version (updated L1b corrections)	04/23/2018	Vince Leslie
2.0	Pathfinder ORR	07/05/2021	Vince Leslie
2.1	Pathfinder updates	01/01/2022	Vince Leslie

Contents

1	Scope	5
2	System Overview.....	5
3	Applicable TROPICS Documents.....	6
4	Payload Characteristics.....	6
4.1	Receiver Architecture	6
4.2	Spatial Response	7
4.3	Polarization	9
5	Data Products.....	11
6	Calibration Background	11
6.1	Transfer Function.....	12
6.2	Scan Pattern	12
6.3	Calibration Sources	13
6.3.1	Deep space	13
6.3.2	Noise diode	17
7	Algorithm Description	18
7.1	Calibration.....	19
7.2	Geolocation	22
7.3	W- and F-band Channel Mixing Correction	24
7.4	Antenna Temperature to Brightness Temperature Conversion.....	25
7.5	Radiometric Bias Removal	26
7.6	Intra-TROPICS Bias Trending.....	27
7.7	Quality Control Flags.....	29
7.8	Algorithm Input and Outputs	30
8	Error Analysis and Correction Factors	30
9	Algorithm Ancillary Data	31
10	Pre-launch Performance Testing	32
10.1	Antenna Pattern Measurements	33
10.2	Spectral Response Functions	33
10.2.1	SRF Temperature Sensitivity Analysis	33
10.2.2	SRF Difference from Ideal Boxcar Passbands.....	34

10.3	Calibration Characterization	35
10.3.1	Calibration Apparatus	36
10.3.2	Calibration Procedure	36
10.3.3	Calibration Results.....	38
10.4	Pre-launch Calibration Verification	38
10.4.1	Verification Procedure	38
10.4.2	Verification Results.....	38
11	References.....	40
Appendix A: Noise Equivalent Delta Noise		42
Appendix B: Antenna Pattern Beamwidths (Full-width Half Max.).....		43
Appendix C: Native Horizontal Spatial Resolution		44
Appendix D: SRF Thermal Sensitivity Results		47
Appendix E: SRF Ideal vs. Measured Results.....		61
Appendix F: TROPICS-01 (Pathfinder) Characterization.....		76
F.1	Calibration Characterization	77
F.2	Calibration Verification	78
F.3	Spectral Response Functions	79
F.4	Antenna Patterns	81

1 Scope

This Algorithm Theoretical Basis Document (ATBD) describes the theoretical background of the TROPICS native radiance calibration algorithms. It also includes TROPICS payload characteristics and the algorithm's ancillary data (i.e., data coming from sources other than the TROPICS Space Vehicle). Details of the native radiance (i.e., Level-1a antenna temperatures and Level-1b brightness temperatures) data product format can be found in the TROPICS Data User's Guide. This ATBD information on the pre-launch testing completed to verify the algorithm. The TROPICS Data User's Guide will contain the post-launch radiance validation.

2 System Overview

The Time-Resolved Observations of Precipitation structure and storm Intensity with a Constellation of Smallsats (TROPICS) mission [1] will provide rapid-refresh microwave measurements over the tropics that can be used to observe the thermodynamics of the troposphere and precipitation structure for storm systems at the mesoscale and synoptic scale over the entire storm lifecycle. TROPICS comprises a constellation of six CubeSats in three low-Earth orbital planes. Each CubeSat will host a high-performance radiometer scanning across the satellite track at 30 RPM to provide temperature profiles using seven channels near the 118.75 GHz oxygen absorption line, water vapor profiles using 3 channels near the 183 GHz water vapor absorption line, imagery in a single channel near 90 GHz for precipitation measurements, and a single channel at 206 GHz for cloud ice measurements. This observing system offers an unprecedented combination of horizontal and temporal resolution to measure environmental and inner-core conditions for tropical cyclones (TCs) on a nearly global scale and is a profound leap forward in the temporal resolution of several key parameters needed for detailed study of high-impact meteorological events (e.g., Tropical Cyclones). TROPICS will demonstrate that a constellation approach to earth Science can provide improved resolution, configurable coverage (tropics, near global, or global), flexibility, reliability, and launch access at extremely cost effective, thereby serving as a model for future missions.



Figure 1 Photo of TROPICS Space Vehicle

3 Applicable TROPICS Documents

1. TROPICS Data Product User Guide: Publicly released document with information on payload and space vehicle characteristics, quality flags, and validation along with full data product format description.
2. TROPICS Unified Resolution Radiometric Product ATBD (Level-2a data product)
3. TROPICS Atmospheric Vertical Profiles ATBD containing the Atmospheric Vertical Profile Temperature Profile (AVTP) and Atmospheric Vertical Moisture Profile (AVMP) ATBD (Level-2b data products) using NOAA MIRS algorithm
4. TROPICS Instantaneous Surface Rain Rate (ISRR) ATBD (Level-2b data product) using the Goddard NASA PRPS algorithm
5. TROPICS Tropical Cyclone Intensity ATBD (Level-2b data product consisting of Minimum Sea-Level Pressure and Maximum Sustained Wind Speed)

4 Payload Characteristics

This section presents the TROPICS payload characteristics. The payload is a total-power radiometer with channels at W, F, and G bands.

4.1 Receiver Architecture

Table 1 contains the spectral passbands, spatial beamwidth, and expected Noise Equivalent Delta Temperature (NEdT) of the channels. TROPICS weighting functions are in the TROPICS Level-2b AVP ATBD. Each SV's NEDT is in Appendix A: Noise Equivalent Delta Temperature. A complete list of individual beamwidths is in Appendix B: Antenna Pattern Beamwidths (Full-width Half Max.).

Table 1 TROPICS spectral and spatial Stats (Footprint from 550-km altitude)

Chan.	Center Freq. (GHz)	Band width (GHz)	RF Span (GHz)	Beamwidth (degrees) Down/Cross	Nadir Footprint Geometric Mean (km)
1	91.655 ± 1.4	1.000	89.756-90.756, 92.556-93.556	3.0/3.17	29.6
2	114.50	1.000	114.00-115.00	2.4/2.62	24.1
3	115.95	0.800	115.55-116.35	2.4/2.62	24.1
4	116.65	0.600	116.35-116.95	2.4/2.62	24.1
5	117.25	0.600	116.95-117.55	2.4/2.62	24.1

6	117.80	0.500	117.55-118.05	2.4/2.62	24.1
7	118.24	0.380	118.05-118.43	2.4/2.62	24.1
8	118.58	0.300	118.43-118.73	2.4/2.62	24.1
9	184.41	2.000	183.41-185.41	1.5/1.87	16.1
10	186.51	2.000	185.51-187.51	1.5/1.87	16.1
11	190.31	2.000	189.31-191.31	1.5/1.87	16.1
12	204.8	2.000	203.8-205.8	1.4/1.76	15.2

The receiver architecture consists of two separate receiver chains. A simplified payload block diagram is shown in Figure 2. The W- and F-band channels (i.e., Chan. 1 through 8) are implemented with a superheterodyne radiometer. The W-band channel is double sideband, and the F-band channels are single sideband. The W/F receiver has a local oscillator with a fundamental frequency of 30.552 GHz. The G-band channels are implemented with a direct-detect radiometer using single sidebands.

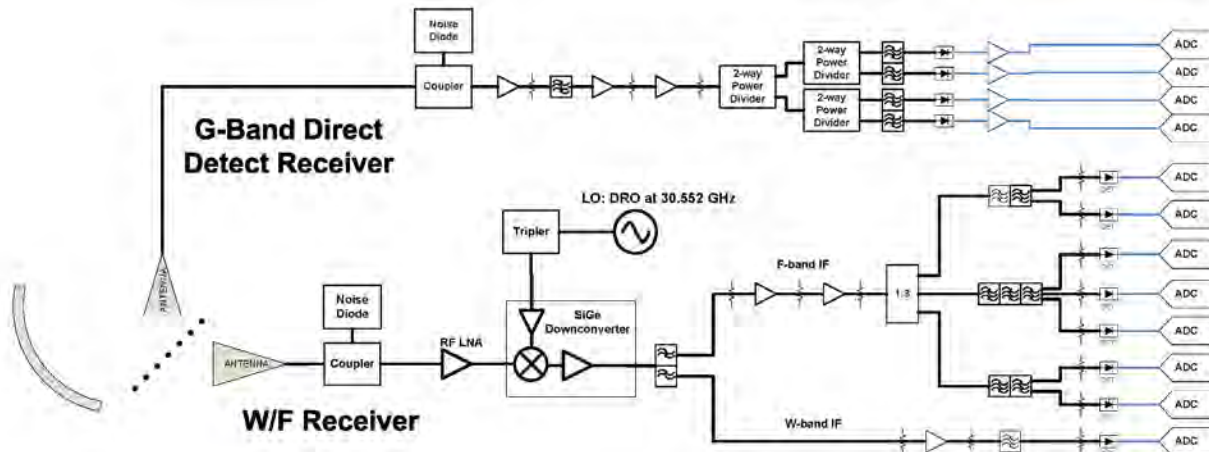


Figure 2 Simplified TROPICS payload block diagram

4.2 Spatial Response

Figure 2 also has a simple illustration of the antenna subsystem. Inside the payload is an offset parabolic reflector with separate feedhorns for the W/F-band receiver and the G-band receiver. The feedhorns illuminate the reflector through a wire gird polarizer, which allow the incoming radiation to be diplexed. More information on polarization is in Sect. 4.3. Figure 3 is an illustration of the TROPICS cross-track scan. The scan is implemented by spinning the entire payload “cube” in reference to the spacecraft bus. Similar to a conical scanner, TROPICS uses a motor and sliring to rotate the payload, but in a cross-track scan pattern on the surface. Table 2 contains the scan pattern details for the cross-track swath projected beneath the space vehicle. There are 81 spots or

beam positions in the Earth View Sector. TROPICS scans during the integration period; therefore, the cross-track dimension will be larger than the down-track dimension. Due to the wire grid, the TROPICS footprints will have minimal offset on the ground, which is a tremendous advantage in post-processing. Sect. 1 has a table of the dimensions of each footprint separated out by band (W, F, G, and 205 GHz) and track. To compare the swath width to ATMS, Figure 4 plots the footprints of the spots on the Earth's surface, along with the ATMS footprints.

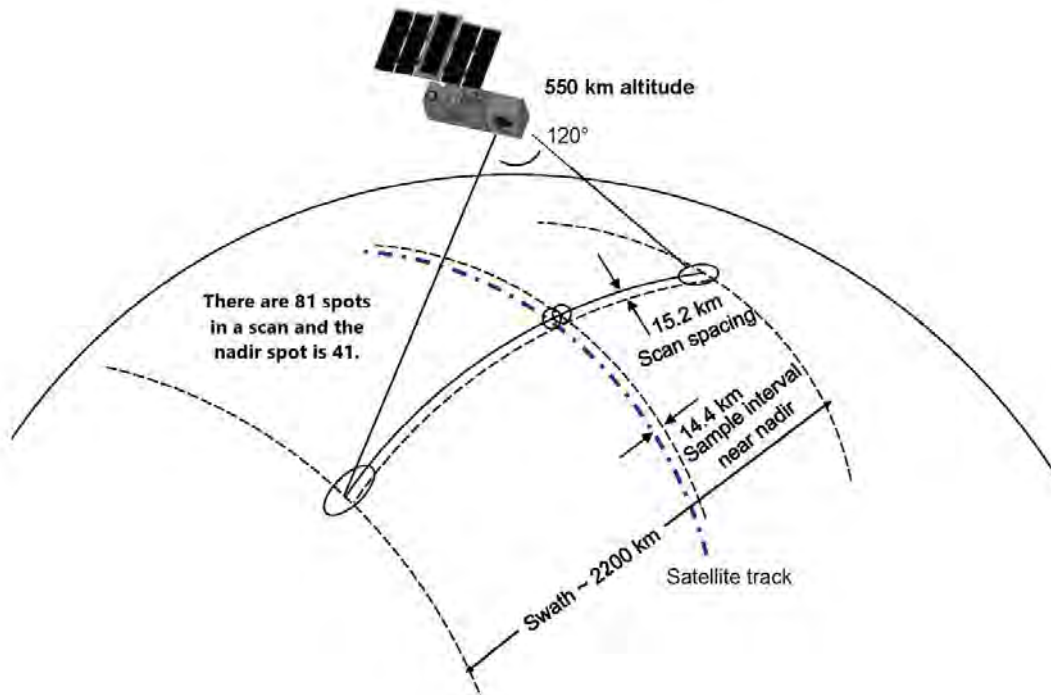


Figure 3 Illustration of the TROPICS cross-track scan pattern.

Table 2 TROPICS scan profile characteristics

Characteristic	Units	Value
Rotation Period	Seconds	2
Maximum Earth View Sector Angle	Degrees	± 60
Scan Type	N/A	Constant velocity (scanning during integration)
Integration time	Seconds	1/120
Number of Earth View Sector Measurements	N/A	81 per scan (one at nadir)

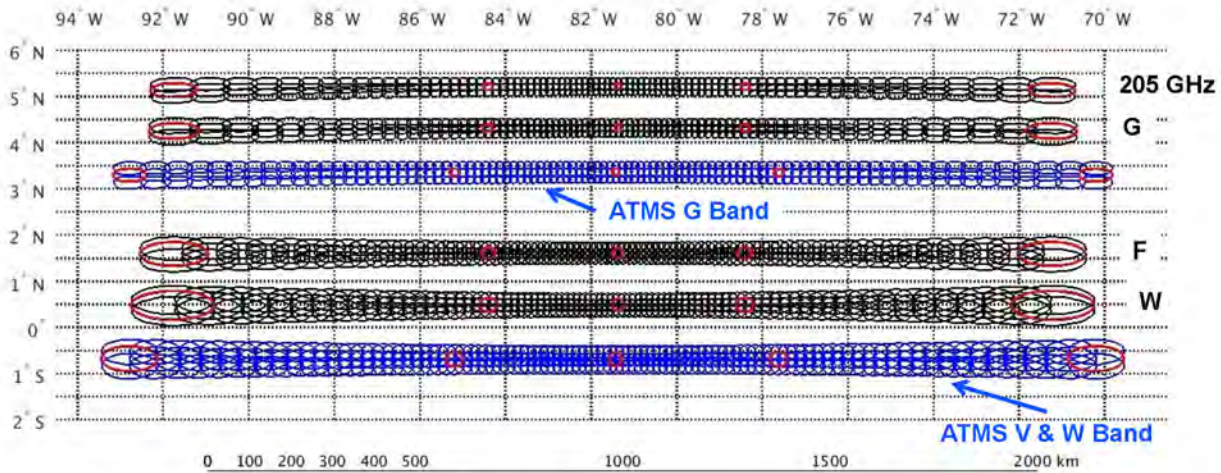


Figure 4 TROPICS swath comparison against ATMS. TROPICS' altitude for this rendering was 550 km.

4.3 Polarization

As previously mentioned, the TROPICS payload has a non-traditional polarization. Figure 5 illustrates the TROPICS polarization, which is a combination of the traditional conical scanner (i.e., fixed angle between reflector and feedhorn) and the cross-track scanner (i.e., scan angle to zenith angle conversion at the surface). As illustrated in the upper left-hand side, the polarization is fixed for the W/F band (i.e., Φ , φ , in the figure, which is called the polarization angle), while the G-band will be separated by 90 deg. from angle φ defined in the figure. This makes the polarization largely the same as the upwelling horizontal and vertical polarization. This is true for all bands. The polarization was measured pre-launch in an antenna range, with W/F band at 70 deg. and G-band at -20 deg., but post-launch assessment of the Pathfinder data derived an empirical W/F-band angle of 0 deg. and G-band at 90 deg.

The mixing equation is in Equation 1. Φ , φ , is typically the scan angle in traditional cross-track

$$\text{Equation 1} \quad T_b = T_b^{hori} * \cos^2(\varphi) + T_b^{vert} * \sin^2(\varphi)$$

radiometers, but the TROPICS feedhorn moves with the reflector (and the entire payload) and therefore remains constant while the entire payload rotates. In the spaceborne radiative transfer equation (not shown), the polarized sources of radiation for the TROPICS instrument is the ocean surface, while the atmosphere and land are largely unpolarized.

Figure 6 is a simulation of the ocean emissivity versus instrument scan angle. The solid black and blue lines are the surface emissivity's vertical and horizontal components, respectively. The solid green is the mixed polarization where the polarization angle is 0 deg. (i.e., horizontal emissivity) for the TROPICS W/F receiver (Channel 1). For Channel 12 (G-band), the solid green is the mixed

polarization where the polarization angle is 90 deg. (i.e., vertical emissivity). For comparison, the typical cross-track “quasi” polarization, which has the same equation as Equation 1, but with Phi, i.e., the polarization angle, replaced with the changing scan angle.

Finally, Figure 7 shows an idealized simulated brightness temperature as a function of scan angle with the fixed 0/90 deg. polarization angle (W & F/G) for a tropical ocean surface. There is limb darkening or brightening due to the change in thickness of the atmosphere and surface emissivity. This simulation does not model antenna pattern sidelobes (i.e., it is a Gaussian beam).

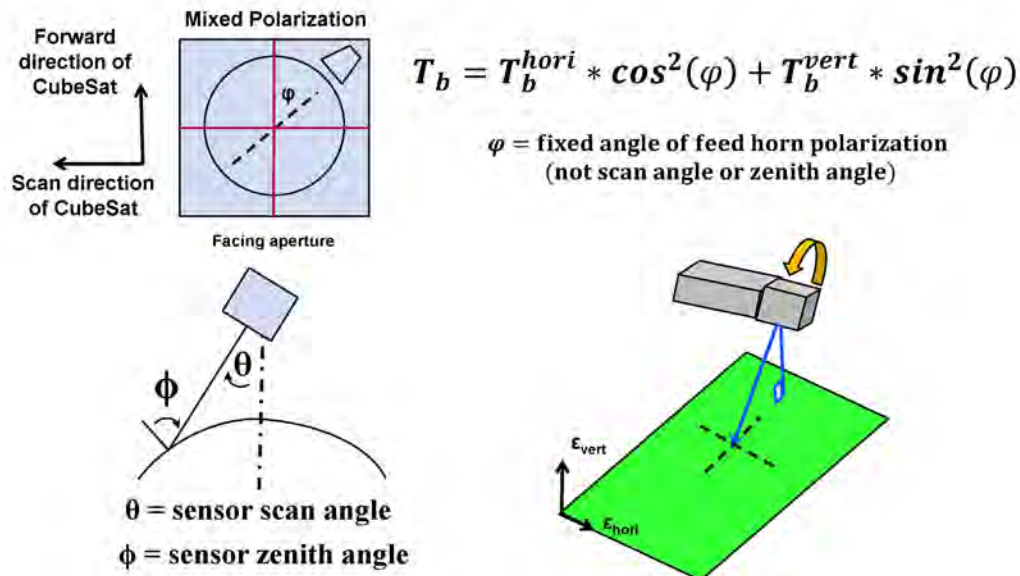


Figure 5 Illustration explaining the TROPICS polarization.

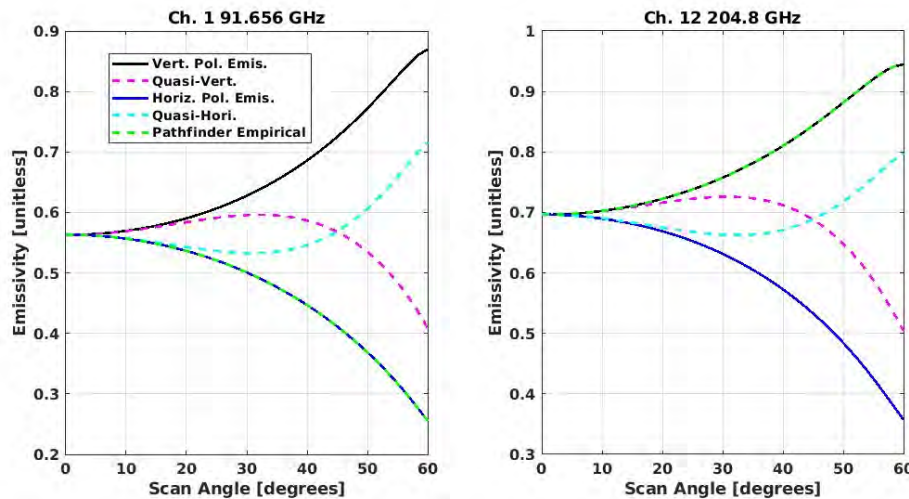


Figure 6 Simulated ocean surface emissivity (fastem v2)

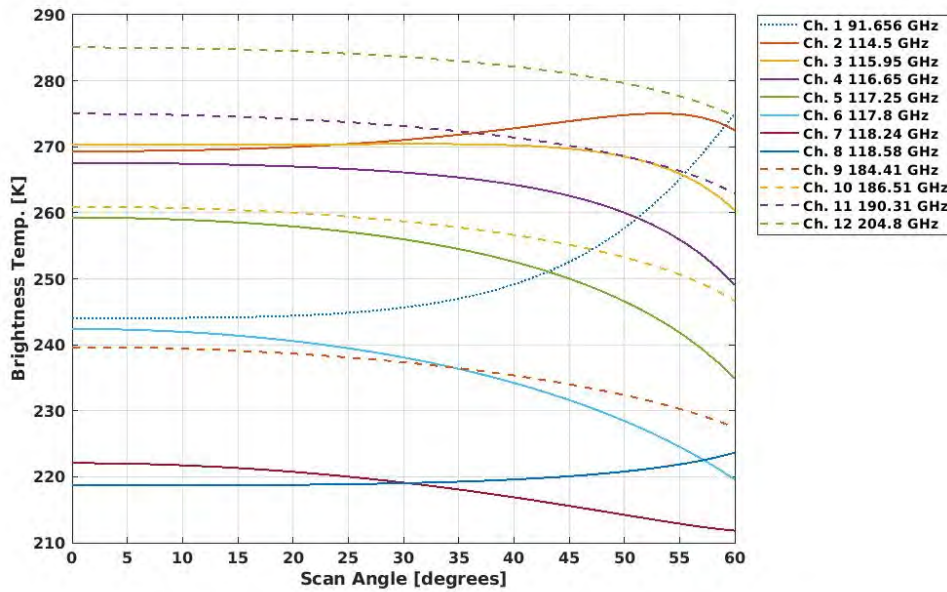


Figure 7 Simulated brightness temperature vs sensor scan angle from the tropical US Standard 1976 atmosphere and fastem version 2 ocean emissivity model. W/F-band at 0 deg. and G-band at 90 deg.

5 Data Products

A comprehensive data product description can be found in the TROPICS Data User's Guide. A high-level description of the data products is given in Table 3.

Table 3 TROPICS data product descriptions

Level Designation	Data Product Description
Level 0	raw CCSDS payload and telemetry from space vehicles
Level 1a	Timestamped, geolocated, calibrated antenna temperature
Level 1b	Timestamped, geolocated, calibrated brightness temperature with bias removed
Level 2a URRP	Unified resolution brightness temperature (F-band resolution)
Level 2b	Atmospheric Vertical Temperature Profile [kelvins]
	Atmospheric Vertical Moisture Profile [g/kg]
	Instantaneous Surface Rain Rate [mm/hr]
	TC Intensity: Minimum Sea-level pressure [mb]
	TC Intensity: Maximum Sustained Wind [m/s]

6 Calibration Background

This section gives the background information on the payload calibration. The first section reviews the typical model for a radiometer regarding the relationship between the incoming radiation and

the measurand (i.e., Analog-to-digital counts). Next, the pertinent aspects of the scan pattern for calibration are explained. Finally, a description is given of the two calibration sources.

6.1 Transfer Function

Total-power radiometers are not completely linear instruments. Instrument non-linearity is characterized at the system level and corrected for in the calibration algorithm. Figure 8 is an illustration of transfer model of a total-power radiometer. The y-axis is the input radiance, which is the antenna temperature, and the x-axis the instrument's measurement in Analog-to-Digital Convert counts (or digital numbers). The blue line is the hypothetical true instrument response, or transfer function. The two-point calibration scheme calculates a linear relationship using two sources of known radiance (green line). There is a residual error from the linear calibration, which is the difference between the green and blue lines. The calibration algorithm will try to correct for the residual non-linearity using measurements in a thermal-vacuum chamber against precision external calibration targets (see Sect. 7.1 and Sect. 10). The constraints of the non-linearity correction factor include being zero at the two on-orbit calibration source temperatures. As shown in the illustration, the non-linearity error is zero at those two points. If assuming a parabolic transfer function, the maximum non-linearity, within the dynamic range of 3 to 330 K, is half way between the calibration sources. For TROPICS, that is approximately half the noise diode temperature.

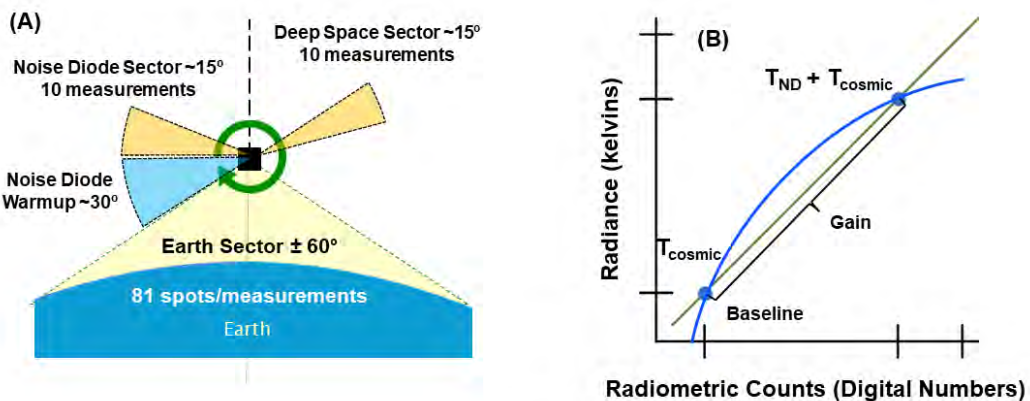


Figure 8 Illustration of TROPICS radiometer transfer function. T_{sv} is the deep space measurement, and T_{ND} is the noise temperature injected into the receiver. Deep space sector is the cold calibration sector and the Noise Diode sector is the hot calibration sector.

6.2 Scan Pattern

The TROPICS payload rotates at 30 RPM, or at a two-second period. The scan pattern acquisition starts after receiving a timing message through the slipring from the payload driver running on the bus processor. As shown in Figure 3 (A), the first sector, i.e., the Noise Diode Sector, the radiometer will turn on the noise diodes, which inject noise into the receiver chain (see Figure 2). There will be adequate noise diode warm up before data is collected in the Noise Diode Sector. After the Noise Diode Sector measurements are complete, the lunar/solar intrusion section is skipped in

normal mode. Afterward, the Deep Space Sector measures the radiance from deep space, which is a standard reference radiance for spaceborne calibrations. These two sector's measurements will include both the radiance of deep space and the noise diode, which allows for a two-point calibration as discussed in Sect. 6.1. The periodic absolute two-point calibration will be repeated every rotation (i.e., every two seconds).

6.3 Calibration Sources

Total-power radiometers with periodic absolute calibration require at least two precise calibration sources with known radiances. Deep space is a common “cold” reference used in space applications. The second most common is the onboard iron-filled epoxy target that has very high emissivity at microwave frequencies, but is bulky and not appropriate for a small 1U payload like TROPICS has. TROPICS uses a different calibration source technique by having a weakly coupled noise source at the front of the receiver chain that can be turned on when viewing deep space.

6.3.1 Deep space

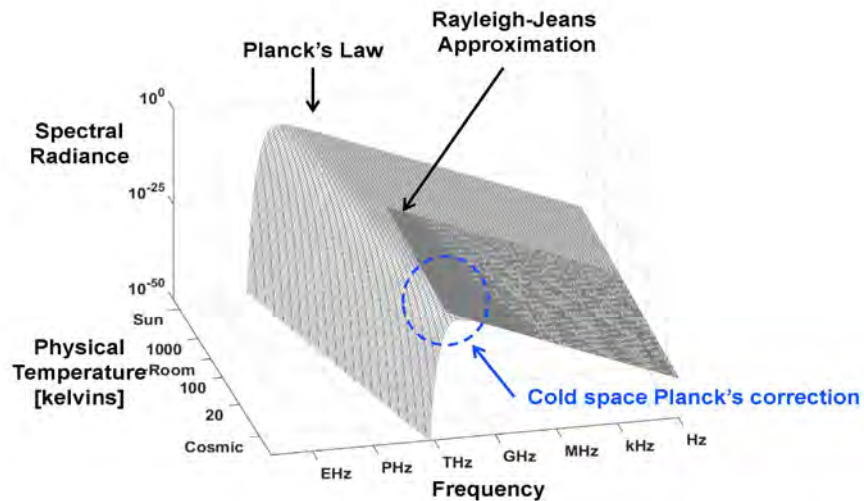
The radiation from deep space is very homogenous at microwave frequencies, and a standard calibration source. There are a few adjustments required:

- Planck function correction for the breakdown of the Rayleigh-Jeans approximation at low radiances and high frequencies
- Earth intercept (i.e., part of the antenna pattern measuring the Earth while viewing deep space)
- Spacecraft intercept

Figure 9 plots Planck’s Law versus frequency and physical (kinetic) temperature. The Rayleigh-Jeans approximation is also plotted for the approximate range of frequencies and physical temperatures that it is valid. There are residual errors of the approximation that are mitigated by adjusting the cold space brightness temperature to minimize the error along the instrument’s dynamic range with the Earth scene brightness temperature range.

Figure 9 Illustration of the breakdown of the R-J approximation at low radiances.

TROPICS calibrates to a Planck-equivalent brightness temperature, which means the brightness temperature is similar to the physical or kinetic temperature of a blackbody. To illustrate what this means, a simple model was used to compare the impact of various calibration source corrections to the thermal calibration sources, whether they were the cosmic background radiation, the precision blackbody targets used in the pre-launch thermal-vacuum calibration, or the equivalent temperature injected into the radiometer by the noise diode.



The model used Planck's radiation law to transform between spectral radiance domain ($W/m^2 \cdot ster \cdot Hz$) to a blackbody temperature (K), i.e., brightness temperature, domain. TROPICS calibration is accomplished in the brightness temperature domain, but this model determined the consistency in the spectral radiance domain. The model consisted of an ideal radiometer transfer function (i.e., no radiometer non-linearity) to solely address the non-linearity of applying the Rayleigh-Jeans linear approximation to the non-linear Planck's law. Figure 10 shows a flowchart of the simple model. The idealized linear radiometer modeled upwelling radiation (K) into radiometric counts that were proportional to the Planck's law, then various calibration techniques were tested by comparing the resulting calibrated radiance against Planck's law radiance. The calibration targets were idealized to have emissivity of one (i.e., perfect black bodies). The model assumed the cold calibration target at 2.73 K and the hot calibration target at 273 K. To maximize the error of the R-J approximation, a frequency from TROPICS's highest frequency channel was chosen (205 GHz).

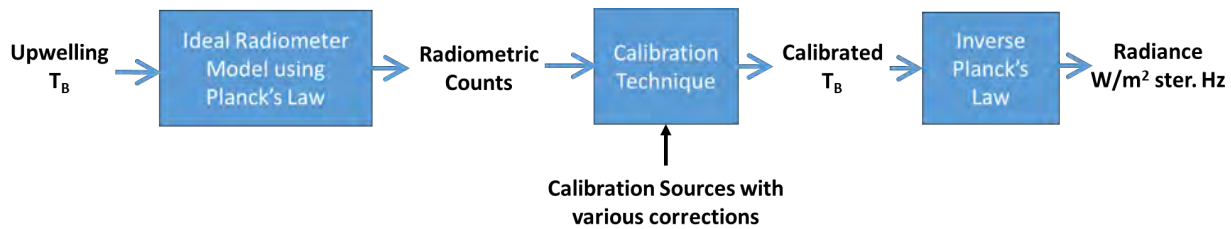


Figure 10 Planck-equivalent model flowchart

There are three calibration techniques evaluated in this analysis:

1. No Planck correction where the calibration target's brightness temperature is equal to the target's physical or kinetic temperature times its emissivity: $T_B = \varepsilon \cdot T \cong T$.
2. Standard Planck correction using the standard Rayleigh-Jeans approximation equal to the Planck's law that gives a relationship between brightness temperature and physical temperature: $T_B^{RJ} = \frac{hf}{k} \cdot (e^{hf/kT} - 1)^{-1}$
3. Modified Planck correction using a modified Rayleigh-Jeans approximation equal to the Planck's law that gives a relationship between the brightness temperature and physical temperature: $T_B^{MRJ} = \frac{hf}{k} \cdot [(e^{hf/kT} - 1)^{-1} + 0.5]$. The modification will align the brightness temperature closer to spectral radiance when using the inverse Planck's law.

In Figure 11 on the left-hand side, each of the three above calibration models were converted back into spectral radiance to compare how closely they match Planck's law. The modified Rayleigh-Jeans correction aligned best with Planck's law in the physical temperature range of the Earth's atmosphere (i.e., 150 to 330 K). Therefore, for TROPICS, all target's physical temperatures were converted to brightness temperatures using the modified Rayleigh-Jeans equation above. The noise diode temperature has the modified R-J correction because it was applied to the external target's temperature measurement from the embedded temperature sensors during TVac calibration. Furthermore, the correction is applied to the cosmic background temperature of 2.73 K. On the right-hand side of Figure 11, the difference between the brightness temperature and physical temperature is shown. A better match to the Planck's law produces a better match between the brightness temperature and the physical temperature. Simulated studies indicated that there was not a sufficient enough breakdown in the monochromatic assumption to warrant correction factors. The only double-sideband channel was only ± 1.5 GHz.

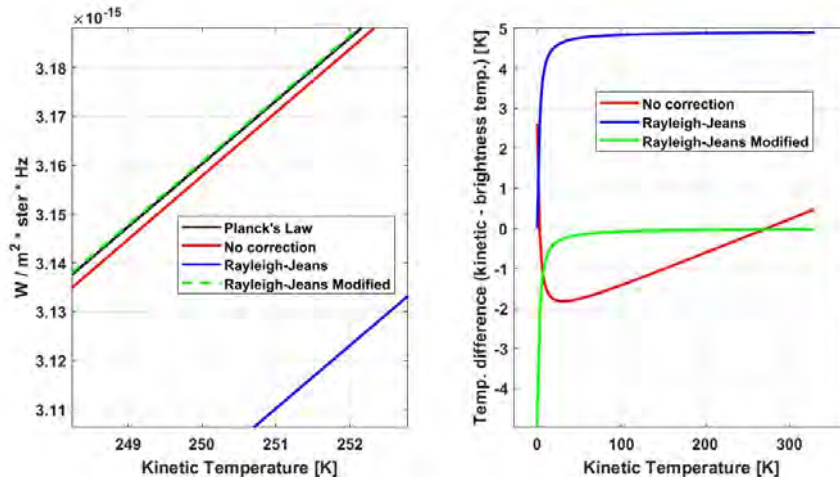


Figure 11 Planck radiation law and calibrating an ideal linear radiometer with various Rayleigh-Jeans approximations to the calibration targets. The left-hand side is the residual error between brightness temperature error and the kinetic temperature (205 GHz).

When taking measurements of deep space, the antenna pattern sidelobes will also measure the Earth and spacecraft. Figure 13 illustrates the Earth intercept against a plot of a simulated antenna pattern. The correction will integrate the angular extent of the Earth normalized by the entire antenna pattern. This fraction of the antenna pattern is multiplied by an assumed Earth brightness temperature (~250 K). The antenna pattern is three-dimensional and a similar intercept is calculated for spacecraft (and solar array) intercept. See Figure 12 for radiometric measurements of the Earth's limb from the MicroMAS-2a and the clear impact near the edges of the Earth with the W-band that has the largest antenna beamwidth has the largest limb brightness temperatures. Note that the two calibration sectors in Figure 8 (A) can be set to be an equal angular distance to within the Earth's limb. Depending on the antenna pattern's symmetry, and due to the fact both calibration sectors are making measurements of the limb (which is not the case for traditional internal calibration targets), the radiometric count difference will cancel out the Earth limb contamination.

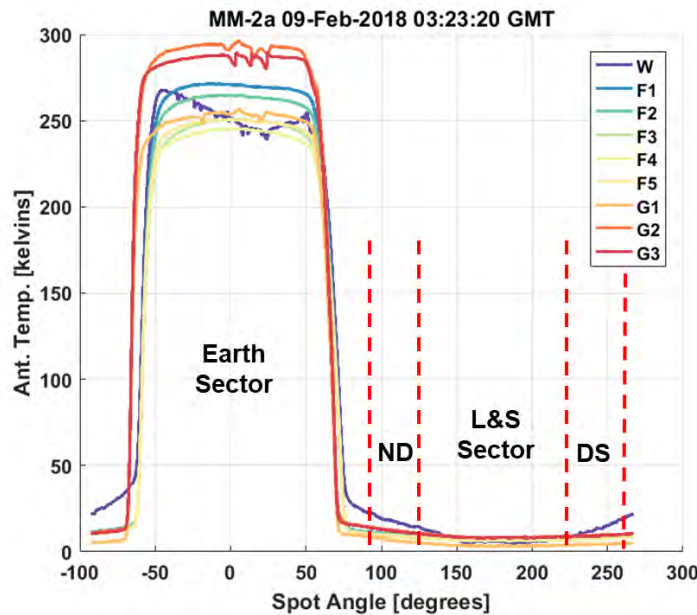


Figure 12 MicroMAS-2a on-orbit radiometric data showing the full rotation of the scan pattern with the calibration sectors identified.

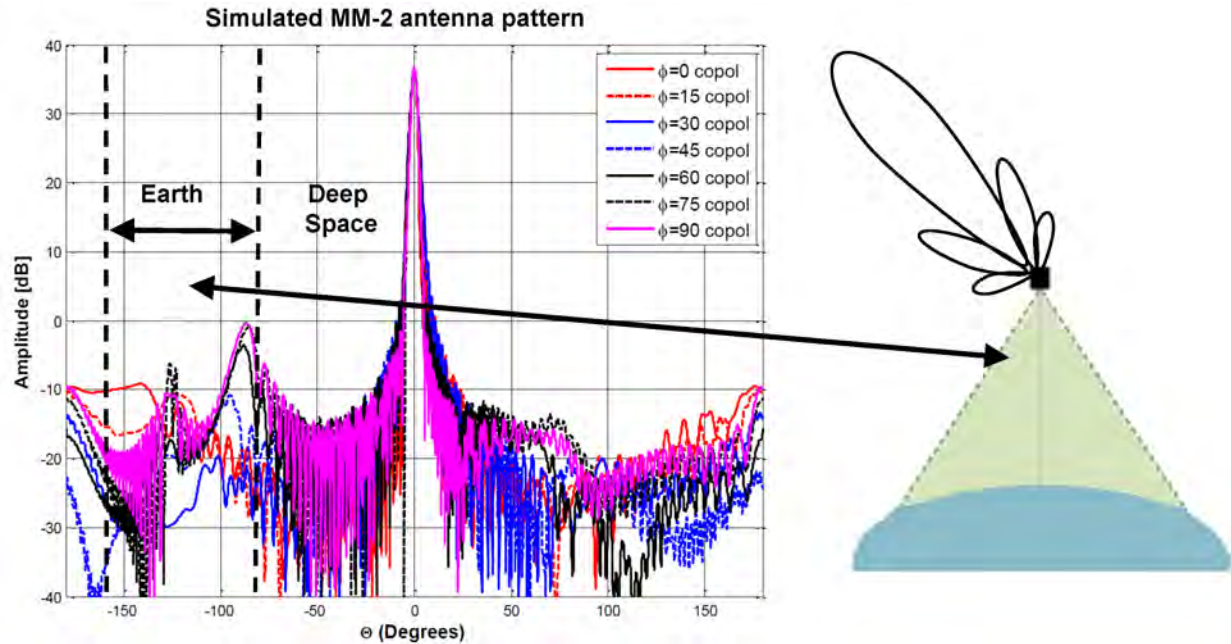


Figure 13 Illustration of the contribution of the Earth intercept during a measurement of deep space.

Another consideration for the angular position of the calibration sectors is the lunar/solar contamination. For the TROPICS constellation orbits, lunar and solar intrusions will occur around $\pm 60^\circ$ from zenith. There is a tradeoff between reducing lunar/solar intrusions and placing the calibration sectors further from the limb. Furthermore, TROPICS has ten calibration measurements covering ~ 15 degrees of angular extent, which is much wider than traditional operational sensors of only four measurements covering ~ 5 degrees. The sun or moon will not intrude all of the ten spots for any of the channels, and TROPICS will have a more robust calibration to solar and lunar intrusion (traditional sensors gave priority to other design decisions, e.g., variable speed scan pattern to maximize integration time in the Earth scene). This tradeoff will be investigated during early orbit checkout.

6.3.2 Noise diode

The TROPICS warm calibration source is a weakly coupled noise diode. The weak coupler minimizes the insertion loss in the main receiver chain, and attenuates the noise diode power to levels within the radiometer's dynamic range (i.e., scene temperature). The drawbacks to the noise diode is the variability of the output power over time. While all instruments need to be characterized (e.g., non-linearity and spectral response), the noise diode requires additional pre-launch characterization. This is discussed further in Sect. 10. The TROPICS noise diode is turned on while viewing deep space to have a homogenous background, and therefore has similar issues of Earth and spacecraft intercept along with lunar intrusion.

Figure 14 shows an example characterization of the injected noise power by the noise diode. This channel is easily parameterized by a quadratic regression against the payload's physical

temperature. To calibrate the channel, the equivalent ND temperature will be determined by the payload temperature sensors provided in the payload telemetry. For example, if the physical temperature is 10°C, the calibration will use 276 K in the calibration for the ND temperature.

Figure 14 Example noise diode temperature characterization of an F-band channel that was easily parameterized using payload physical temperature and a parabolic fit.

The Pathfinder (TROPICS-01) was the qualification unit from the constellation and had seen the most vigorous testing, but not to the levels that wouldn't make it flight worthy. The G-band receiver had the most unstable noise diode, which required a more complex parameterization than the constellation SV. Instead of a single predictor variable like Figure 14 used payload temperature, two predictor variables are required to characterize the Pathfinder G-band noise diode temperatures.

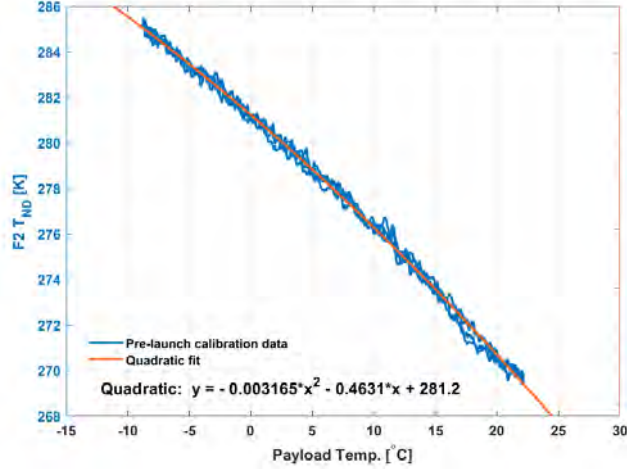
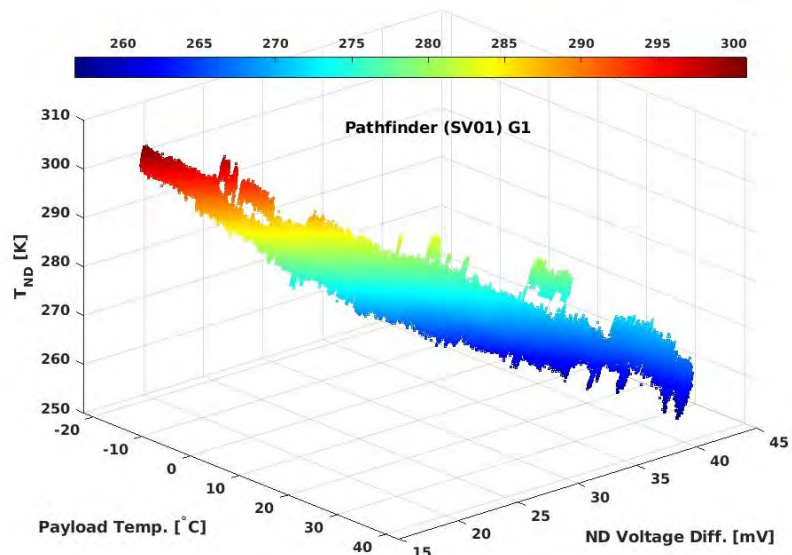


Figure 15 Pathfinder G-band example of the ND temp. regression that required two predictor variables. Besides G-band receiver temperature, the voltage difference between the two calibration sectors (i.e, ND on and off) is used. Colorbar is the T_{ND} calibrated using the external calibration targets in TVac (same as Z-axis).



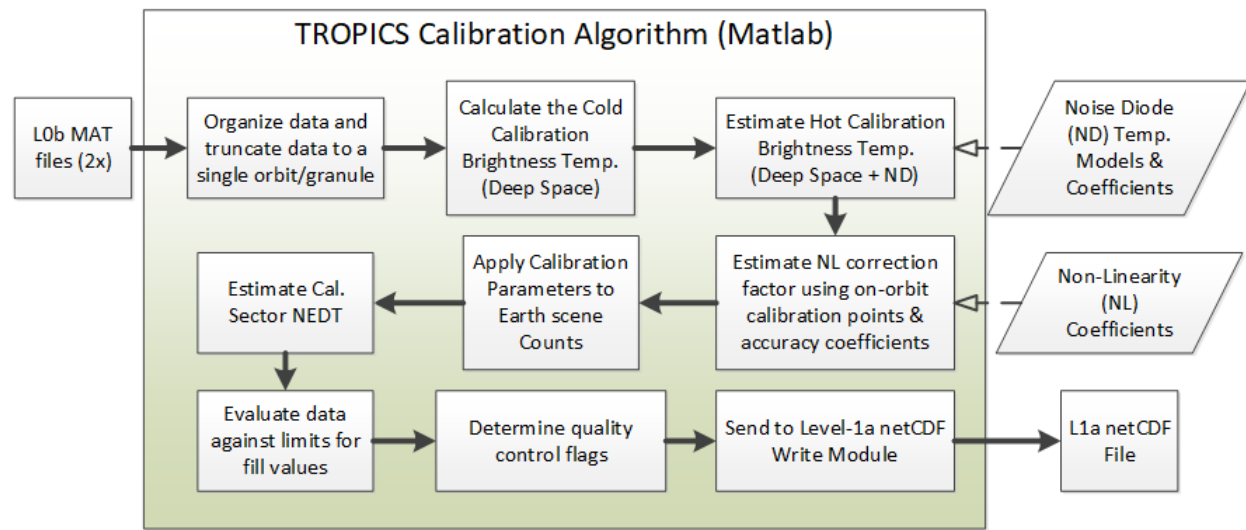
7 Algorithm Description

This section describes the calibration procedure for the Level-1a and Level-1b data products. Level-1a are timestamped, geolocated antenna temperatures with a non-linearity correction term. Level-1b will have three added corrections: 1) a 1st principle scan bias correction to reduce the impact of sidelobes using the antenna pattern measurements and simple Earth model, 2) a

calibration correction on the noise diode temperature to account for on-orbit drift over the lifetime of the mission (i.e., bias removal), and 3) an empirical scan bias correction using the GEOS-5 NWP.

7.1 Calibration

Calibration converts the radiometric counts from the radiometer analog-to-digital converter to radiance. TROPICS payload is a total-power radiometer architecture and the radiometric counts are proportional to the power of the upwelling radiation (i.e., square law device). A flow diagram of the TROPICS Calibration Algorithm is shown in Figure 16. This section will discuss each block



in this diagram.

Figure 16 Calibration block diagram

The input to the TROPICS Calibration Algorithm is two L0b mat files. The L0b mat files contain up to 100 minutes of data each. L0b is an intermediate data product that is not available to the public. L0b converts that raw payload binary file's telemetry into engineering units (e.g., voltages), prepares the timestamp, and geolocates the Earth sector's measurements on the surface of the Earth (see next section for more details on geolocation).

The first step in the calibration algorithm is to concatenate and truncate the data to a single orbit's worth, which is the L1 granule size. The orbit granule is bookended by ascending equatorial crossings. Two 100-min. L0b are required to assure an orbit has two ascending equatorial crossings. The next step is to organize the radiometer output data into the three sectors and flag outliers in the cold and hot calibration sectors. Flagged outliers are excluded from calibration. The thresholds for outliers in the cold and hot sectors are measured as the number of standard deviations from the orbital median value and are tunable parameters found in a payload specific .dat file (i.e., each payload has a unique .dat file). The .dat file contains other tunable parameters, and payload specific measurements that are used throughout the algorithm.

<https://tropics.ll.mit.edu>

The next step in the algorithm is to compute the cold scene calibration brightness temperature and its matching radiometric counts. The cold scene sector consists of 10 samples collected when the radiometer is viewing deep space with the ND turned off. A ND turn-off transient was noted during pre-launch testing. The calibration process was modified to ensure the transient is completely settled before the start of the cold scene sector (i.e., enough separation between ND sector and deep space sector).

The spectral radiance of deep space is the intensity as represented on Planck's 2.725 Kelvin blackbody curve. To calculate this value, we use the modified Rayleigh-Jeans equation described in Sect. 6.3.1, which provides the Planck equivalent brightness temperature. The equation for the final cold calibration brightness temperature is:

$$\text{Equation 2} \quad \tilde{T}_c = RJM_{corr}^{ch}(T_c + T_{sidelobe}^{ch})$$

The sidelobe term includes the Earth and spacecraft intercept, which is different for each antenna pattern measured. RJM is the modified Rayleigh-Jeans approximation equation in described in Sect. 6.3.1

Next the algorithm estimates the hot scene calibration brightness temperature and matching radiometric counts. The hot scene consists of 25 samples collected when the radiometer is viewing deep space with the ND turned on. A turn-on transient was noted during pre-launch testing, and the calibration process has a ND warm up period. The transient settles before the final 10 samples and therefore only the final 10 samples are used for calibration.

To estimate the hot scene brightness temperature, we need to know both the brightness temperature of deep space and the brightness temperature the ND injects into the radiometer chain. Unlike the cold calibration point, the deep space brightness temperature does not get the Planck correction factor because it's added to the ND temperature, which is warm enough to have minimal error introduced by the R-J approximation. The brightness temperature of the ND is determined by using the model coefficients derived during pre-flight TVAC calibration testing and that scan's current values reported in the payload telemetry. Each channel in each payload has its own unique model and set of coefficients based on its behavior. The equation for the hot calibration brightness temperature is

$$\text{Equation 3} \quad T_h = T_c + T_{ND}(X) + T_{sidelobe}^{ch}$$

where T_c is the cosmic background radiation (2.725 K), T_{ND} is the model output based on the telemetry values, X . The sidelobe contribution is for the Earth and spacecraft intercept, which is similar as the cold calibration sector if the hot calibration sector is as close to the Earth's limb in angle and the cold calibration sector (and the antenna pattern is largely symmetrical). If this is the case, then this term can largely cancel out during the gain calculation coming up.

Next, an on-orbit estimate of the non-linearity correction factor is determined. The non-linearity of each channel in each payload was characterized during pre-flight TVac calibration testing. See Figure 17A for an example of accuracy verses input brightness temperature. The two-point

calibration will have a maximum deflection at the half-way point (i.e., furthest distance from the calibration points). The maximum deflection or T_{NL} is measured as the payload temperature is changed. Figure 17B shows examples of the T_{NL} as a function of payload temperature that can be easily parameterized with a quadratic regression using the average temperature of all of the payload temperature sensors. The quadratic coefficients for each channel and payload are unique and stored in look-up tables. On orbit, the quadratic regression is used with the current scan's telemetry from the payload temperature sensors to estimate the non-linearity (i.e., maximum deflection) for each channel. The non-linearity value is then rebased according to the on-orbit cold and hot calibration temperatures, which are inevitably different than the cold and hot calibration temperatures measured during TVAC calibration testing (e.g., TVac calibration was between 100 K and 350 K, while on orbit is ~ 3 K to T_{ND}). Furthermore, T_{ND} is continuously changing with payload temperature throughout the orbit.

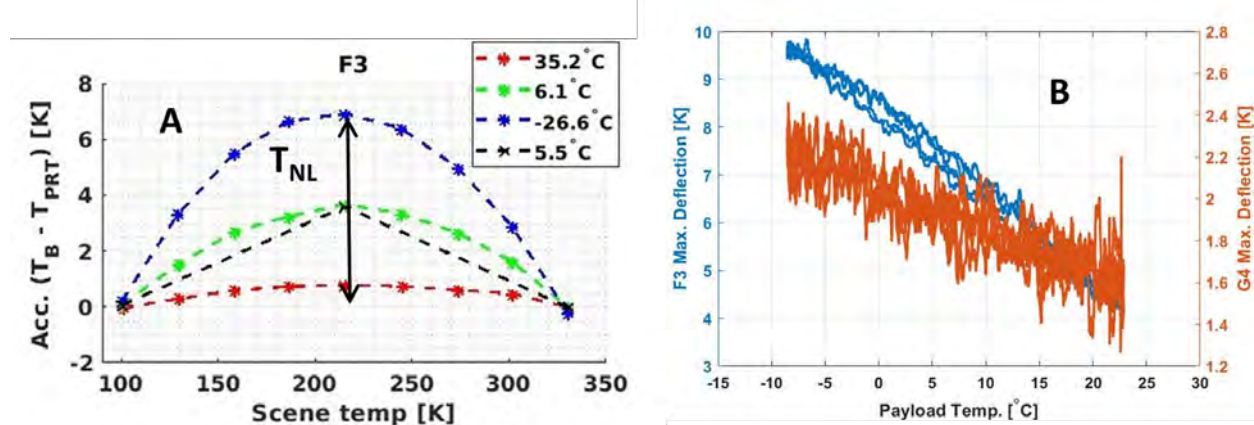


Figure 17 Explanation of non-linearity characterization and model. "A" is the calibration accuracy as a function of input brightness temperature. Each curve is the accuracy at a different payload temperature. "B" is plotting the maximum deflection as a function of payload temperature and can be clearly modeled by a quadratic. (Note that F3 in B is a different payload than F3 in A, which is why they don't match.)

These values are now sufficient to apply the calibration to the Earth scene measurements. The calibration equation is presented in Equation 4 with the output being the Level-1a antenna temperature. The inputs are the radiometric counts, C, and antenna temperatures, T. The subscript C is the cold scene and the subscript ND is the hot scene. Finally, the subscript S is the Earth scene.

$$\text{Equation 4} \quad T_A = \tilde{T}_C + \frac{T_H - \tilde{T}_C}{C_{ND} - C_C} \cdot (C_S - C_C) + T_{NL}(T_{instr}) \cdot 4 \cdot (s - s^2) \quad s = \frac{C_S - C_C}{C_{ND} - C_C}$$

The calibration is anchored with the cold scene brightness temperature, and the scene counts have the cold scene counts removed before being multiplied by the scalar gain. This implements the green curve in Figure 8.

The remainder of the equation removes the difference between the blue and green curve (i.e., the blue is the true response that is not linear). The non-linearity correction needs to be zero at the

two calibration sources, which is provided by the remaining non-linearity equation shown (i.e., other than the T_{NL}).

The calibration source measurements include the instrument noise, i.e., NEdT. Instrument noise has two mechanisms: 1) thermal or white noise and 2) flicker or 1/f noise. Thermal noise can be reduced by averaging calibration source measurements, but too much averaging will cause the noise to increase due to the flicker noise [Hersman 1981]. Each calibration sector within a scan will have ten measurements to reduce thermal noise. Calibration measurements from neighboring scans (the calibration period is two seconds) can be used to reduce thermal noise further, but due to the flicker noise in the TROPICS receiver front ends, minimal scan-to-scan filtering of the radiometric counts is done. The L1a calibration algorithm does have the functionality to filter the gain, which should be a continuous function in time and the filtering can reduce random noise and some of the residual ND fluctuations as shown in Figure 15 for the G-band Pathfinder channels.

The next three blocks in Figure 16 consist of calibration quality control. First, we calculate the NEDT of the instrument in cold and hot scene's independently. For more details, see TROPICS Data User Guide. Any sudden changes in these values from scan to scan may be an indication that the calibration is degraded. Next, the calibrated antenna temperatures reviewed and any out-of-family values are overwritten with fill values, i.e., anything outside the range of 0 to 350 K gets a fill value of -999. As a final step, quality control flags are determined consisting of quality checks and calibration conditions for trending (e.g., ascending or descending orbit). For a complete listing and description of the various quality flags, see the TROPICS Data User Guide. The final step is sending the data to a module that writes the L1a netCDF output file.

7.2 Geolocation

The TROPICS geolocation algorithm is described in this section, which requires the timestamp as a prerequisite. The spacecraft bus has an Attitude Determination and Control System (ADCS) with star trackers, which allows for precise attitude knowledge. The spacecraft bus also has a GPS receiver for precision positioning. A third component is the scanning assembly's encoder for knowledge of the payload orientation relative to the bus (and therefore the ADCS frame of reference).

The payload's line-of sight vector, \vec{u}_{PCS} , is derived from antenna measurements. There are 2 feeds in the radiometer for W/F-band and G-band that have slightly different line-of-sight vectors. In this sense, there is a unique geolocations solution for each: one for W/F-band and one for G-band. For simplicity, the rest of this section will discuss how the geolocation algorithm handles a single line-of-sight vector.

Figure 18 has the TROPICS coordinate systems illustrated with nomenclature required for the rotation of the line-of-sight vector to its geodetic intersection with earth's surface. Note that $\theta_{Encoder}$ is the instrument scan angle.

TROPICS coordinate system nomenclature:

- Payload Coordinate System (PCS)
- Payload Alignment Coordinate System (PACS)
- ADCS Body Coordinate System (BCS)
- Earth Centered Earth Fixed (ECEF)

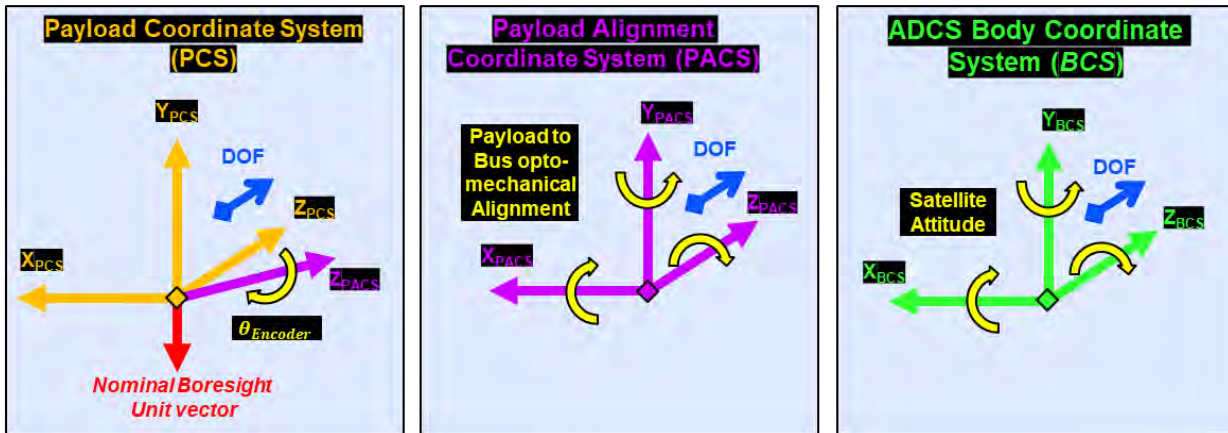


Figure 18 TROPICS coordinates and definitions

The rotation matrix needed to move the radiometer line-of-sight, \vec{u}_{PCS} , from PCS to ECEF is:

$$\mathbf{q}_{PCS2ECEF} = (\mathbf{q}_{PCS2PACS} \mathbf{q}_{PACS2BCS}) \mathbf{q}_{BCS2ECEF}$$

$$\mathbf{R}_{PCS2ECEF} = \text{quat2dcm}(\mathbf{q}_{PCS2ECEF})$$

The rotation from PCS to PACS is done by building a quaternion. The quaternion accounts for slight misalignments of the scan axis and the current instrument scan angle as represented in the data. The slight misalignment of the scan axis are unique for each payload and are derived from payload mechanical inspection measurements.

The rotation from PACS to BCS is derived from an opto-mechanical alignment performed by BCT. It accounts for slight misalignments between the payload and the bus as well as the precise alignment of the ADCS within the bus. A unique directional cosine matrix (DCM) is provided in the report for each TROPICS satellite. The DCM's are transformed into quaternions for use in the geolocation algorithm.

The rotation from BCS to ECEF incorporates the current satellite attitude as reported in the bus data. It is provided as a quaternion.

To rotate the line-of-sight from PCS to ECEF the following equation is used:

$$\vec{u}_{ECEF} = \mathbf{R}_{PCS2ECEF} \cdot \vec{u}_{PCS}$$

The radiometer line-of-sight, \vec{u}_{ECEF} , is used along with the satellite position reported by the onboard GPS to find the intersection with the WGS84 ellipsoid. See Figure 19 for a geolocation

flow chart. Based on post-launch analysis of ascending and descending orbits, a corrective rotation matrix might be added [9].

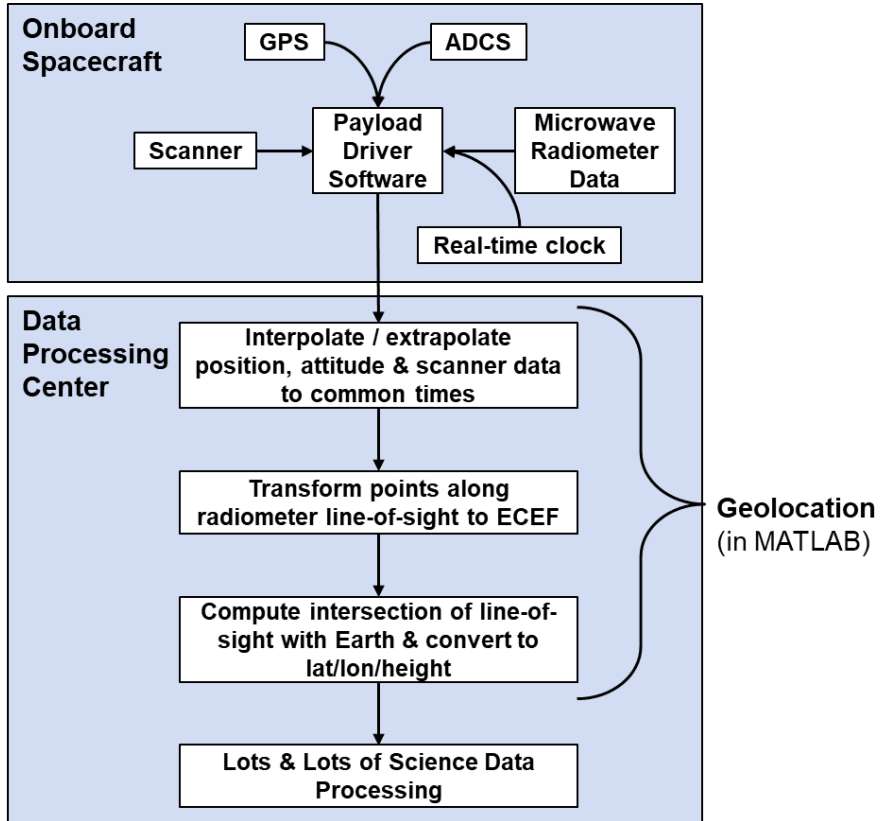


Figure 19 TROPICS geolocation flow chart

7.3 W- and F-band Channel Mixing Correction

During post-launch cal/val of the Pathfinder mission, the on-orbit data indicated mixing of the W/F-band channels that could not be explained by radiative transfer (i.e., not an issue with the passband or spectral response function measurements). This was most apparent when channels with high-altitude weighting functions (i.e., Ch. 8) had a negative brightness temperature perturbations when transitioning from ocean to land surfaces. ECMWF and Met Office found similar behavior in the FY-3 MWTS-2 data [17], and no root cause was identified, but a simple and robust correction was derived.

TROPICS derived a similar set of correction factors as the ECMWF & Met Office team [17] using the O-B outlined in Section 7.5. The correction coefficients were derived by linear regression using clear-sky

$$T_A^{Ch8 \text{ fixed}} = 0.711 \cdot T_A^{Ch8} + 0.272 \cdot T_A^{Ch3}$$

Equation 5 Example mixing correction equation for Pathfinder channel 8.

ocean near-nadir O-B. Equation 5 is an example of the correction for Pathfinder channel 8. The analysis indicated that channels 4 through 8 were primarily corrupted by channel 3, and channel 1 by both channel 2 and channel 3. Channel 2 and 3 showed little indication in mixing in the O-B data. The mixing correction

<https://tropics.ll.mit.edu>

had its initial validation by checking the retrieval error of the L2b Atmospheric Vertical Temperature Profile data, but further evaluating of the correction is underway. It is assumed this issue will also be found on the constellation space vehicles, and similar corrections will be derived during their Initial Orbit Checkout.

7.4 Antenna Temperature to Brightness Temperature Conversion

Microwave radiometers typically correct for “stray” radiation, which is outside the general area of the antenna’s main beam [3,7]. Even though the stray radiation comes from the angle with very little sensitivity (i.e., sidelobes), the radiometric contrast can cause a non-negligible radiance error. This is the first of three L1b corrections, and it is considered a “1st principle” scan bias correction because of the use of measured antenna patterns. Equation 5 relates the antenna temperature to the brightness temperature. The antenna pattern, or radiation pattern, D, sums to 4π steradians. Figure 20 has a simulated MM-2 antenna pattern on the left-hand side.

$$\text{Equation 6} \quad T_A = \frac{1}{4\pi} \int \oint \mathbf{D}(\theta, \phi) \cdot \mathbf{T}_B(f, \theta, \phi) d\Omega df \text{ [kelvins]}$$

The antenna pattern can be segregated between radiation upwelling from the Earth and deep space. As illustrated in Figure 20, the antenna pattern can be divided into sections that can be weighted, which can rewrite Equation 5 as:

$$T_A = \eta_{SC} \cdot T_{SC} + \eta_{DS} \cdot T_{DS} + \eta_E \cdot T_B$$

Where η is the integrated antenna pattern within the angular extent of the spacecraft, deep space, or Earth. The antenna temperature conversion to brightness temperature simply becomes:

$$T_B = \frac{T_A - \eta_{DS} \cdot T_{DS} - \eta_{SC} \cdot T_{SC}}{\eta_E}$$

The η will be calculated for each of the 81 beam positions at each of the four bands (W, F, G, and 205 GHz) using the antenna patterns measured at the antenna range. The brightness temperature of the spacecraft and deep space will be approximate values (e.g., 290 K and 3 K, respectively).

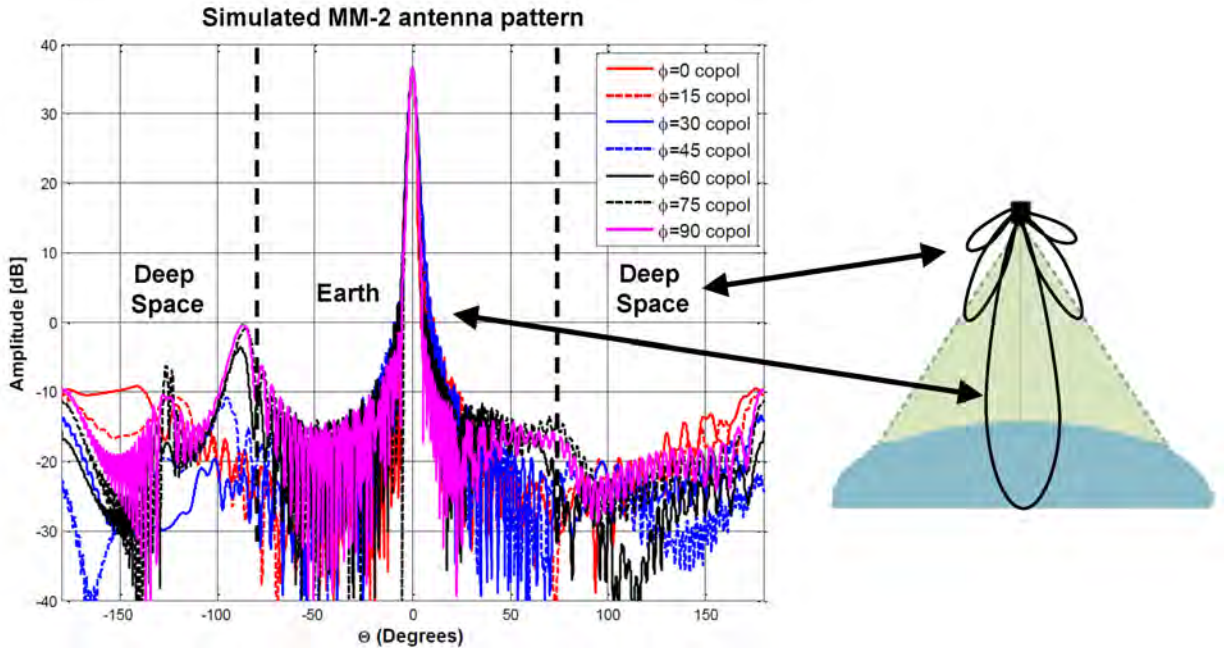


Figure 20 Simulated antenna pattern with illustration of sidelobe contamination.

7.5 Radiometric Bias Removal

Similar to the Global Precipitation Measurement Mission (GPM), TROPICS will have an extensive intercalibration of its CubeSat constellation [11]. Each CubeSat will have its radiometric bias benchmarked against a number of validation sources such as Numerical Weather Prediction model output, GPS radio occultation retrievals, radiosondes, and operational microwave sounders. Any consistent bias recorded will be corrected by adjusting the TND parameterizations in the calibration algorithm. While ND have shown to be stable on orbit, they have exhibited some post-launch settling [5,6]. This section discusses the other two L1b corrections: 1) noise diode drift and 2) empirical scan-bias correction.

The first step will be comparing the measured TROPICS radiances against validation sources, which typically require a radiative transfer model and instrument model. The TROPICS near real-time bias monitoring consists of comparing the GEOS-5 Forward Processing Assimilation model output analysis (available every three hours) combined with a line-by-line radiative transfer model [15]. To minimize the radiative uncertainty, bias is only calculated over ocean and under clear-air conditions. The clear-air conditions are determined using the GOES-16 and GOES-17 Binary Cloud Mask, which is available in 10 min. increments and is blurred to the TROPICS spatial resolution. For every orbit, TROPICS can conservatively expect 1,500 clear-air spots over ocean to compare against the measured radiances during a single CubeSat (~98 min.). The bias is then projected to the ND temperature as shown in Figure 21 (A). Using the cosmic background as an anchor point, the clear-air ocean pixel radiances and matching radiometric counts are used to calibrate the apparent temperature of the ND versus telemetry. It will be important to also include

the non-linearity correction, which is not shown in the illustration. Based on the example in Figure 5, each CubeSat will have approximately 1,500 spots to use each orbit over the eight deg. C temperature swing expected every orbit. Once a bias is confirmed, an affine transform of the T_{ND} parameterization will be derived using the updated T_{ND} values. The transform will have a timestamp based on when the bias data was collected. Figure 21 (B) has an exaggerated example of how the corrected T_{ND} data points would define a new T_{ND} relationship with the parameterization using predictive variables from the telemetry. Depending on the span of time the data points are collected, the new data would only cover a subset of the telemetry range, e.g., a day's worth of data would only cover a temperature range of about eight deg. C ($\pm 4^{\circ}\text{C}$). The affine transform is in the form of: $z(t) = a(t) \cdot y + b(t)$. The coefficients $a(t)$ and $b(t)$ will be linearly interpolated in time to the scene being calibrated. The initial condition for $a(t=0)$ at launch will be one and b will be zero. Data collected during early-orbit checkout will baseline the various validation data's error sources (e.g., radiative transfer model errors), then after early-orbit checkout, deviations will be monitored.

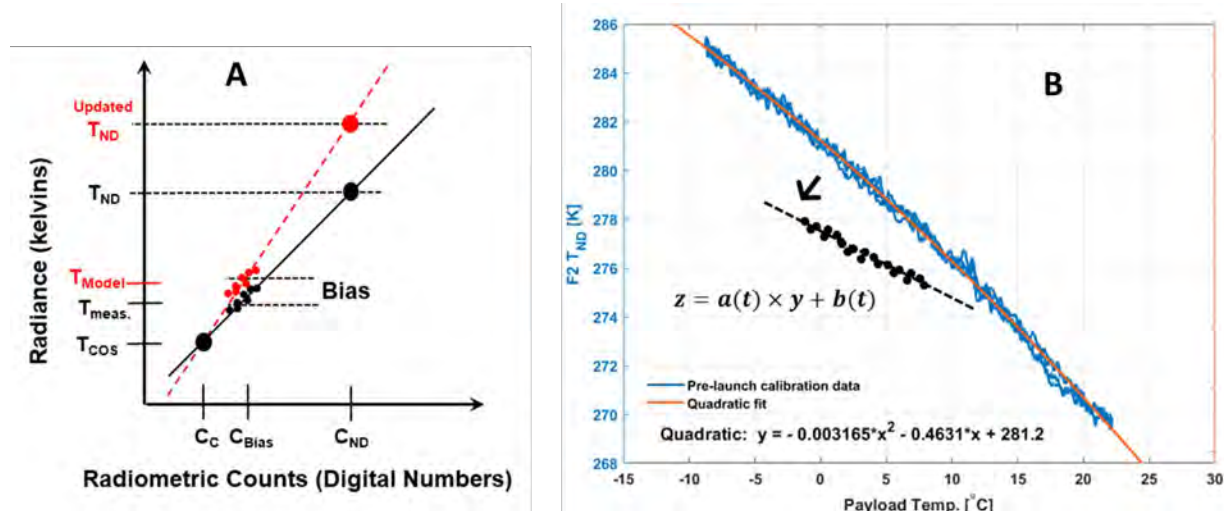


Figure 21 On-orbit ND drift recalibration technique. A) Using clear-air ocean simulations projected to noised diode temperature B) Simple affine technique to adjust the pre-launch ND temp. parameterization.

The empirical scan-bias will be characterized using the same technique as the noise diode drift using the GMAO GEOS-5 NWP and line-by-line radiative transfer model. The correction will remove any residual scan bias after the 1st principle correction from the antenna pattern measurements that was outlined above.

7.6 Intra-TROPICS Bias Trending

A standard technique for monitoring bias is to compare the observed radiances (Observation) against simulated radiances from a paired radiative transfer model and a source of the atmospheric

state (Background). This is called Observation minus Background or O-B. During the TROPICS Initial Orbit Checkout, a TROPICS spacecraft will be chosen with the minimum O-B using the Community Radiative Transfer Model ([CRTM](#)) and several atmospheric states: 1) [NASA GMAO GEOS-5 NWP](#), 2) radiosondes (e.g., [NOAA IGRA](#) or [GCOS GRUAN](#)), and 3) GNSS Radio Occultation. O-B will be measured over ocean and tropical rainforest to get both a low and high radiance. The spacecraft with the minimum bias will become the “reference” TROPICS spacecraft, but the O-B will be monitored throughout the mission for all six TROPICS spacecraft.

The other five TROPICS spacecraft will be monitored through the double difference technique [11-13]. The double difference technique removes the RTM’s 1st order bias [11]. Figure 22 illustrates the procedure for the TROPICS radiometric bias monitoring. It is important to correct for any spacecraft unique attributes like the antenna pattern or spectral response function, so the bias monitoring starts with brightness temperature and uses the CRTM with the “as built” Spectral Response Function (SRF) of the particular TROPICS spacecraft being monitored. The SRF is measured before launch. The procedure is:

1. Identify TROPICS radiance that is free of clouds and precipitation
2. Simulate the radiance using the NWP and RTM with the appropriate geometry, spatial resolution, polarization, and spectral response function
3. Calculate the O-B between 1 and 2 above, which is Single Difference (e.g., SD1 in the figure).
4. All other TROPICS spacecraft will follow the same O-B procedure (SD2, etc.)
5. Another difference will be made with each SD against the reference spacecraft, mentioned above, to produce the DD bias.

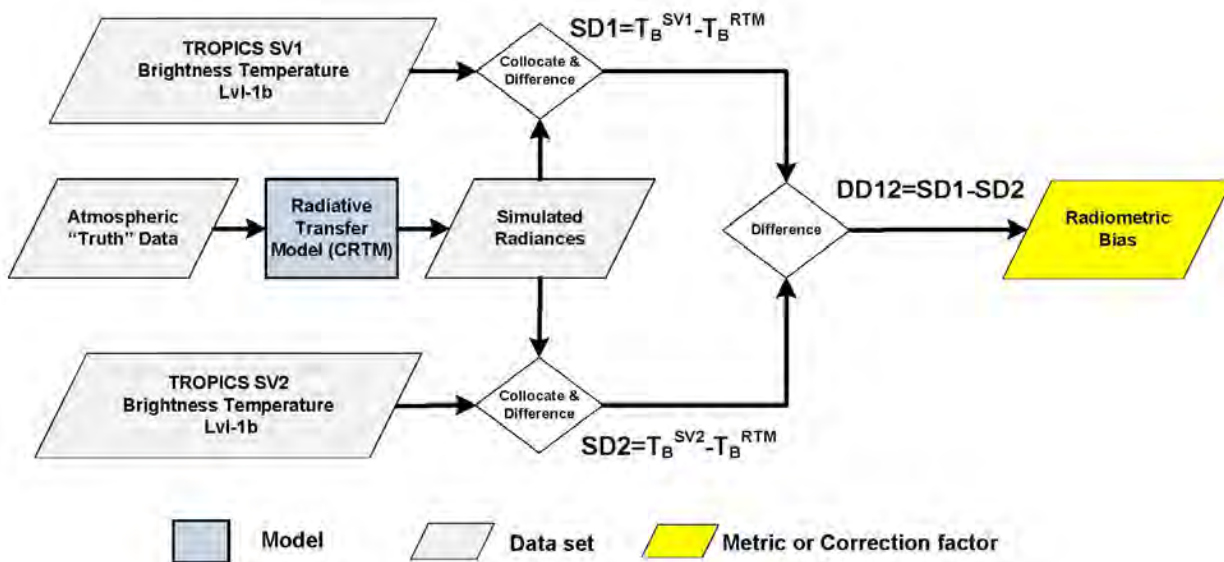


Figure 22 TROPICS bias monitoring block diagram

7.7 Quality Control Flags

A full description of the Level-1 quality flags can be found in the TROPICS Data User Guide. Here is brief description of Calibration Quality Flag is:

- Non-ocean flag: indicates whether the measurement (i.e., spot) is over non-ocean surface, which can be land, coastline, or an undefined geolocation of the spot.
- Lunar/solar intrusion flag: indicates that the calibration sectors may have had lunar or solar intrusion based solely on ephemeris modelling (i.e., not by evaluating the radiometric data).
- Space Vehicle maneuver flag: indicates that the space vehicle is in an active maneuver.
- Cold calibration consistency flag: evaluates subpar conditions in the cold calibration measurements.
- Hot calibration consistency flag: evaluates subpar conditions in the hot (i.e., noise diode) calibration measurements.
- Ascending/Descending flag: indicates whether the scan has the space vehicle in an ascending or descending part of the orbit.
- Day/night flag: indicates whether the spot is illuminated by the sun
- Payload orientation flag: indicates space vehicle orientation with one indicating the payload is facing the velocity direction. A zero is the bus is facing the velocity direction.

There is other information in the radiance data products:

- a scan-by-scan estimate of the NEDT from the two calibration sectors

<https://tropics.ll.mit.edu>

- payload temperatures
- more elaborate non-ocean flag with values for non-ocean, land/coastline, and undefined

7.8 Algorithm Input and Outputs

The principal input is the Level-0 payload data packets, which has been re-structured and timestamped. The on-board payload driver collects bus telemetry for attitude determination, positioning, and absolute timing and appends it to the payload data, making the Level-0 data largely self-sufficient. There are tunable parameter files with thresholds and output of the payload characterization described in Sect. 10. The output will be the netCDF Level-1a and Level-1b data products. See the TROPIC Data Product User Guide for more details on the output files.

			E_{NL}	E_{ND}	E_c	E_s				
Channel	Designation	On-orbit CBE (±K)	Residual Non-linearity	Noise Diode Cal. Point	Cold Cal. Point	Geolocation (Static)	Antenna Artifacts (Dyn.)	Passband Artifacts (Dyn.)	Gain drift (Dyn.)	Polarization (Dyn.)
1	W-band	1.213	0.125	0.377	0.061	-0.05	0.378	0.193	0.02	0.556
2	F-band 1	0.807	0.15	0.345	0.03	-0.06	0.301	0.144	0.026	0.072
3	F-band 2	0.907	0.175	0.345	0.03	-0.06	0.242	0.338	0.026	0.022
4	F-band 3	1.031	0.3	0.345	0.03	-0.05	0.242	0.325	0.027	0.006
5	F-band 4	0.989	0.3	0.345	0.03	-0.03	0.242	0.243	0.028	0.001
6	F-band 5	0.936	0.325	0.345	0.03	-0.015	0.242	0.058	0.029	0
7	F-band 6	0.826	0.325	0.345	0.03	-0.005	0.126	0.023	0.026	0
8	F-band 7	0.715	0.325	0.345	0.03	-0.06	0.068	0.008	0.031	0
9	G-band 1	0.81	0.09	0.601	0.005	-0.03	0.129	0.009	0.064	0
10	G-band 2	0.816	0.09	0.601	0.005	-0.05	0.156	0.023	0.064	0
11	G-band 3	0.839	0.09	0.601	0.005	-0.08	0.211	0.033	0.065	0
12	204-GHz	0.788	0.09	0.601	0.005	-0.1	0.18	0.001	0.066	0

Table 4 Current Best Estimate (CBE) of the on-orbit calibration accuracy.

8 Error Analysis and Correction Factors

Before launch, TROPICS uses an extensive radiometric calibration accuracy error budget that utilizes antenna pattern measurements and radiative transfer model to estimate the on-orbit calibration accuracy (i.e., the difference between the incoming scene brightness temperature and the L1b calibrated brightness temperature). Table 4 is the latest roll-up of the calibration accuracy error budget. The “E” are the errors from non-linearity (NL), noise diode calibration source (ND), space calibration source (C), and the scene brightness temperature (S). The E_{ND} , E_c , E_s – antenna, and E_s – passbands also have a breakdown of contributors. The CBE is the sum of static errors (e.g., T_{ND} drift) and the root sum square of the dynamic errors (e.g., sidelobes near the main beam). The error budget does account for each payload to have pre-launch characterization. Table 5 outlines the measurements and what error they mitigate. Note some of these measurements are used in the L1 algorithm (e.g., antenna to brightness temperature conversion uses the antenna

pattern measurements) or in the fast radiative transfer model (CRTM) used in the L2b algorithm and validation activities.

The ENL, END, Ec, and Es are weighted based on the scene temperature due to the calibration equation. Using propagation of errors on Equation 2, the on-orbit accuracy is in Equation 5.

$$\text{on-orbit accuracy} = x * E_{ND} + (1 - x) * E_C + E_{NL} + E_S \quad x = \frac{T_S - T_C}{T_{ND} - T_C}$$

$$E_{NL} = 4 * (x - x^2) * T_{NL}^{\text{residual}}$$

Equation 7 On-orbit calibration error budget weighting of the error sources based on scene temperature.

Table 5 lists some of the main error sources found in Table 4, and lists the mitigation technique that uses pre-launch measurements of each payload characteristics (e.g., sidelobes).

Table 5 A list of some of the main calibration accuracy error sources and the pre-launch mitigation measurements.

Error Source	Mitigation	Notes
Antenna sidelobes	Antenna pattern measurements used in deep space and scan bias corrections (e.g., Tb)	Impacts both calibration and Earth sector scan bias (Ec & Es antenna artifacts)
Geolocation	Measurements of electrical boresight and rotation/translation matrices before launch; there is also an on-orbit correction derived from land/sea boundaries crossings	
Polarization uncertainty	Pre-launch polarization measurement	Polarization angle is included in RTM, but the residual is Es polarization.
Non-linearity	Pre-launch characterization and on-orbit correction	Limited by no on-orbit measurement opportunities; window channels can potentially use vicarious calibration sources on the surface (residual is ENL)
Spectral response	Pre-launch characterization through SRF measurement	SRF used in RTM (residual error is in Es Passband Artifacts)
Calibration drift	On-orbit bias monitoring and removal	Will track both noise diode

9 Algorithm Ancillary Data

The Level-1a data product does not need ancillary data, but does have tunable parameters and files containing the pre-launch characterization. The Level-1b bias monitoring and removal will require extensive ancillary data (see Sect. 7.4).

10 Pre-launch Performance Testing

Pre-launch testing of each satellite not only verifies the performance (e.g., NEdT), but also characterizes each payload's spatial, spectral, and input/output responses. The three main characterizations:

- Measurements of the antenna subsystem in an antenna test range:
 - Antenna pattern in the principal polarization in both the along track and cross track directions
 - Antenna pattern in the cross-polarization in both the along track and cross track directions
 - Polarization angle
 - Beam characteristics: beamwidth and beam pointing
- Spectral Response Function measures the response of the instrument per frequency. Total-power radiometers combine, i.e., average, the frequencies across the passband, but weigh the frequencies differently across the passband. The SRF is important to measure when simulating the radiances. TROPICS measures the response using transmitted RF frequency tones that enter through the antenna and go to the detector. The SRF is made at three physical temperatures: low, nominal, and high. Sensitivity studies (see Section 10.2.1) indicated that the simulated radiance differences between low and high SRF has minimal radiance impacts, and the nominal (i.e., 24°C) temperature SRF were used to make the TROPICS CRTM and RTTOV sensor coefficients.
- Payload thermal-vacuum calibration [16]:
 - Uses three precise external calibration targets
 - Verifies NEdT over instrument temperature and across scene radiance
 - Measures non-linearity through accuracy and the two-point external calibration (i.e., T_{NL} from Sect. 7.1)
 - Characterizes the noise diode temperature (T_{ND}) over instrument temperature or telemetry
 - Quantifies the residual accuracy after applying non-linearity correction and using noise diode as the warm calibration source (i.e., not using the external targets for calibration)
 - Tests the calibration repeatability with a thermal profile very similar to the on-orbit thermal predictions
 - Monitors noise diode stability over duration of test

10.1 Antenna Pattern Measurements

The antenna pattern were measured for each payload and at frequency near the center of each channel's passband. Measurements were made at the MIT LL RF System Test Facility in a compact antenna test range. Two sets of measurements were made: 1) baseline measurement around the antenna pattern peak (± 5 deg.) at 0.1 degree increments and 2) beam efficiency measurement ± 90 deg. at a coarser 0.5 deg. increments. Both sets were measured at two orientations relative to the satellite velocity vector: 1) along satellite track and 2) cross satellite track. Also, both the principal polarization and cross-polarization were measured. These measurements were used to adjust the geolocation by measuring the electrical boresight. The antenna measurements also determined the polarization scheme angle from Section 4.3.

10.2 Spectral Response Functions

To design and manufacture a compact payload that fits into a small volume, a number of passband specifications that are common to operation sensors were not levied onto the TROPICS passbands. Instead, precise measurements of the passbands replaced stringent TROPICS passband requirements. Each payload had a comprehensive measurement of its Spectral Response Functions (SRF) using a millimeter-wave source input at the receiver front ends and the resulting voltage is recorded from the detector (i.e., the radiometer's backend). The output was made into a frequency weighting that is used to make the radiative transfer coefficient for the TROPICS payloads. As shown in the following sections, it is imperative to use the SRF in the radiance simulations, but we don't need to have multiple SRFs to model at different payload temperatures.

10.2.1 SRF Temperature Sensitivity Analysis

The SRF were measured at three payload temperature: -20°C, 24°C, and 40°C. To quantify the radiance change due to temperature changes occurring in the SRF, the passbands from the three temperatures were simulated using an absorption-only Line-by-line radiative transfer model [15] and the NOAA88b radiosonde dataset. NOAA88b is known to be polar heavy and Figure 23 is a scatterplot of the Total Precipitable Water (TPW) verses the latitude of the radiosonde location. Note that the TROPICS constellation only measures $\pm 35^\circ$ latitude. Appendix D has, for each channel, a pair of plots with the top plot showing the minus 20°C and positive 40°C passbands along with the design goal (e.g., boxcar). The bottom plot is the radiometric difference of that channel between the -20 and 40 degree Celsius passband (i.e., 60 degree Celsius change). Note that the on-orbit thermal simulations indicate that the orbital variation will be $\pm 4^\circ\text{C}$ and the yearly variation approximately -5°C to 18°C. All of the radiance differences for the 60 degree change in payload temperature indicted that using the 24°C SRF as the primary or main SRF with provide minimal spectral error in the radiative transfer models. Both the CRTM and RTTOV developers have incorporated the 24°C SRFs into their TROPICS coefficients. Table 6 has the maximum error (K) of the NOAA88b simulation differences for TPW greater than 20 mm, which is represents profiles most common in tropical latitudes (see Figure 23). The SRF used the 24°C SRF and the

on-orbit thermal simulations predict a range of -5°C to 18°C. Regarding Ch. 3, this is the error over 60°C range. Using 24°C SRF will have a temp. difference between 6°C to 30°C, a which will result in the worst-case error of half shown in the table.

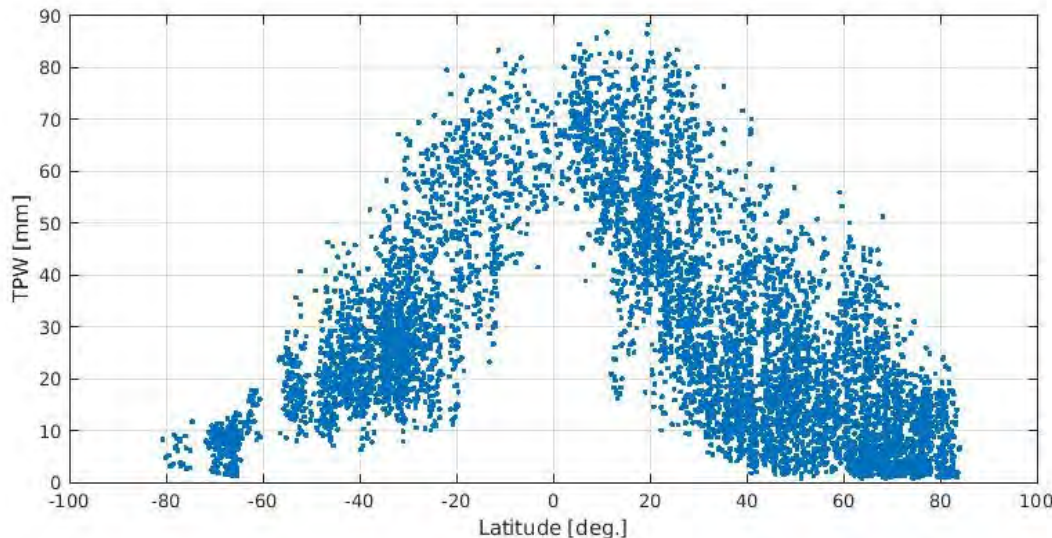


Figure 23 NOAA88b radiosonde global dataset used to evaluate the differences in SRF. One metric to evaluate an individual profile in the dataset is the Total Precipitable Water. Higher TPW indicates a profile that is closer to the equator.

Table 6 Max. error (kelvins) from NOAA88b ensemble simulations with TPW > 20 mm (~tropical profile)

Ch.	1	2	3	4	5	6
Box-SRF	0.35	0.60	1.20	-0.30	0.012	-0.40
-20°C vs 40°C	0.013	0.050	-0.250	-0.030	-0.100	0.035
Ch.	7	8	9	10	11	12
Box-SRF	0.007	-0.025	0.0	-0.20	-0.10	-0.005
-20°C vs 40°C	-0.080	-0.060	0.0	-0.050	-0.050	-0.080

10.2.2 SRF Difference from Ideal Boxcar Passbands

After picking the nominal temperature SRF, simulations of the difference in radiance for the NOAA88b radiosonde dataset between the idealized boxcar passbands and the nominal temperature SRF were made. Examples of how the SRF were digitized can be found in F.3. Data points were taken throughout the passband and then down the sides to approximately -15 dB to -

20 dB down from the peak (i.e., passband maximum value). Similar to the previous section, Appendix E: SRF Ideal vs. Measured Results has the passband weights for each channel along with the ideal or design passband goal. Each channel also has analysis from the NOAA88b radiosonde dataset described above where the simulated radiance difference between the ideal and nominal Pathfinder SRF is shown. These difference (note that some axis are $\times 10^{-3}$) are not negligible and any radiance comparisons to validate the TROPICS data products will require using the SRFs. Table 6 has the maximum error (K) of the NOAA88b simulation differences for TPW greater than 20 mm, which represents profiles most common in tropical latitudes (see Figure 23).

10.3 Calibration Characterization

This section describes the pre-launch calibration and performance verification of the TROPICS payloads, and the repeated calibration of a payload after its integration onto the spacecraft bus, in a thermal-vacuum (TVac) chamber. Each payload is calibrated separately and has its own characterization that can be very different between payloads due to manufacturing variability within payload components.

The first calibration step characterizes the radiometer's non-linearity and Noise Diode (ND) temperature. The precise characterization of the ND output power is crucial because it replaces the onboard calibration target typically used in traditional sensors. The next step uses the first step's calibration characterization and the standard periodic absolute calibration equations (see Section 7.1), to verify the radiometer's performance: 1) Noise Equivalent Delta Temperature, ΔT_{rms} , and 2) radiometric calibration accuracy. This verification step uses the ND characterization, on-orbit data acquisition mode, and an orbital thermal profile similar to what is expected on orbit. This methodology is the closest to "test as you fly" that has been accomplished by a passive microwave spaceborne payload. Upcoming sections cover the overall calibration procedure, calibration Ground Support Equipment (GSE), verification procedure, and general verification results, but individual payload's characterization and verification results will be in separate appendices.

10.3.1 Calibration Apparatus

MIT LL has designed and built a state-of-the-art and unique calibration apparatus for compact radiometers. The Ground Support Equipment (GSE) includes three precision iron-filled epoxy calibration targets that represented the three calibration sectors (i.e., Earth view, deep space, and deep space with ND). See Figure 24 (A) for a photo of the apparatus holding the targets with the payload or Space Vehicle (SV) situated in the middle to allow the targets to be at the same angles as the TROPICS calibration sectors (B). The GSE also included a robust thermal control system that allowed nearly orbital payload thermal profiles during characterization and verification (both in range and rate). An extensive design effort required a full analysis of all error sources and greatly reduced stray radiation and thermal gradients in the GSE's targets. The end-to-end calibration accuracy of the GSE was determined to be 0.2 K peak-to-peak by assessing the variance of linear-channel's calibration accuracy across nine scene temperatures varying between 100 to 350 K. Calibration accuracy requirements were approximately ± 1 K. More details of the GSE can be found in [16].

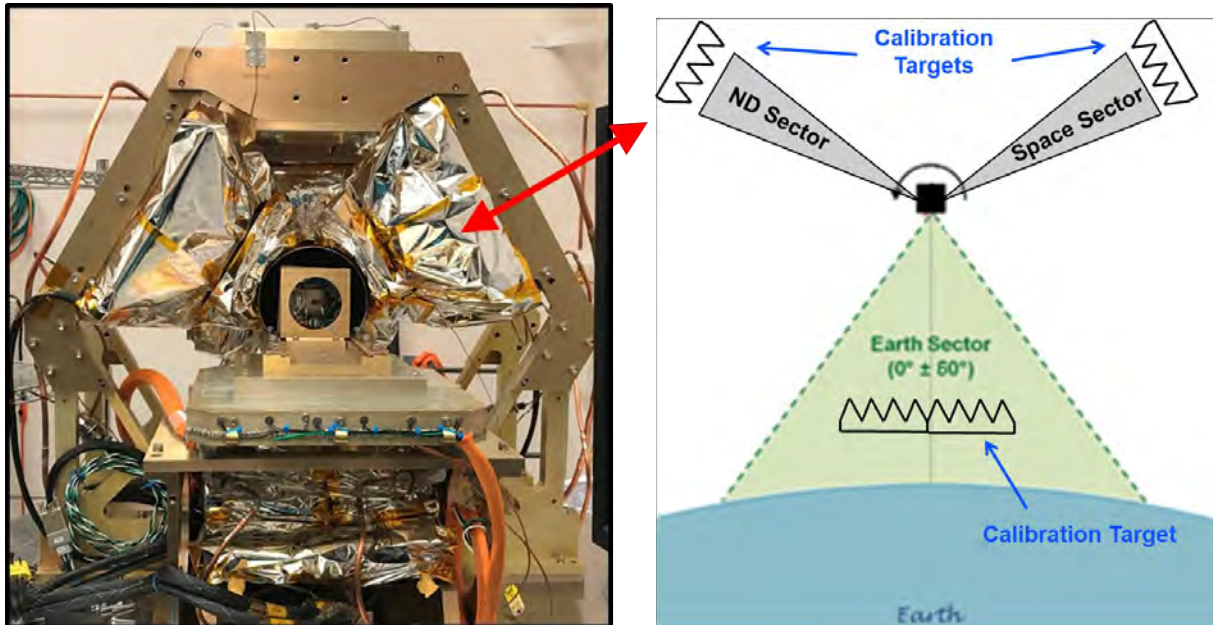


Figure 24 Photo of the calibration apparatus without the chamber cover on (left). The external targets are placed in approximately the same angles as the on-orbit calibration sectors (right).

10.3.2 Calibration Procedure

The ND calibration consisted of a “through the antenna” characterization of the ND power injected into the radiometer’s receiver chain, which adds to the incoming scene radiance. This is accomplished by transferring the known radiances of the external calibration targets onto the increased radiometric output voltage when the ND was turned on. The ND output power varies with the physical temperature of the instrument, and therefore is characterized across the range of expected on-orbit temperatures.

Figure 25 Example profiles from the characterization and verification thermal profiles. On-orbit predicted thermal profiles are also show for the coldest and hottest cases.

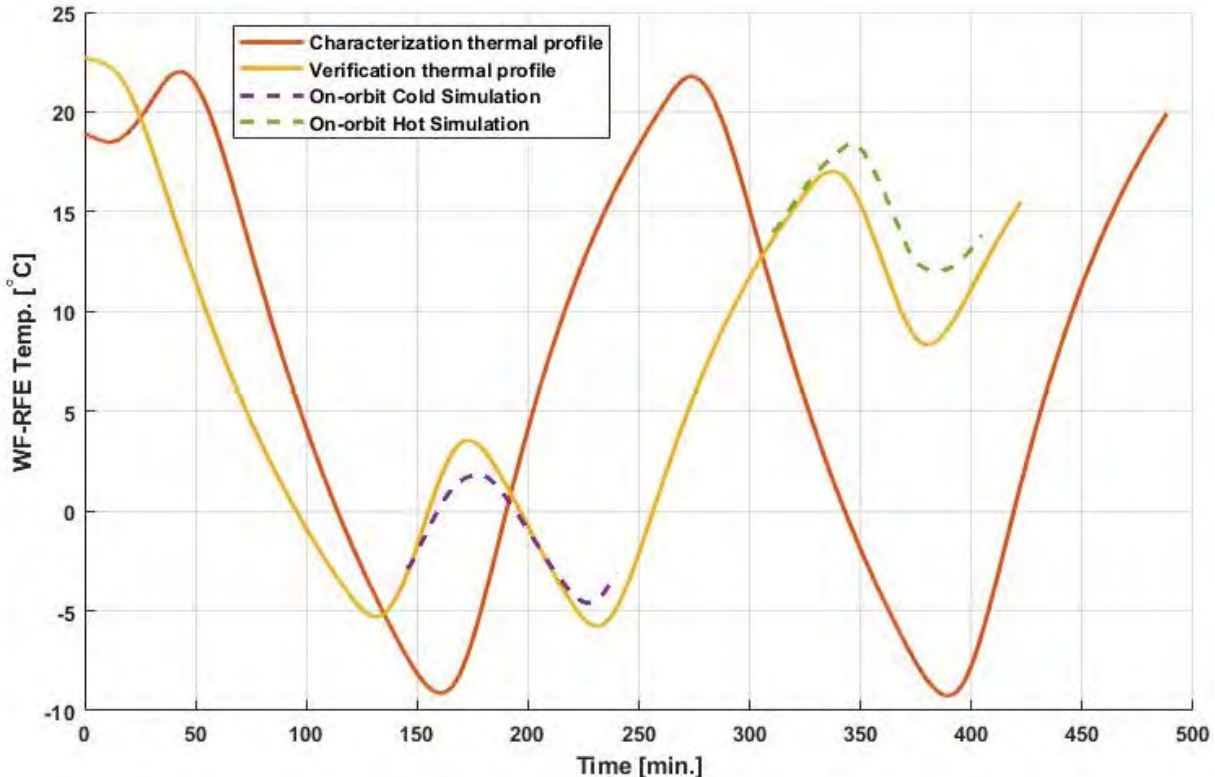


Figure 25 has the characterization thermal profile that is used to derive the ND temperature and non-linearity parameterization. It exceeded the predicted temperature range and rate of temperature change. The on-orbit payload thermal balance will be different, but it is critical to have the payload's temperature changing during calibration. Note that the verification profile was different from characterization profile to emulate the inevitable on-orbit differences. Non-linearity is derived using the maximum radiance deflection from the two-point calibration by placing the scene brightness temperature at the half-way point between the two external calibration target temperatures.

10.3.3 Calibration Results

The final calibration characterization results in a parametrization of the ND temperature (or other payload telemetry) and instrument non-linearity as a function of payload data telemetry. The payload telemetry consists primarily of temperature sensors placed on or in key payload components (e.g., receiver front end), but can also be voltage and current telemetry or even another channel's radiometric telemetry. The parameterization of each payload will be presented as a separate appendices.

10.4 Pre-launch Calibration Verification

The next crucial aspect is verifying the derived calibration parameters in conditions similar to on-orbit, which consist of 1) using the complete calibration algorithm and calibration parameterization, 2) payload in operational mode, and 3) a nearly orbital thermal profile.

10.4.1 Verification Procedure

Figure 25 has the verification thermal profiles with the on-orbit thermal predictions overlaid. Using this nearly on-orbit thermal profile, along with the ND and non-linearity characterization, provided a unique assessment of the payload performance on the SV. Figure 26 has an example of the operational-mode radiometric data used for verifying the calibration. The targets used in the calibration sectors were controlled to ~100 K, and the scene is at ~250 K. The 100-K scenes in the

calibration sectors represent the deep space radiance that would be seen on orbit.

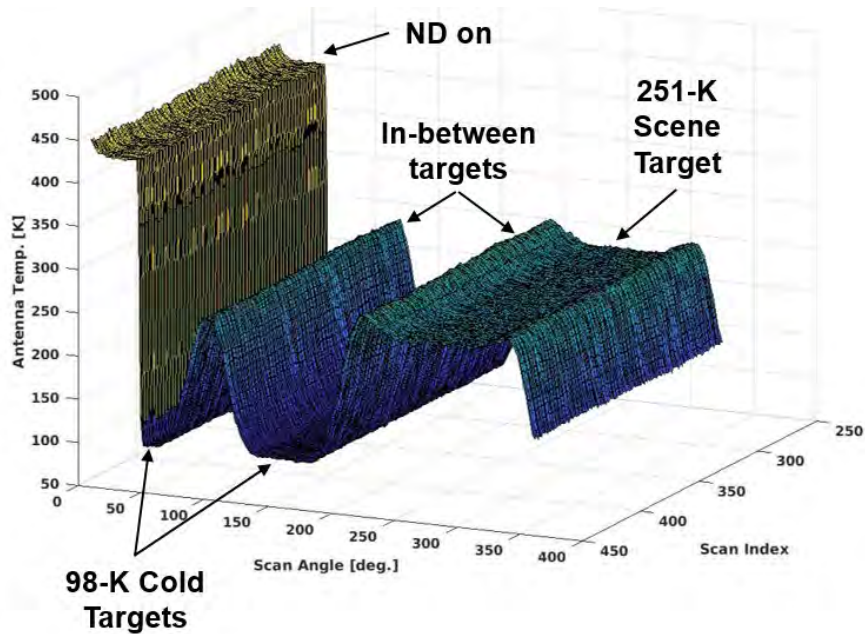


Figure 26 Example radiometric data while verifying the calibration parameters in the on-orbit operational mode.

10.4.2 Verification Results

The external targets were only used for the “truth” brightness temperature and the calibration algorithm only uses the ND and non-linearity parameter while the payload temperature varied over

the verification thermal profile in Figure 25. Each payload's calibration characterization is presented as an appendices, but an example of a SV that was calibrated three separate times is described here. Figure 27 shows the calibration accuracy of the TROPICS-02 SV from the orbit-like thermal profiles in operational mode. The same data configuration was repeated after the payload was integrated onto the bus. Additional curves come from data collected in Dec. 2019 and Jan. 2021 but still used the calibration characterization from the March 2019 calibration. During these nine months, the payload was turned on for about nine days, and an additional three days during Jan. 2021.

Some on-orbit ND settling is expected and differences in Figure 27 are assumed to be ND settling that previous spaceborne mission with ND have experienced (Draper 2015 & 2018). The GMI settling occurred during the first couple of months after launch. There is evidence in the TROPICS recalibration that settling occurred between calibrations, but settled to a new steady state (or even the previous state) within days. Any longer term ND settling will be mitigated by monitoring and corrective action as described in Section 7.4.

In general, verification results lacking a strong temperature dependence is a sign of a successful calibration, i.e., robust ND temperature parameterization and non-linearity correction across

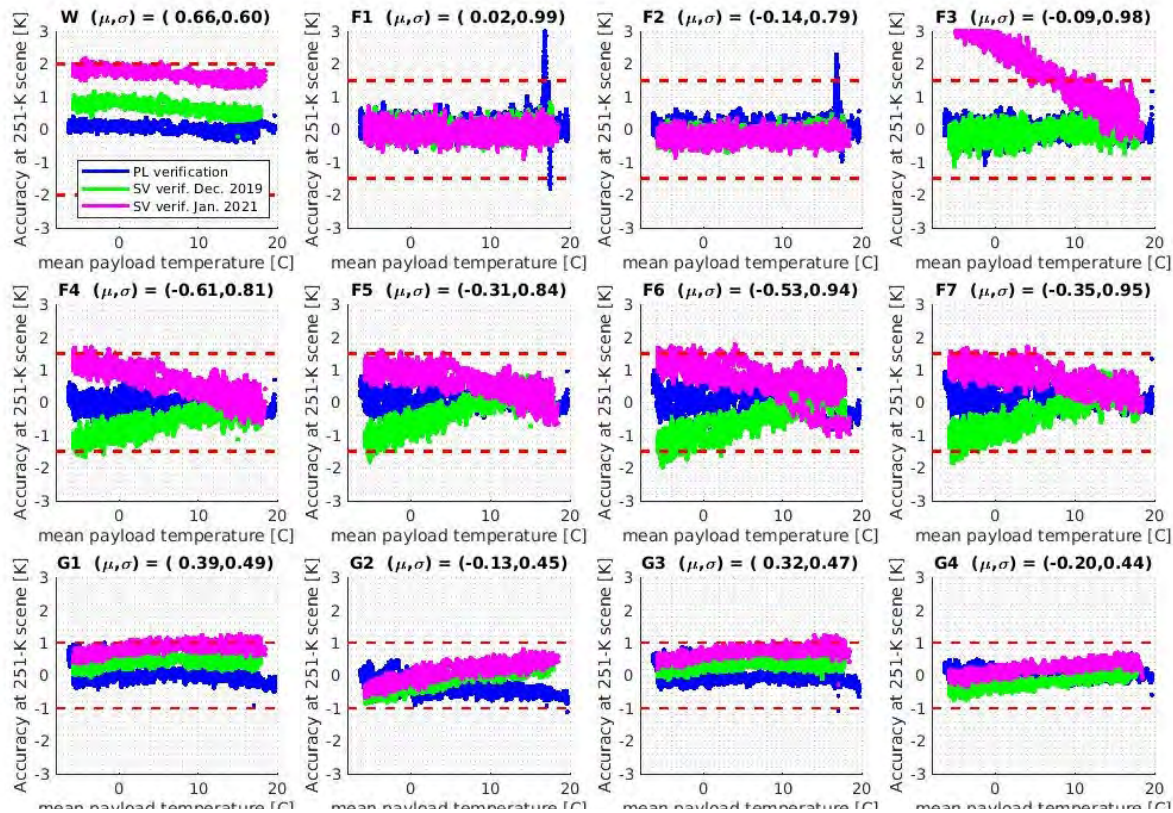


Figure 27 TROPICS-02 calibration accuracy using the March 2019 calibration characterization on data collected during SV TVac in Dec. 2019 and Jan. 2021.

changing instrument temperature. The parameterizations for each channel will be presented in that payload's characterization appendices.

11 References

1. W. J. Blackwell, et al., "An overview of the TROPICS NASA Earth Venture Mission," Quarterly Journal of the Royal Meteorological Society, 144 (Suppl. 1): pp. 16-26, 2018 doi:10.1002/qj.3290
2. Hersman, Michael S. and Gene A. Poe, "Sensitivity of the Total Power Radiometer with Periodic Absolute Calibration," IEEE Transactions on Microwave Theory and Techniques, Vol. MTT-29, No. 1, January 1981
3. Advanced Technology Microwave Sounder (ATMS) Algorithm Theoretical Basis Document, https://www.star.nesdis.noaa.gov/jpss/documents/ATBD/D0001-M01-S01-001_JPSS_ATBD_ATMS-SDR_A.pdf
4. F. Weng and X. Zou, "Errors from Rayleigh–Jeans approximation in satellite microwave radiometer calibration systems," Appl. Opt., 52, 505-508 (2013).
5. Draper, David W.; David A. Newell; Darren S. McKague; and Jeffrey R. Piepmeier, "Assessing Calibration Stability Using the Global Precipitation Measurement (GPM) Microwave Imager (GMI) Noise Diodes," IEEE Journal of Selected Topics in Applied Earth Observations and Remote Sensing, Vol. 8, No. 9, September 2015
6. D. Draper and D. Newell, "Global Precipitation Measurement (GPM) Microwave Imager (GMI) After Four Years On-Orbit," 2018 IEEE 15th Specialist Meeting on Microwave Radiometry and Remote Sensing of the Environment (MicroRad), Cambridge, MA, 2018, pp. 1-4. doi:10.1109/MICRORAD.2018.8430702
7. Meissner, Thomas; Frank Wentz; and David Draper, "GMI Calibration Algorithm and Analysis Theoretical Basis Document," http://images.remss.com/papers/gmi_ATBD.pdf, Version G, April 2012
8. Maiwald, Frank; et al., "Reliable and Stable Radiometers for Jason-3," IEEE Journal of Selected Topics in Applied Earth Observations and Remote Sensing, Vol. 9, No. 6, June 2016
9. Moradi, Isaac; Huan Meng; Ralph R. Ferraro; & Stephen Bilanow, "Correcting Geolocation Errors for Microwave Instruments Abroad NOAA Satellites," IEEE Transactions on Geoscience and Remote Sensing, Vol. 51, No. 6, June 2013
10. Atkinson, Nigel; James Cameron; Brett Candy; and Steve English; "Bias correction of satellite data at the Met Office," ECMWF Presentation, <https://www.ecmwf.int/sites/default/files/elibrary/2005/14209-bias-correction-satellite-data-met-office.pdf>, 2005
11. Biswas, Sayak K.; Spencer Farrar; Kaushik Gopalan; Andrea Santos-Garcia; W. Linwood Jones; Stephen Bilanow, "Intercalibration of Microwave Radiometer Brightness Temperatures for the Global Precipitation Measurement Mission," IEEE Transactions on Geoscience and Remote Sensing, Vol. 51, No. 3, March 2013

12. Gyanesh Chander, Tim J. Hewison, Nigel Fox, Xiangqian Wu, Xiaoxiong Xiong, and William J. Blackwell, "Overview of Intercalibration of Satellite Instruments," *IEEE TRANSACTIONS ON GEOSCIENCE AND REMOTE SENSING*, VOL. 51, NO. 3, MARCH 2013
13. R. W. Saunders, T. Blackmore, B. Candy, P. N. Francis, and T. J. Hewison, "Monitoring satellite radiance biases using NWP models," *IEEE Trans. Geosci. Remote Sens.*, vol. 51, no. 3, pp. 1124-1138, Mar. 2013.
14. Yang, Hu, "Developing Vicarious Calibration for Smallsat Microwave Instruments using Lunar Radiation," AMS 98th Annual Meeting, Austin, TX 2018
15. H. J. Liebe, "MPM—An atmospheric millimeter-wave propagation model," *Int.J. Infrared Millimeter Waves*, 10(6), 631–650, 1989
16. R. V. Leslie, W. J. Blackwell, A. Cunningham, M. DiLiberto, J. Eshbaugh and I. A. Osaretin, "Pre-launch Calibration of the NASA TROPICS Constellation Mission," *2020 16th Specialist Meeting on Microwave Radiometry and Remote Sensing for the Environment (MicroRad)*, 2020, pp. 1-4, doi: 10.1109/MicroRad49612.2020.9342614.
17. Lu, Qifeng, *et al.* , "An evaluation of FY-3C satellite data quality at ECMWF and the Met Office," ECMWF Technical Memoranda 767, Nov. 2015, URL
<https://www.ecmwf.int/node/14692>, DOI 10.21957/3l7g9nqun

Appendix A: Noise Equivalent Delta Noise

TROPI CS Chan.	Center Freq. (GHz)	SV1/Path Measured NEDT (K)	SV2 Measured NEDT (K)	SV3 Measured NEDT (K)	SV4 Measured NEDT (K)	SV5 Measured NEDT (K)	SV6 Measured NEDT (K)	SV7 Measured NEDT (K)
1	91.656 ± 1.4	0.76	0.60	0.52	0.33	0.33	0.37	0.37
2	114.50	0.92	0.99	0.84	0.81	1.14	0.72	0.84
3	115.95	0.81	0.79	0.70	0.68	0.72	0.65	0.69
4	116.65	0.93	0.98	0.86	0.80	1.64	0.94	1.01
5	117.25	0.85	0.81	0.77	0.71	1.14	0.86	0.90
6	117.80	0.88	0.84	0.79	0.72	1.11	0.83	0.97
7	118.24	0.95	0.94	0.90	0.87	1.41	0.93	1.02
8	118.58	1.10	0.95	0.94	0.90	1.37	0.86	0.99
9	184.41	0.62	0.49	0.64	0.45	0.61	0.47	0.57
10	186.51	0.70	0.45	0.54	0.50	0.64	0.56	0.59
11	190.31	0.69	0.47	0.42	0.37	0.43	0.38	0.45
12	204.8	0.66	0.44	0.49	0.42	0.53	0.45	0.63

<https://topics.ll.mit.edu>

Appendix B: Antenna Pattern Beamwidths (Full-width Half Max.)

Chan.	Freq. GHz	Req. (deg)	SV1 (deg)	SV2 (deg)	SV3 (deg)	SV4 (deg)	SV5 (deg)	SV6 (deg)	SV7 (deg)
1	90.1	<3.0	2.81	2.83	2.79	2.83	2.84	2.85	2.83
1	93.1	<3.0	2.72	2.71	2.7	2.7	2.72	2.71	2.72
2	114.5	<2.4	2.28	2.27	2.26	2.24	2.27	2.25	2.28
3	115.9	<2.4	2.28	2.3	2.26	2.22	2.29	2.28	2.30
4	116.5	<2.4	2.29	2.31	2.26	2.24	2.28	2.27	2.29
5	117.3	<2.4	2.29	2.31	2.25	2.23	2.26	2.25	2.27
6	117.7	<2.4	2.29	2.31	2.26	2.22	2.26	2.25	2.27
7	118.3	<2.4	2.29	2.32	2.26	2.23	2.28	2.26	2.28
8	118.5	<2.4	2.30	2.31	2.26	2.23	2.26	2.27	2.27
9	184.3	<1.5	1.52	1.53	1.52	1.46	1.48	1.47	1.48
10	186.3	<1.5	1.52	1.51	1.49	1.44	1.48	1.46	1.46
11	190.3	<1.5	1.52	1.52	1.46	1.44	1.47	1.46	1.45
12	204.8	<1.5	1.41	1.40	1.40	1.40	1.42	1.40	1.41

<https://tropics.ll.mit.edu>

Appendix C: Native Horizontal Spatial Resolution

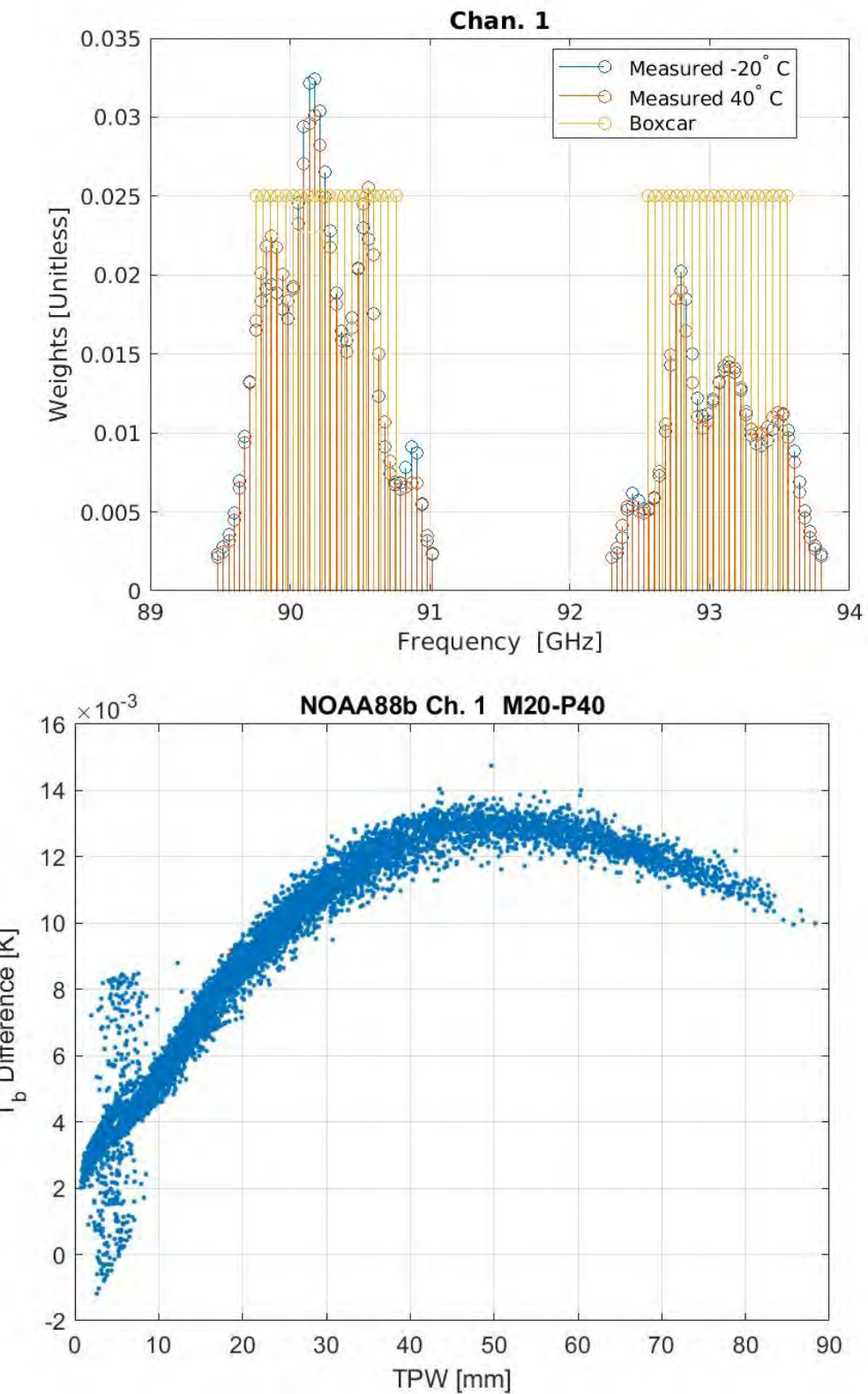
BP #	Scan Angle (Deg.)	F-Band 2.4° FWHM			W-Band 3.0° FWHM		
		Cross Track (km)	Down Track (km)	Geometric Mean (km)	Cross Track (km)	Down Track (km)	Geometric Mean (km)
1	60	177.1	54.5	98.3	215.1	68.1	121.1
2	58.5	148.4	50.9	86.9	180	63.6	107
3	57	127.5	47.9	78.1	154.5	59.9	96.2
4	55.5	111.5	45.3	71.1	135.1	56.7	87.5
5	54	98.9	43.1	65.3	119.8	53.9	80.3
6	52.5	88.8	41.1	60.4	107.5	51.4	74.4
7	51	80.5	39.4	56.3	97.4	49.3	69.3
8	49.5	73.5	37.9	52.8	89	47.4	64.9
9	48	67.7	36.5	49.7	81.9	45.6	61.1
10	46.5	62.6	35.3	47	75.8	44.1	57.8
11	45	58.3	34.1	44.6	70.5	42.7	54.9
12	43.5	54.5	33.1	42.5	66	41.4	52.2
13	42	51.2	32.2	40.6	62	40.2	49.9
14	40.5	48.3	31.3	38.9	58.4	39.2	47.8
15	39	45.7	30.5	37.4	55.3	38.2	46
16	37.5	43.4	29.8	36	52.6	37.3	44.3
17	36	41.4	29.2	34.8	50.1	36.5	42.7
18	34.5	39.6	28.6	33.6	47.9	35.7	41.3
19	33	37.9	28	32.6	45.9	35	40.1
20	31.5	36.5	27.5	31.7	44.1	34.4	38.9
21	30	35.1	27	30.8	42.5	33.8	37.9
22	28.5	33.9	26.6	30	41	33.2	36.9
23	27	32.8	26.2	29.3	39.7	32.7	36
24	25.5	31.9	25.8	28.7	38.5	32.2	35.2
25	24	31	25.4	28.1	37.5	31.8	34.5
26	22.5	30.2	25.1	27.5	36.5	31.4	33.9
27	21	29.5	24.8	27.1	35.6	31.1	33.3
28	19.5	28.8	24.6	26.6	34.8	30.7	32.7
29	18	28.2	24.3	26.2	34.1	30.4	32.2
30	16.5	27.7	24.1	25.9	33.5	30.2	31.8
31	15	27.2	23.9	25.5	32.9	29.9	31.4
32	13.5	26.8	23.8	25.2	32.4	29.7	31
33	12	26.5	23.6	25	32	29.5	30.7
34	10.5	26.2	23.5	24.8	31.6	29.3	30.5
35	9	25.9	23.4	24.6	31.3	29.2	30.2
36	7.5	25.7	23.3	24.4	31	29.1	30

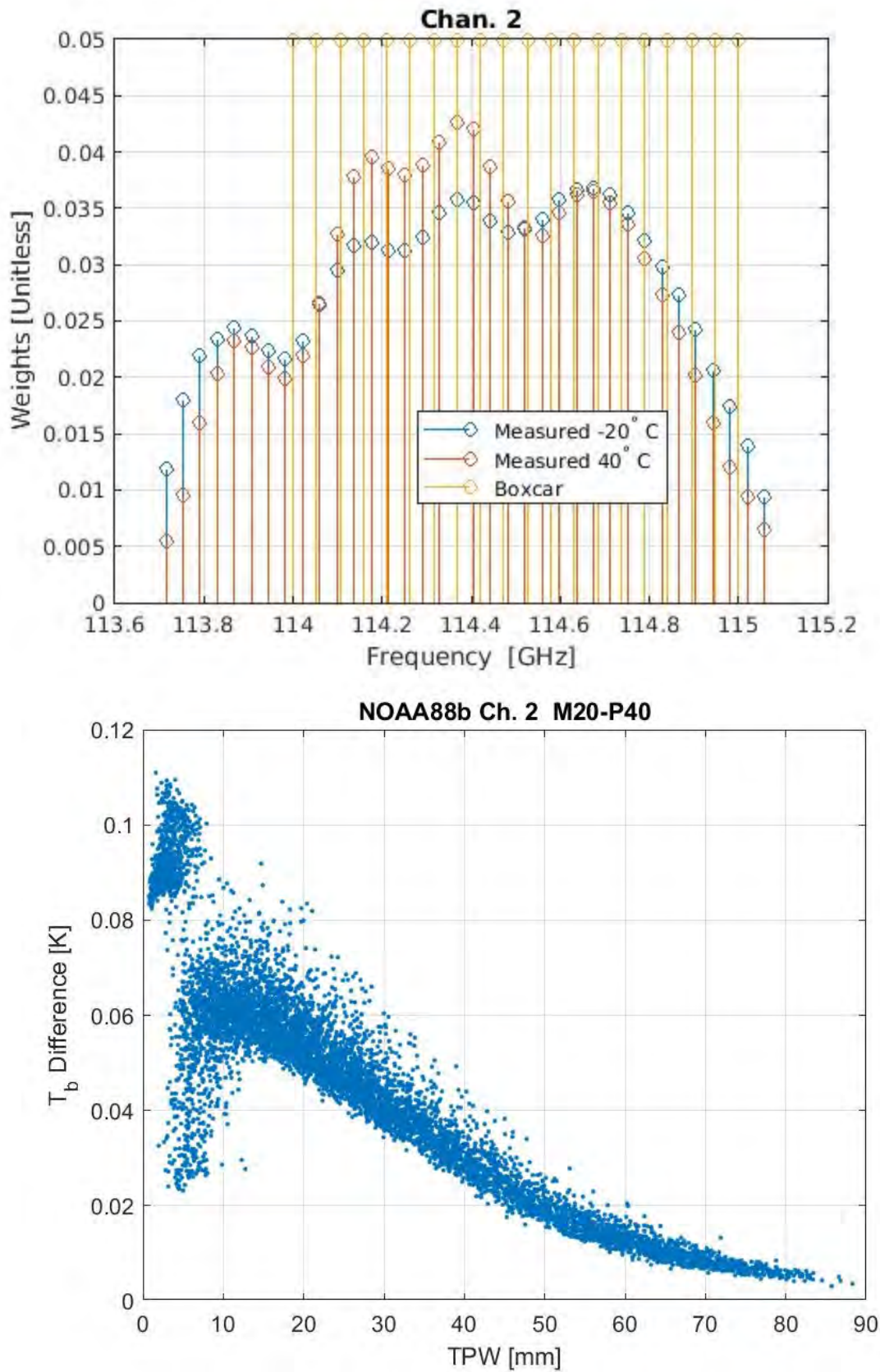
37	6	25.5	23.2	24.3	30.8	29	29.9
38	4.5	25.3	23.1	24.2	30.6	28.9	29.8
39	3	25.2	23.1	24.1	30.5	28.8	29.7
40	1.5	25.2	23.1	24.1	30.5	28.8	29.6
41	0	25.2	23	24.1	30.4	28.8	29.6

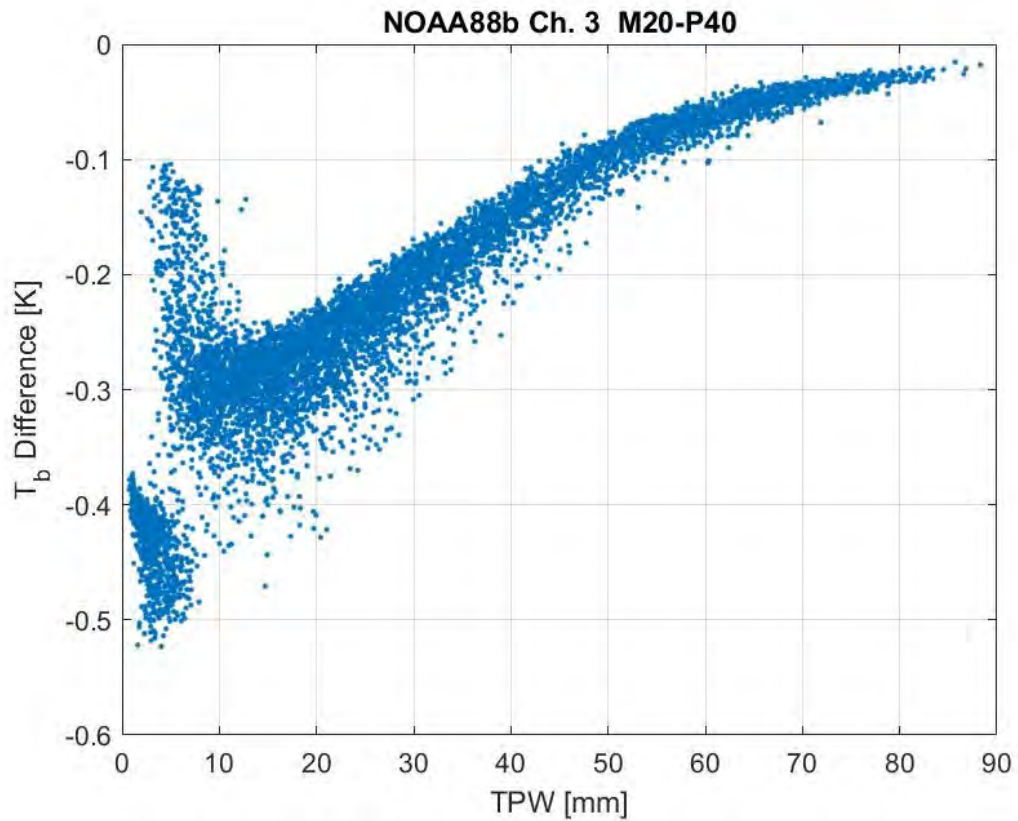
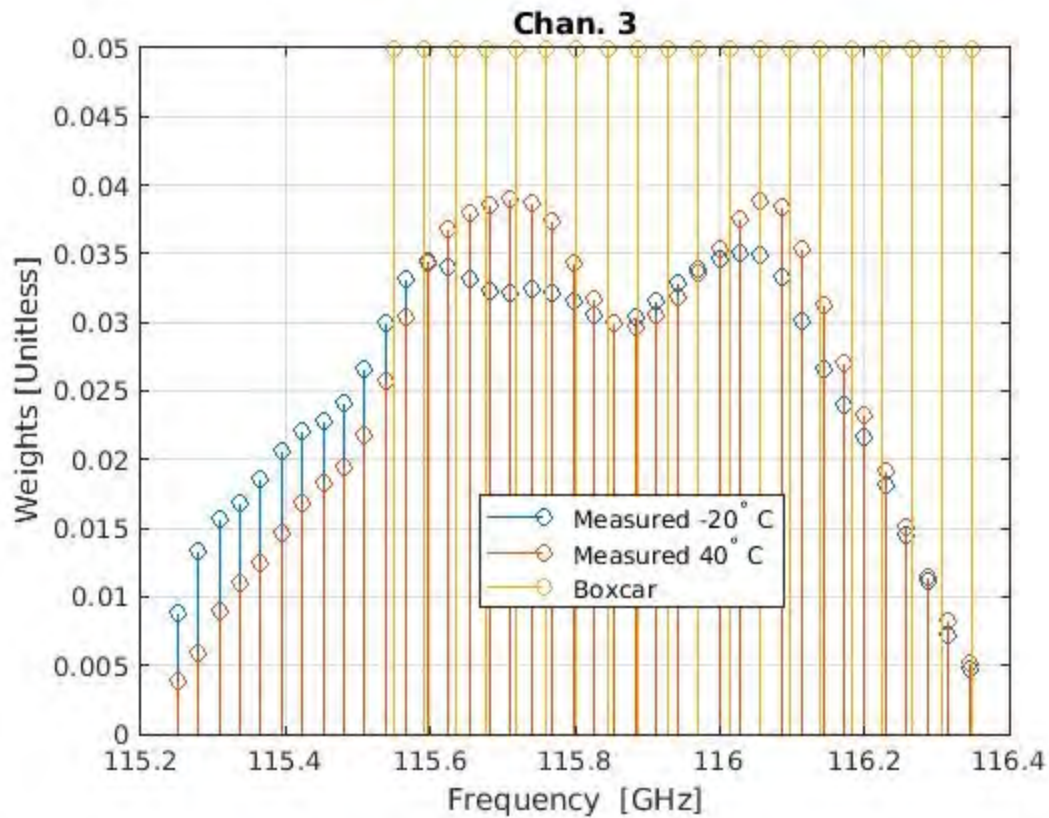
BP #	Scan Angle (Deg.)	G-Band 1.5° FWHM			205 GHz 1.4° FWHM		
		Cross Track (km)	Down Track (km)	Geometric Mean (km)	Cross Track (km)	Down Track (km)	Geometric Mean (km)
1	60	125.6	34.1	65.4	121.1	31.8	62
2	58.5	105.4	31.8	57.9	101.6	29.7	54.9
3	57	90.6	29.9	52.1	87.3	27.9	49.4
4	55.5	79.3	28.3	47.4	76.4	26.4	44.9
5	54	70.4	26.9	43.5	67.8	25.1	41.3
6	52.5	63.2	25.7	40.3	60.9	24	38.2
7	51	57.3	24.6	37.6	55.2	23	35.6
8	49.5	52.3	23.7	35.2	50.4	22.1	33.4
9	48	48.2	22.8	33.1	46.4	21.3	31.4
10	46.5	44.6	22	31.3	43	20.6	29.7
11	45	41.5	21.3	29.8	40	19.9	28.2
12	43.5	38.8	20.7	28.3	37.4	19.3	26.9
13	42	36.5	20.1	27.1	35.2	18.8	25.7
14	40.5	34.4	19.6	26	33.2	18.3	24.6
15	39	32.6	19.1	24.9	31.4	17.8	23.6
16	37.5	30.9	18.6	24	29.8	17.4	22.8
17	36	29.5	18.2	23.2	28.4	17	22
18	34.5	28.2	17.8	22.4	27.2	16.7	21.3
19	33	27	17.5	21.7	26	16.3	20.6
20	31.5	26	17.2	21.1	25	16	20
21	30	25	16.9	20.6	24.1	15.7	19.5
22	28.5	24.2	16.6	20	23.3	15.5	19
23	27	23.4	16.3	19.6	22.6	15.3	18.6
24	25.5	22.7	16.1	19.1	21.9	15	18.1
25	24	22.1	15.9	18.7	21.3	14.8	17.8
26	22.5	21.5	15.7	18.4	20.7	14.7	17.4
27	21	21	15.5	18	20.2	14.5	17.1
28	19.5	20.5	15.4	17.8	19.8	14.3	16.8
29	18	20.1	15.2	17.5	19.4	14.2	16.6
30	16.5	19.7	15.1	17.2	19	14.1	16.4
31	15	19.4	15	17	18.7	14	16.2

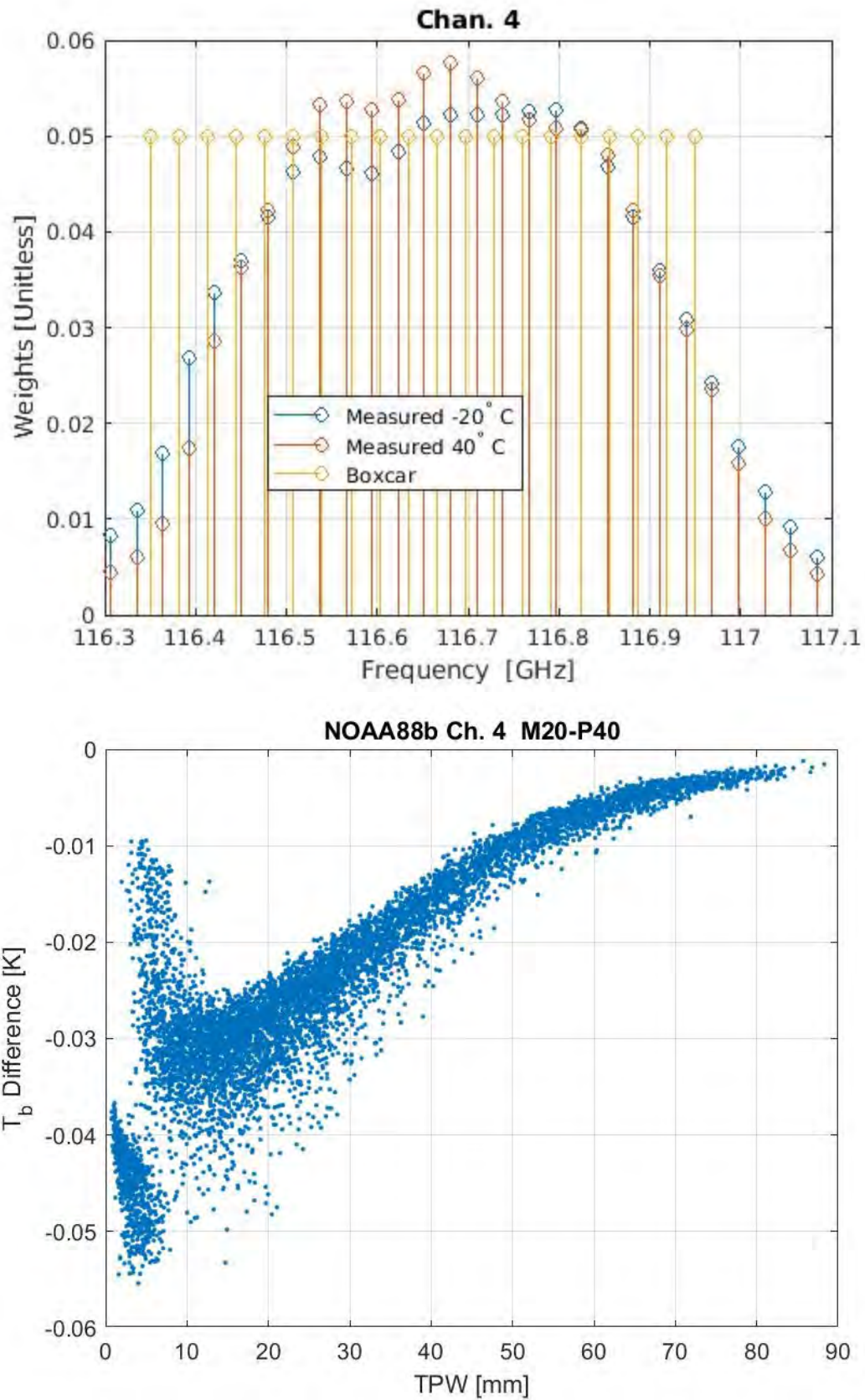
32	13.5	19.1	14.8	16.8	18.4	13.9	16
33	12	18.9	14.8	16.7	18.2	13.8	15.8
34	10.5	18.6	14.7	16.5	18	13.7	15.7
35	9	18.4	14.6	16.4	17.8	13.6	15.6
36	7.5	18.3	14.5	16.3	17.6	13.6	15.5
37	6	18.2	14.5	16.2	17.5	13.5	15.4
38	4.5	18.1	14.4	16.2	17.4	13.5	15.3
39	3	18	14.4	16.1	17.3	13.5	15.3
40	1.5	17.9	14.4	16.1	17.3	13.4	15.2
41	0	17.9	14.4	16.1	17.3	13.4	15.2

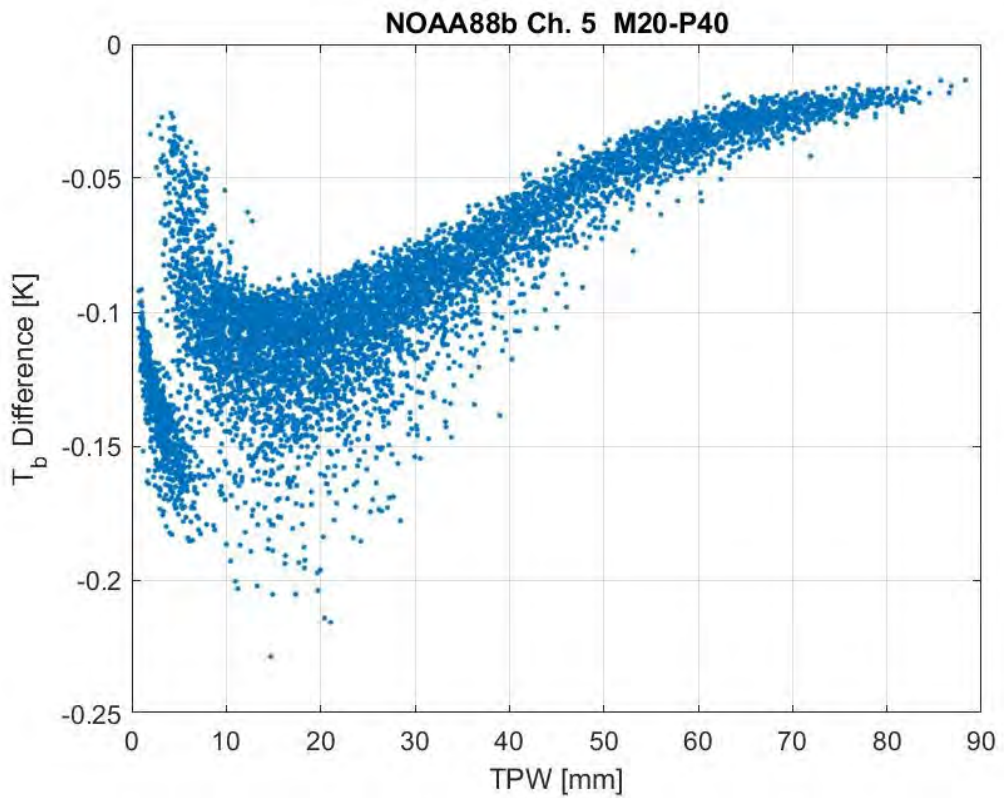
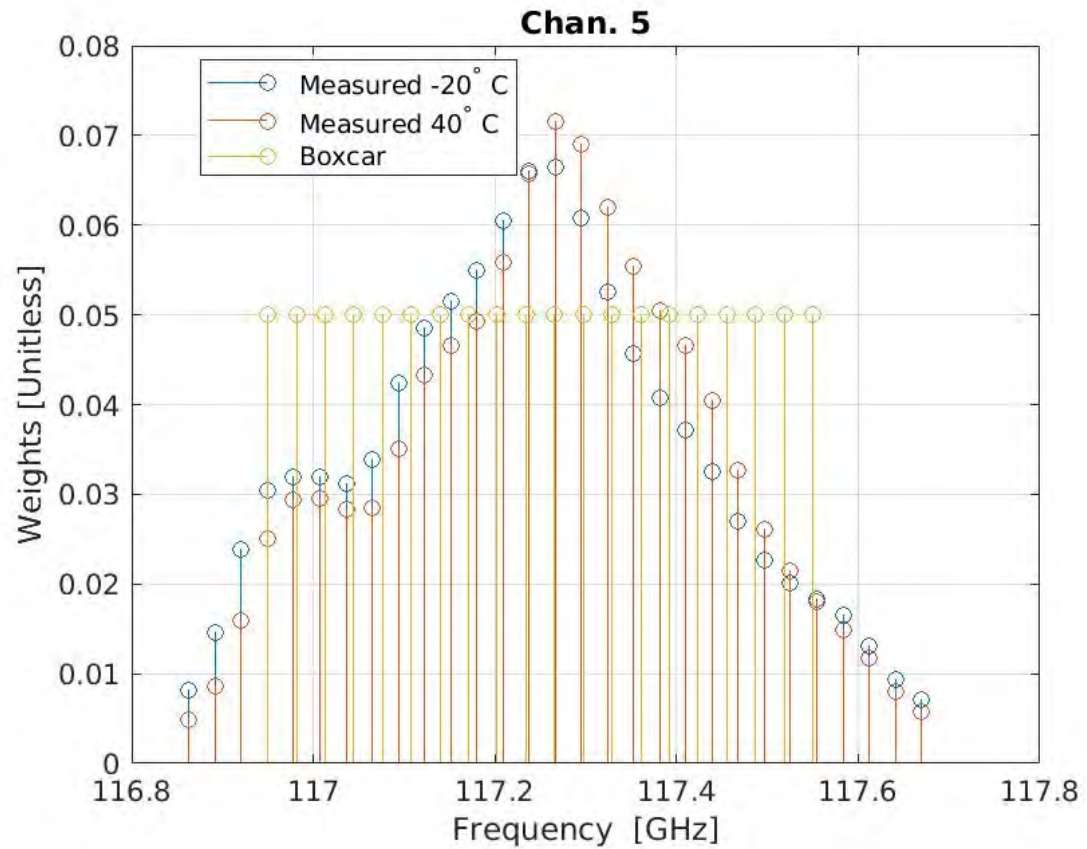
Appendix D: SRF Thermal Sensitivity Results

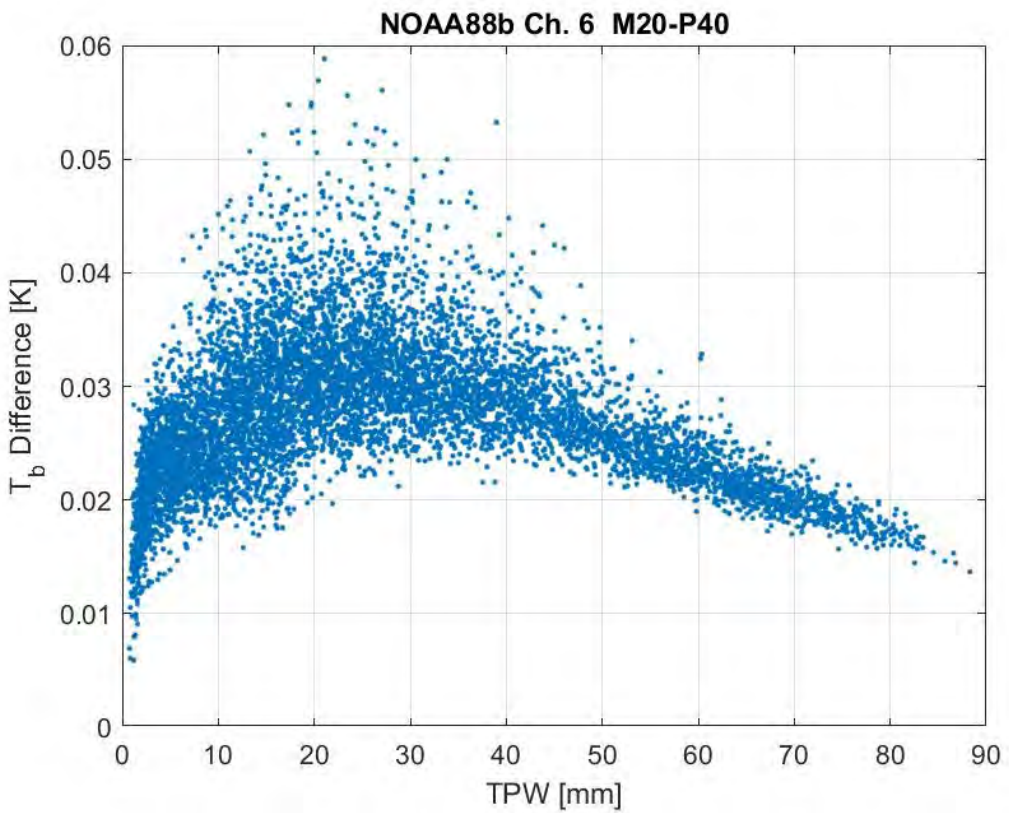
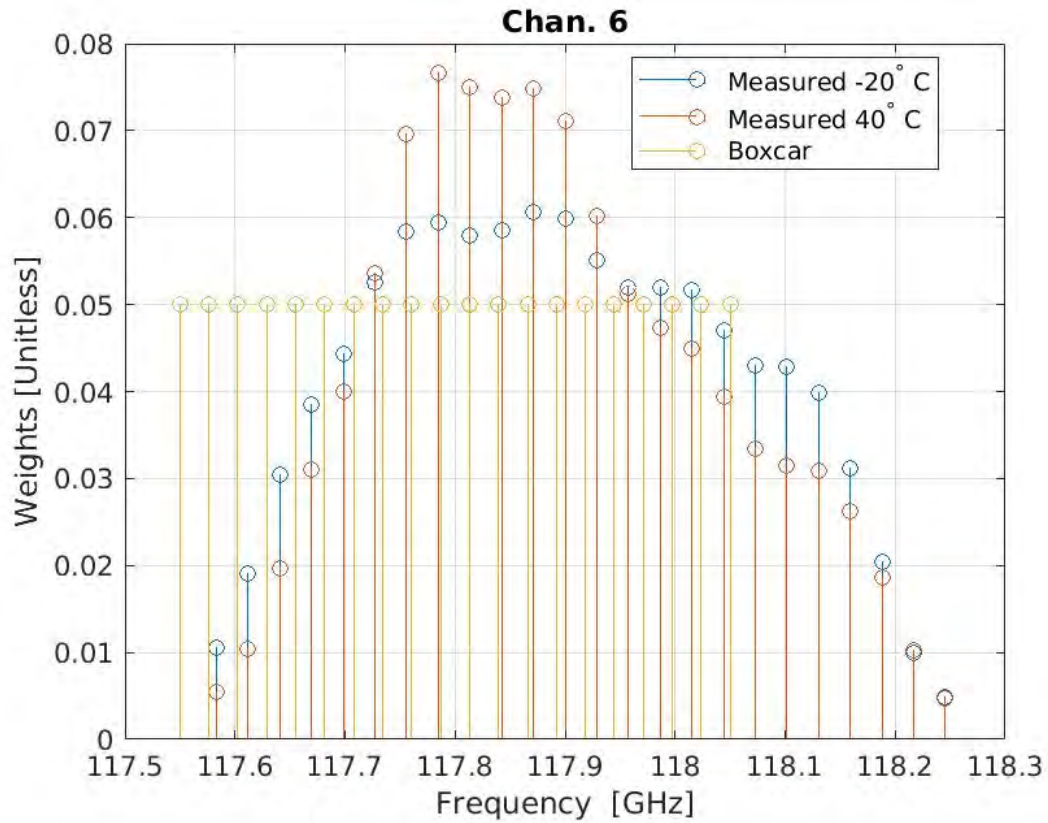


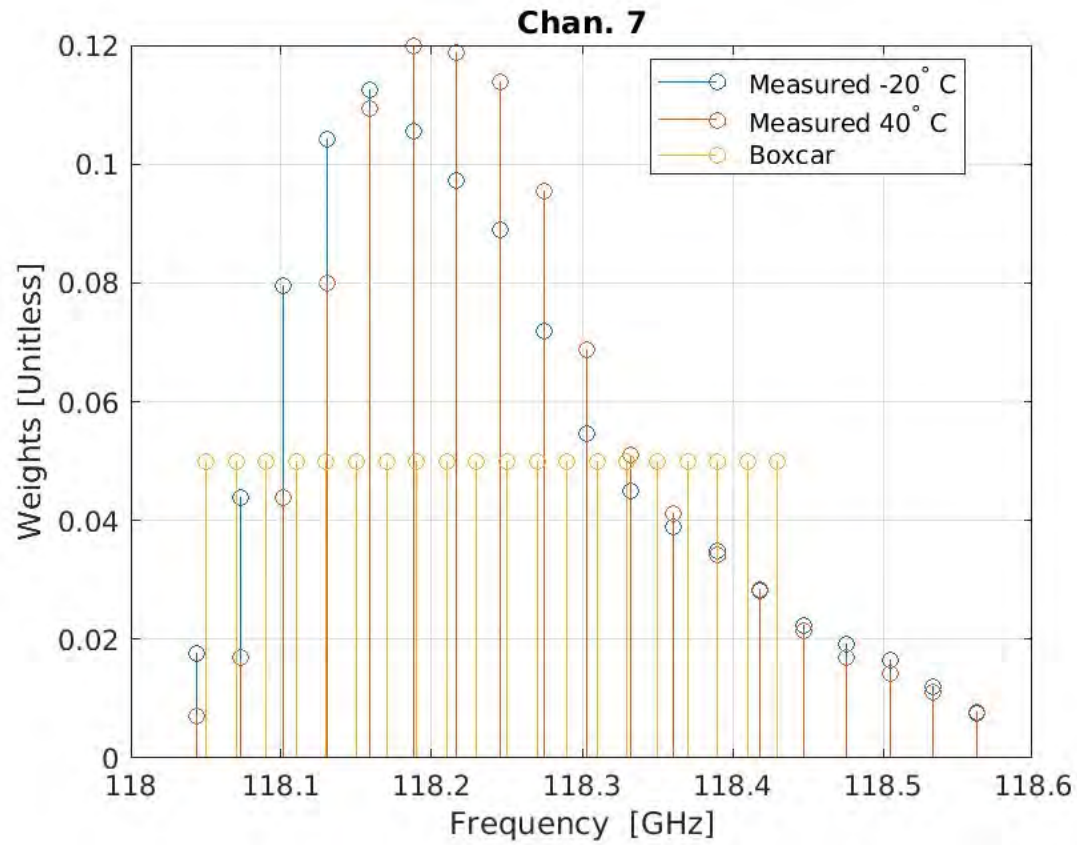


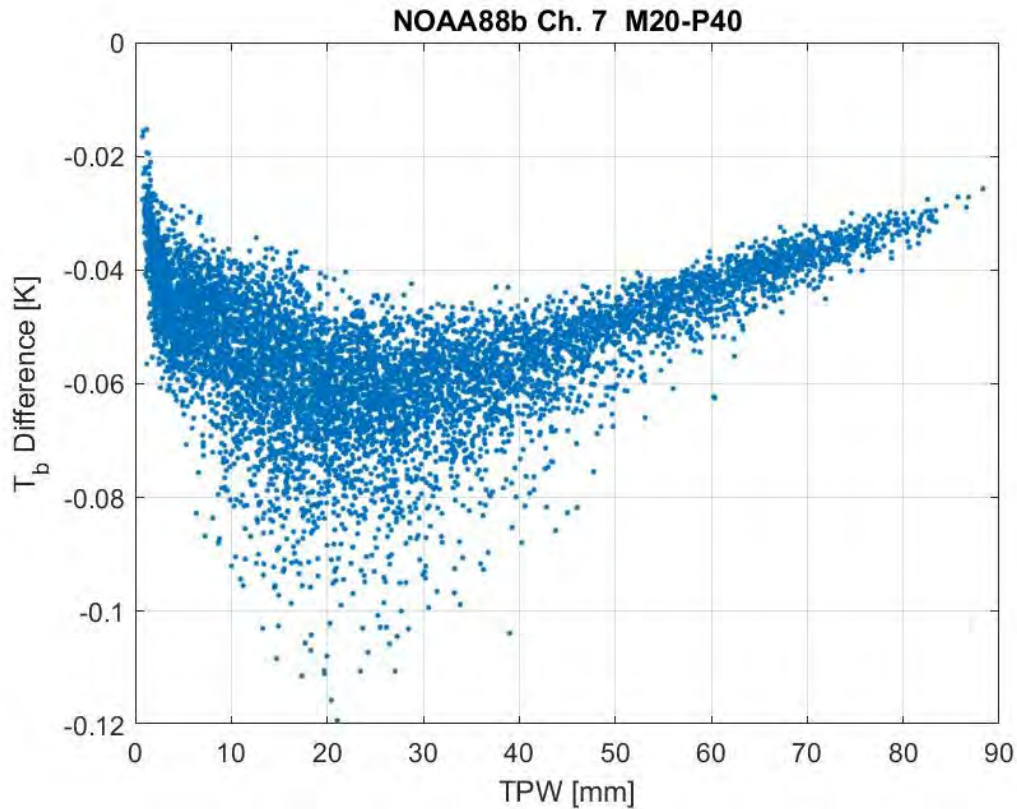


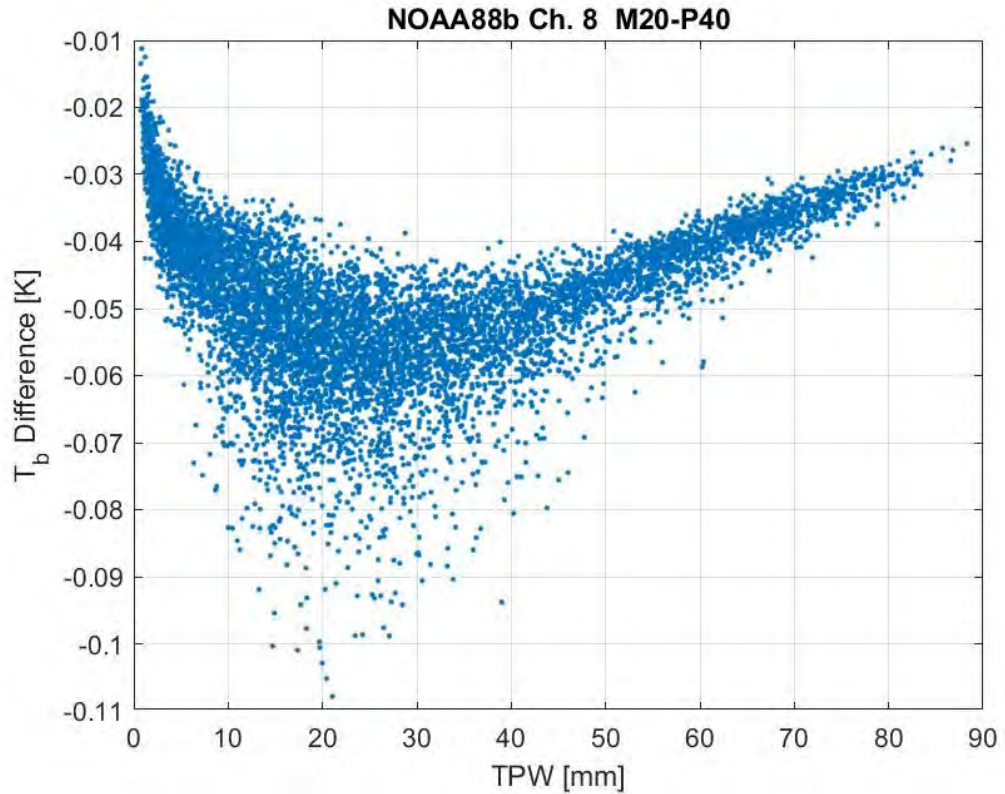
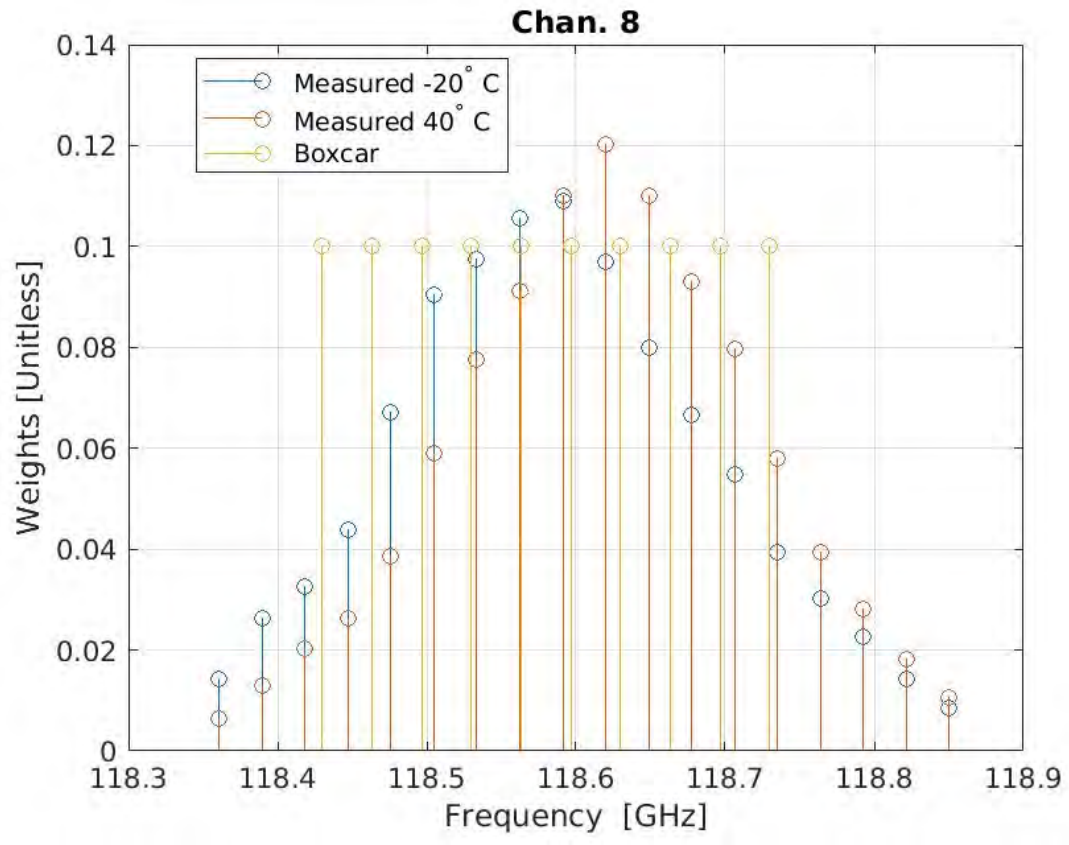


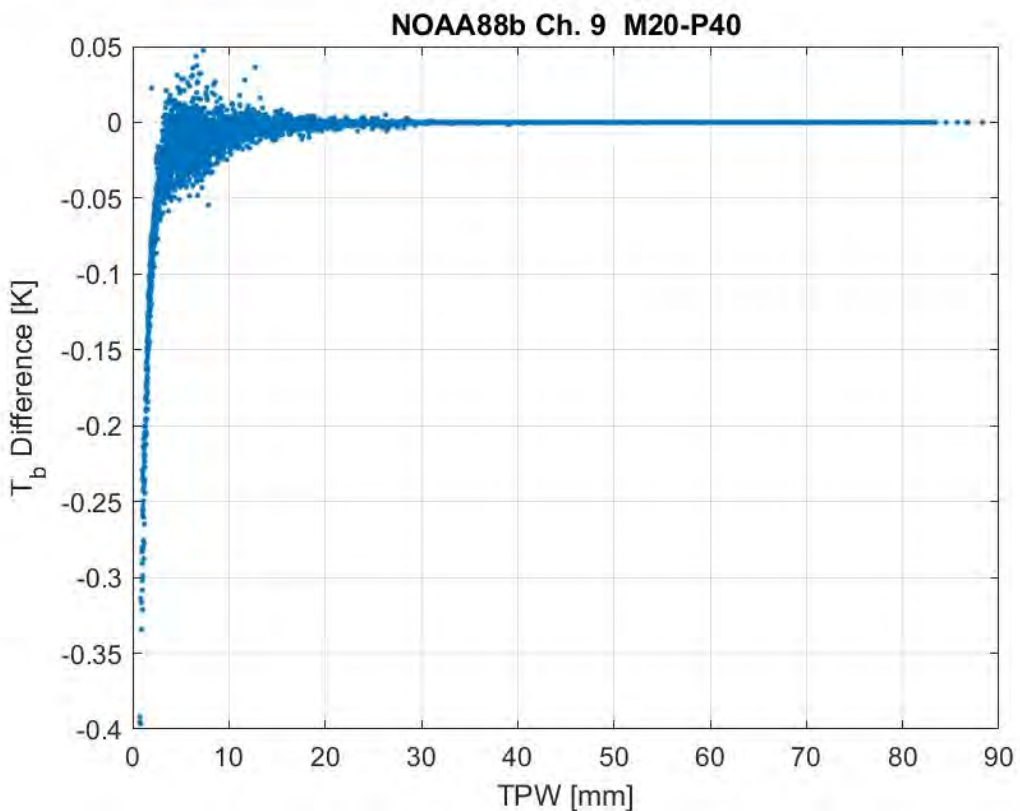
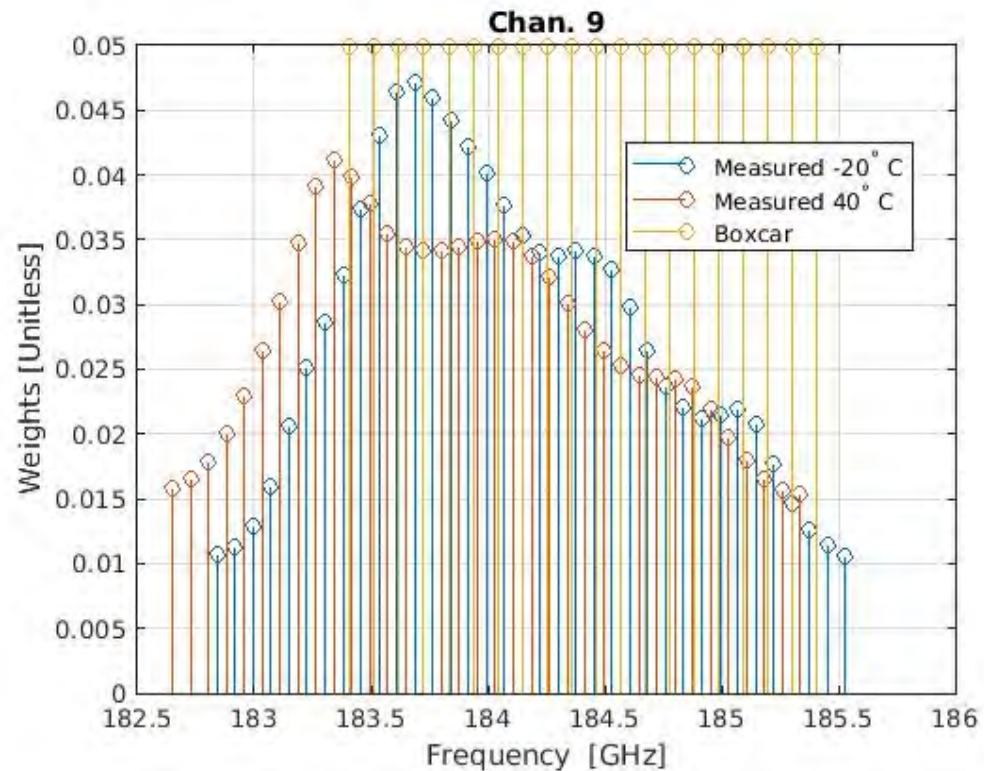


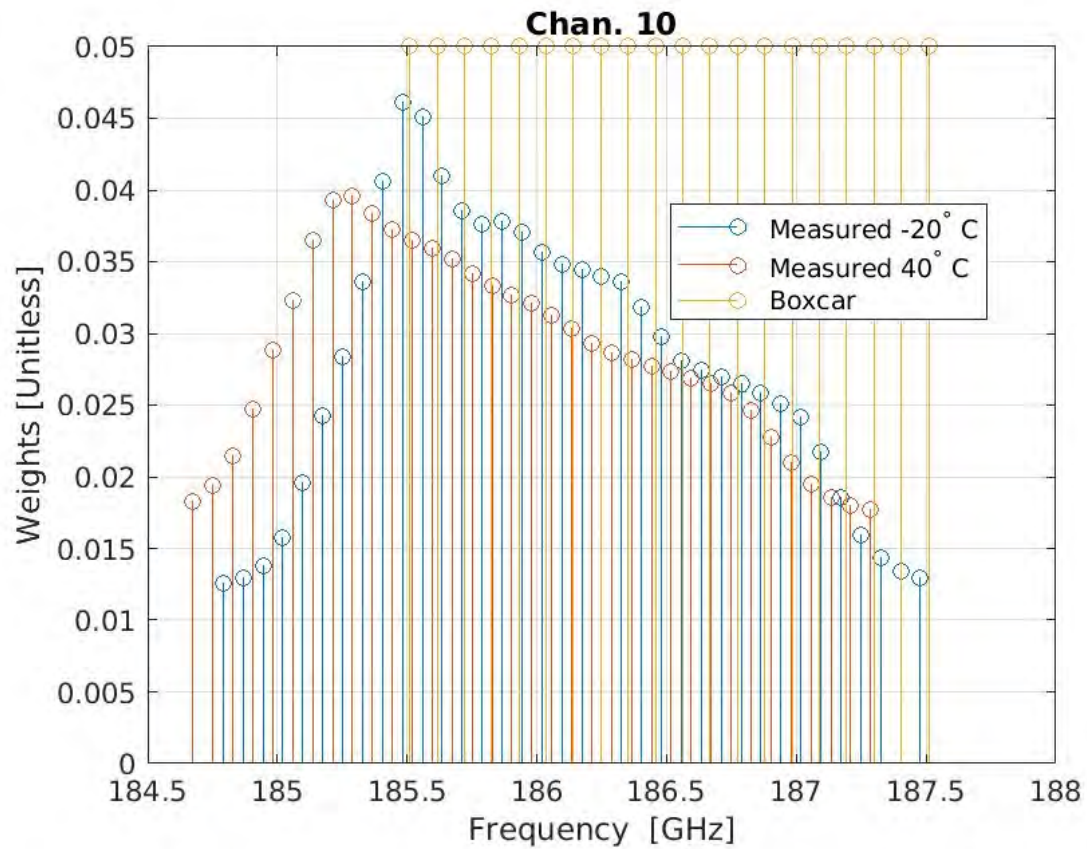


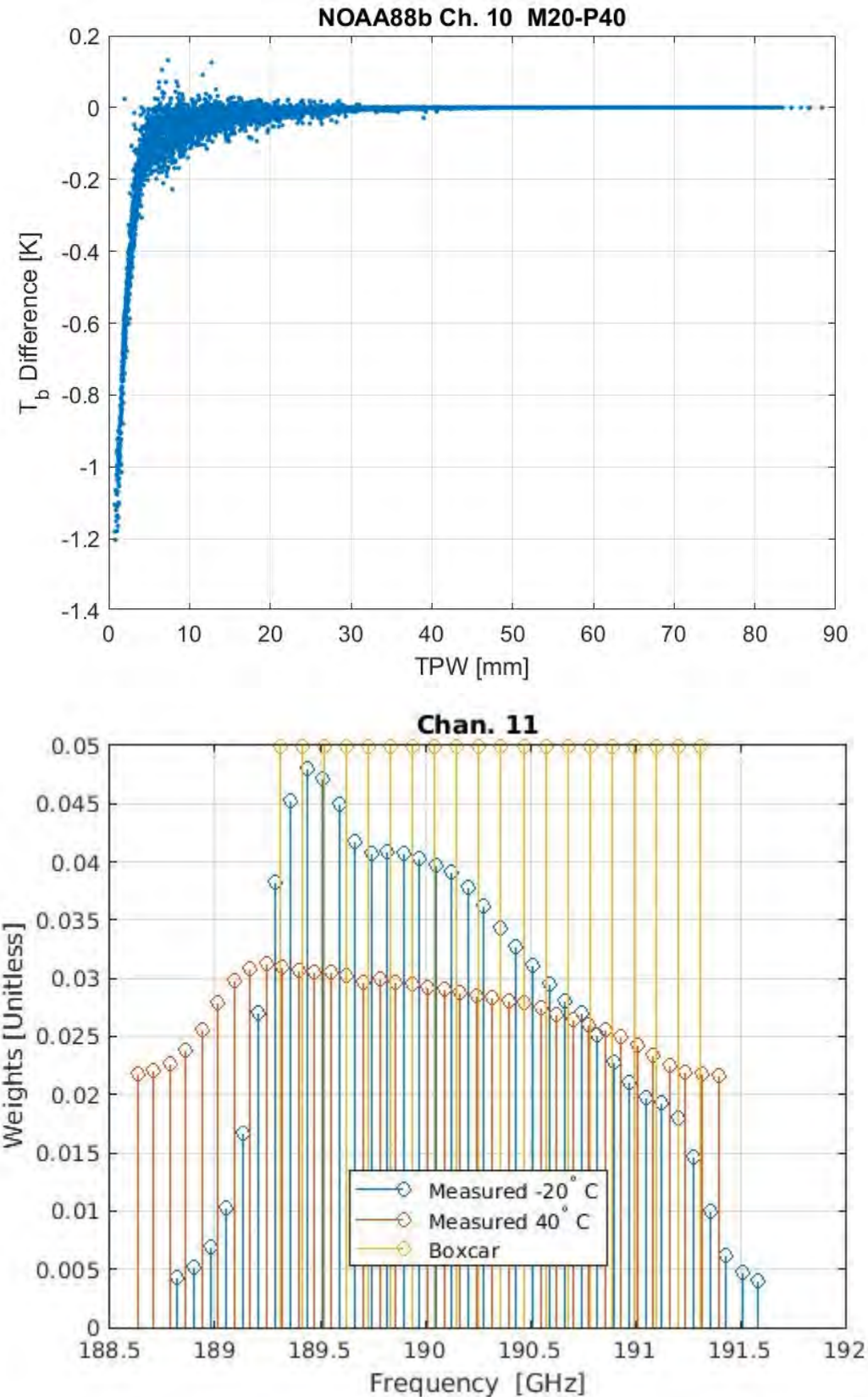


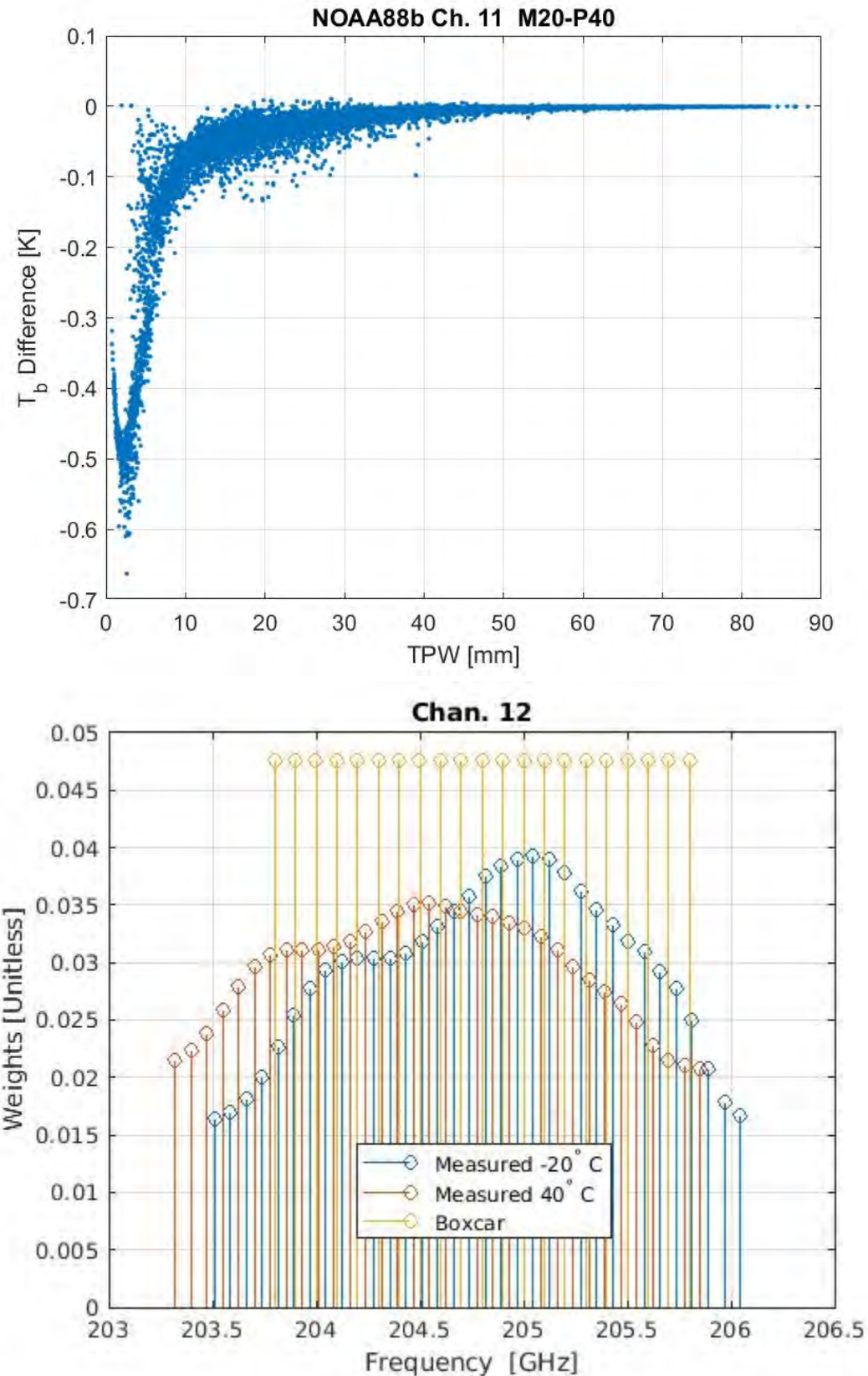


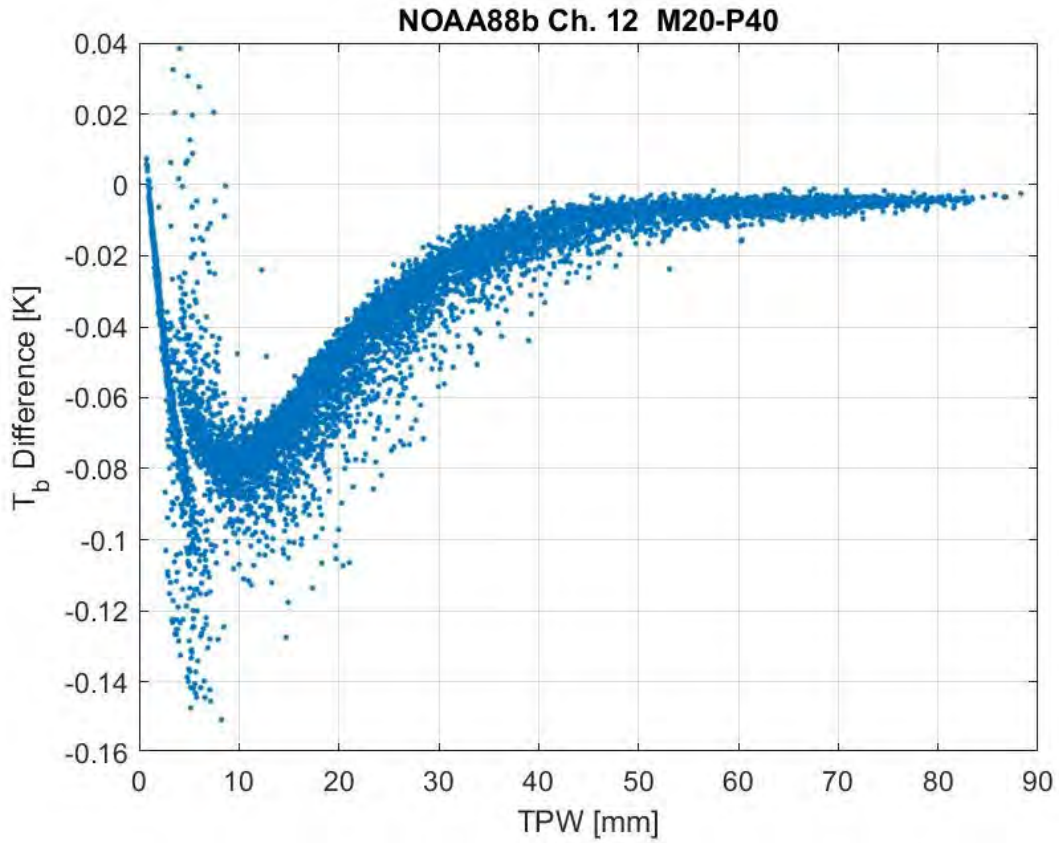




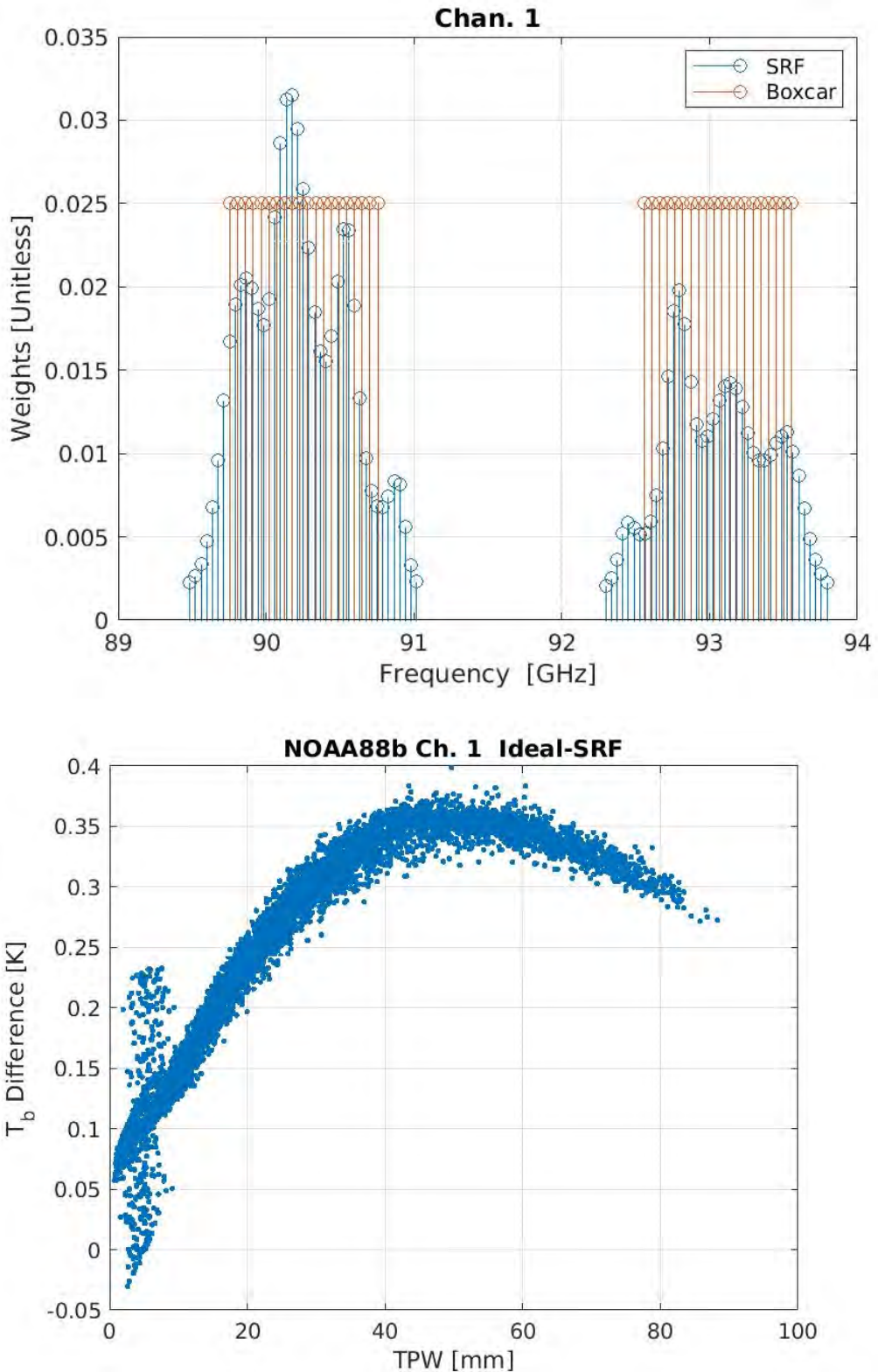


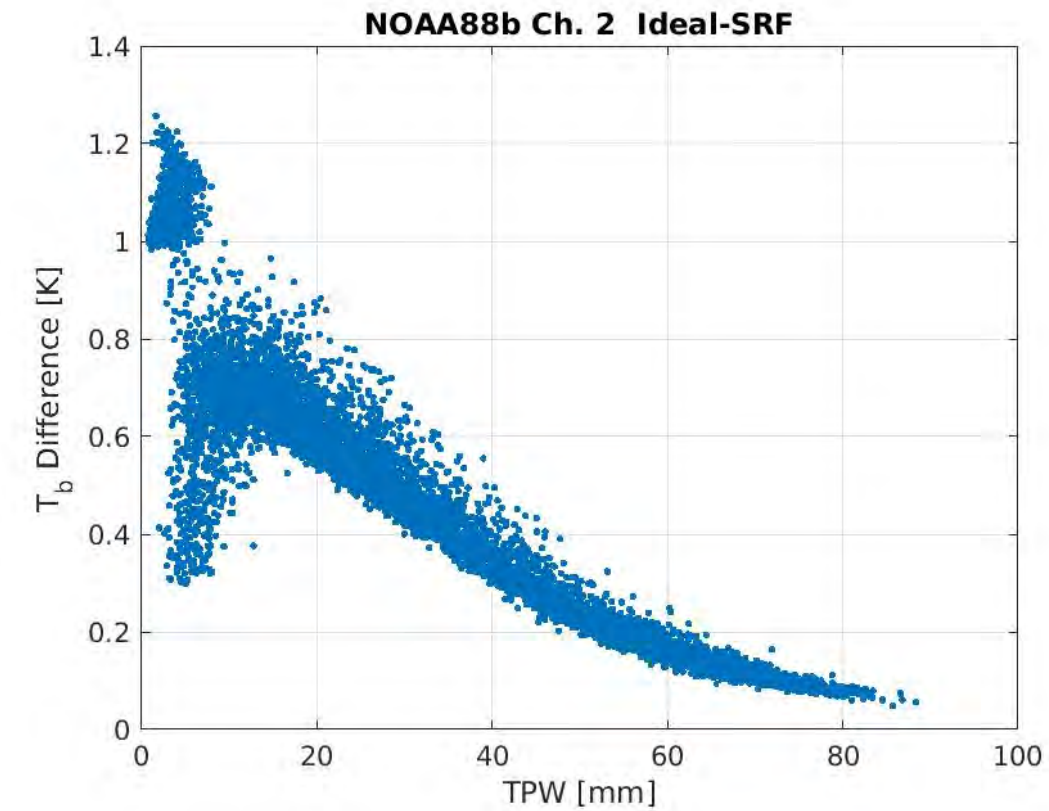
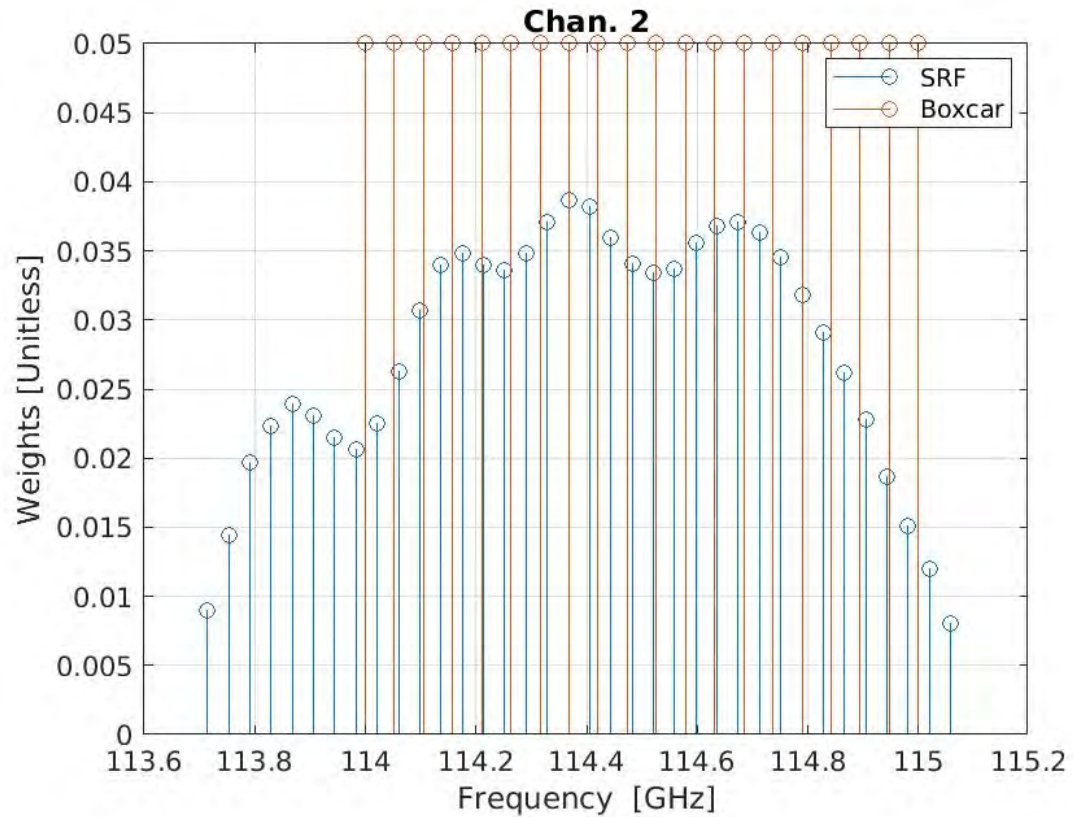


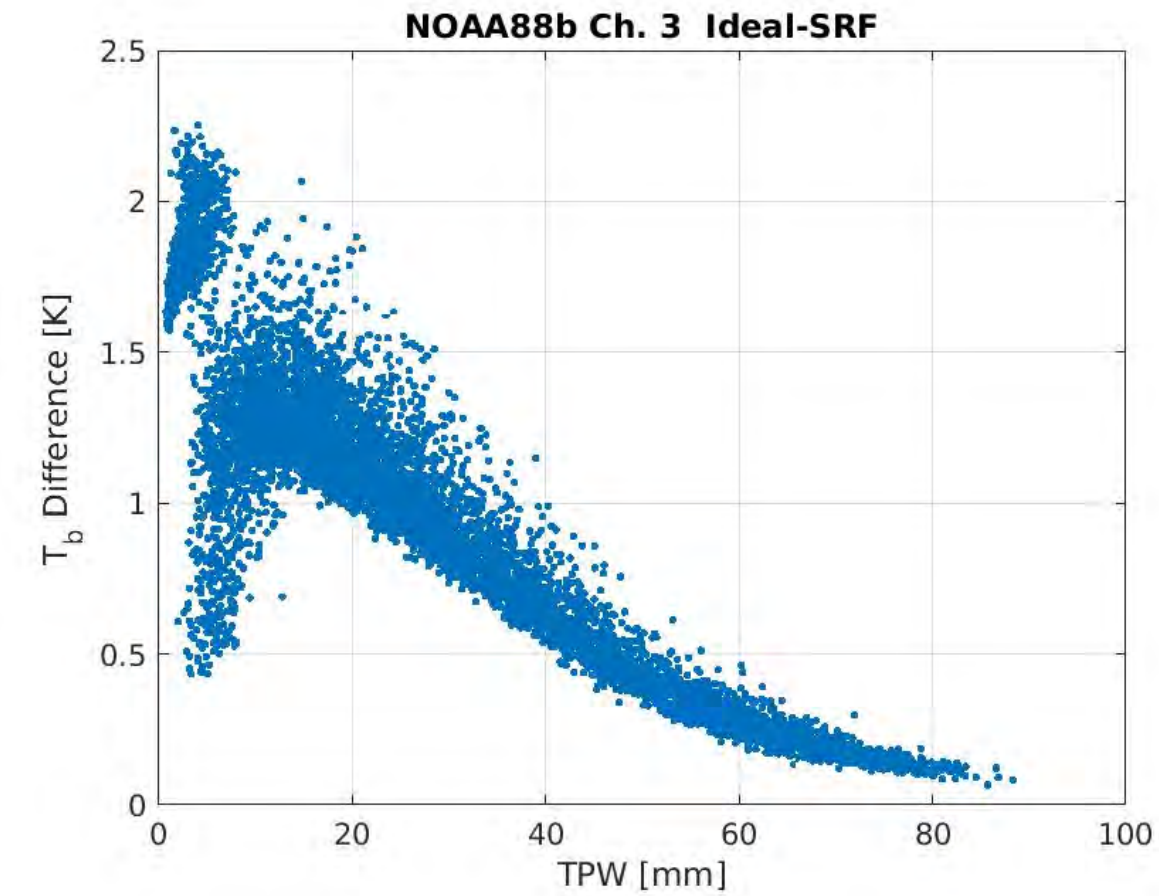
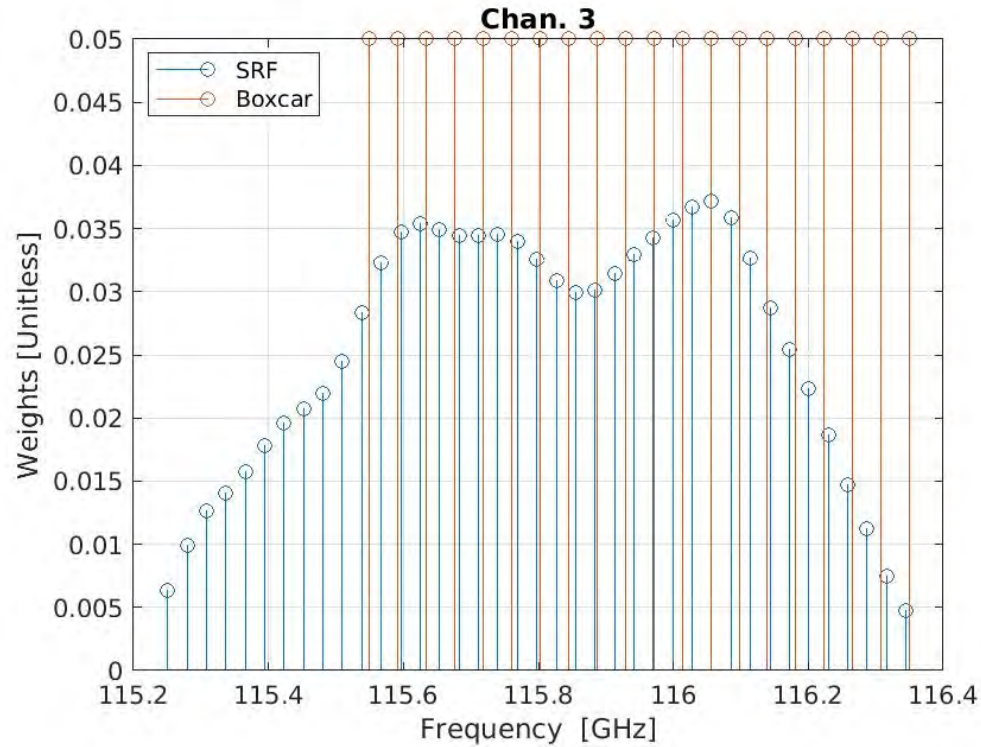


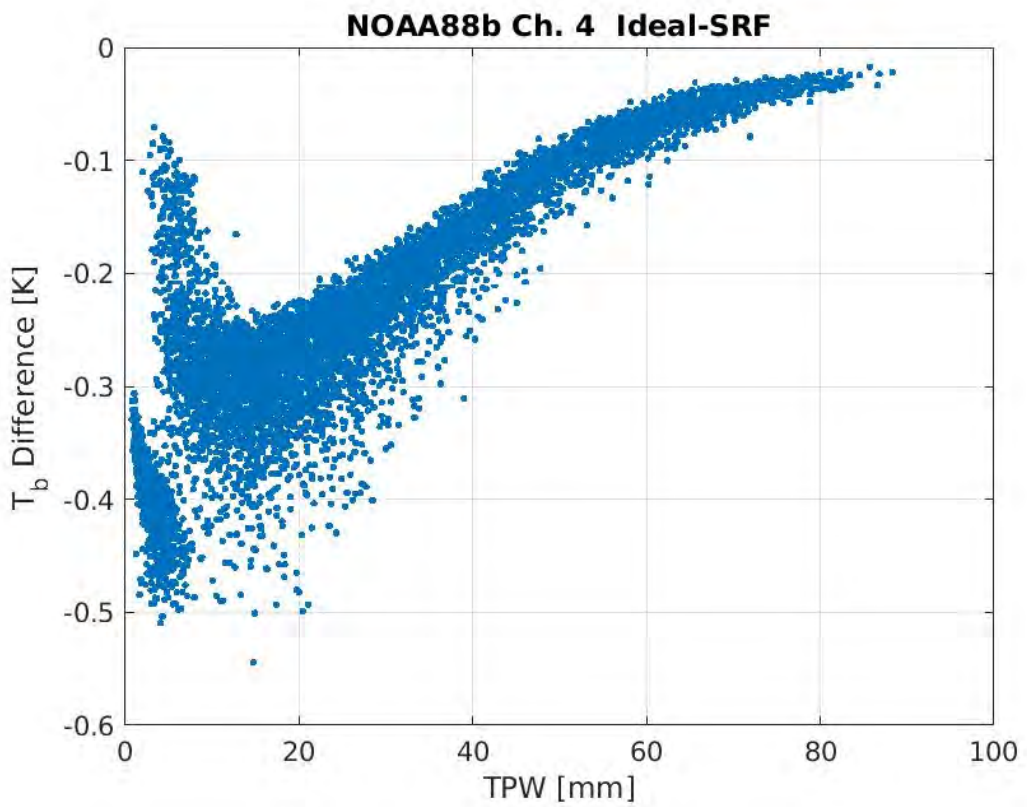
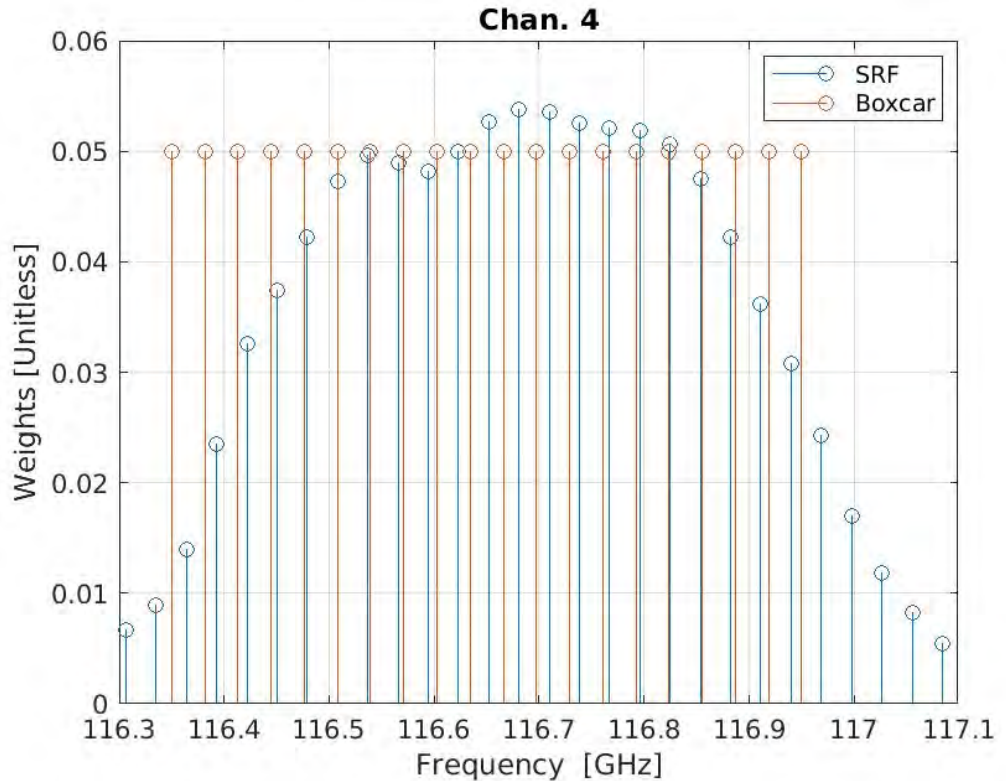


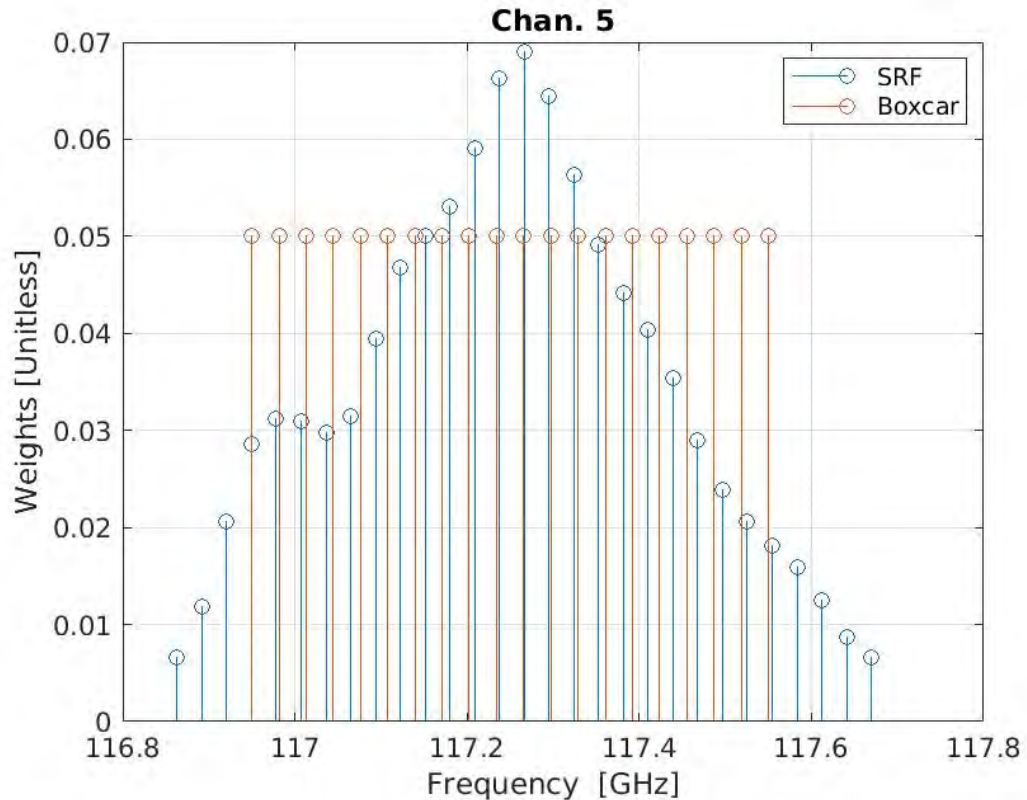
Appendix E: SRF Ideal vs. Measured Results

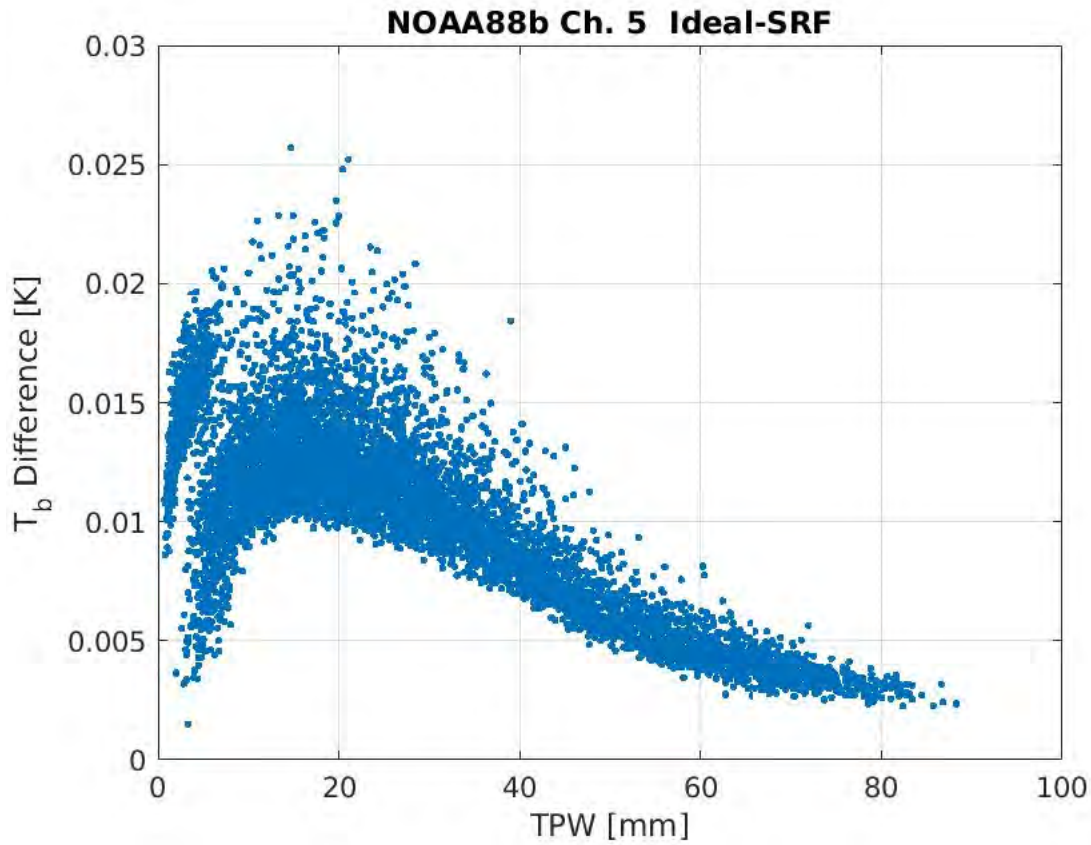


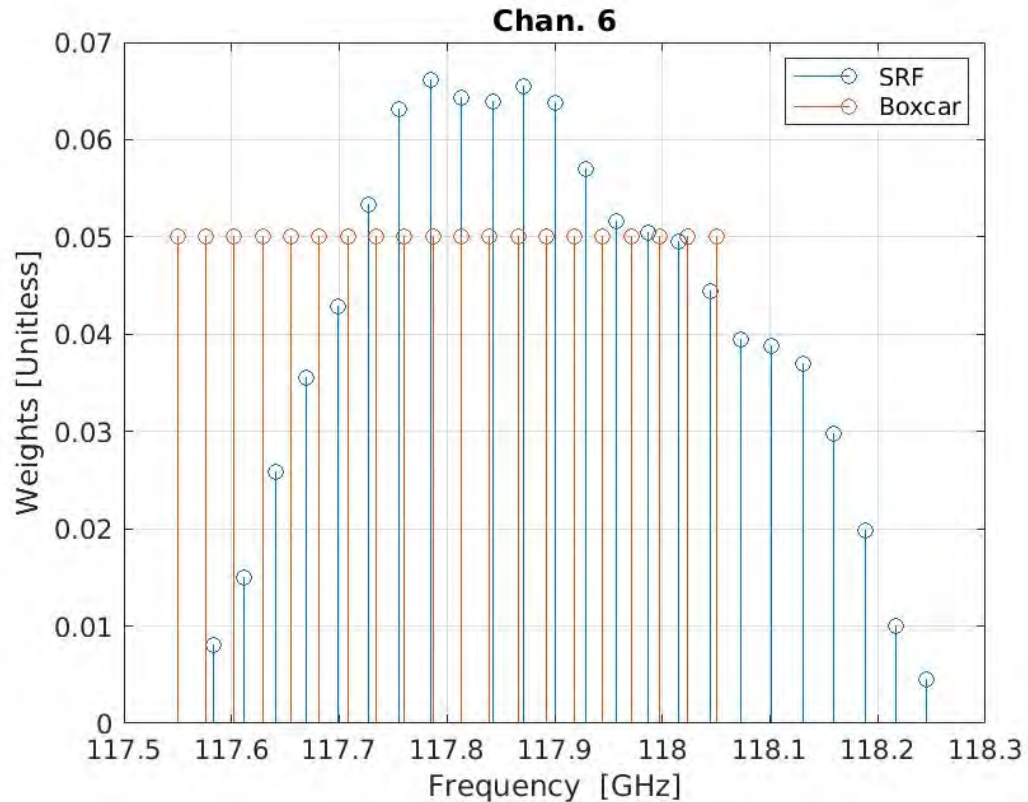


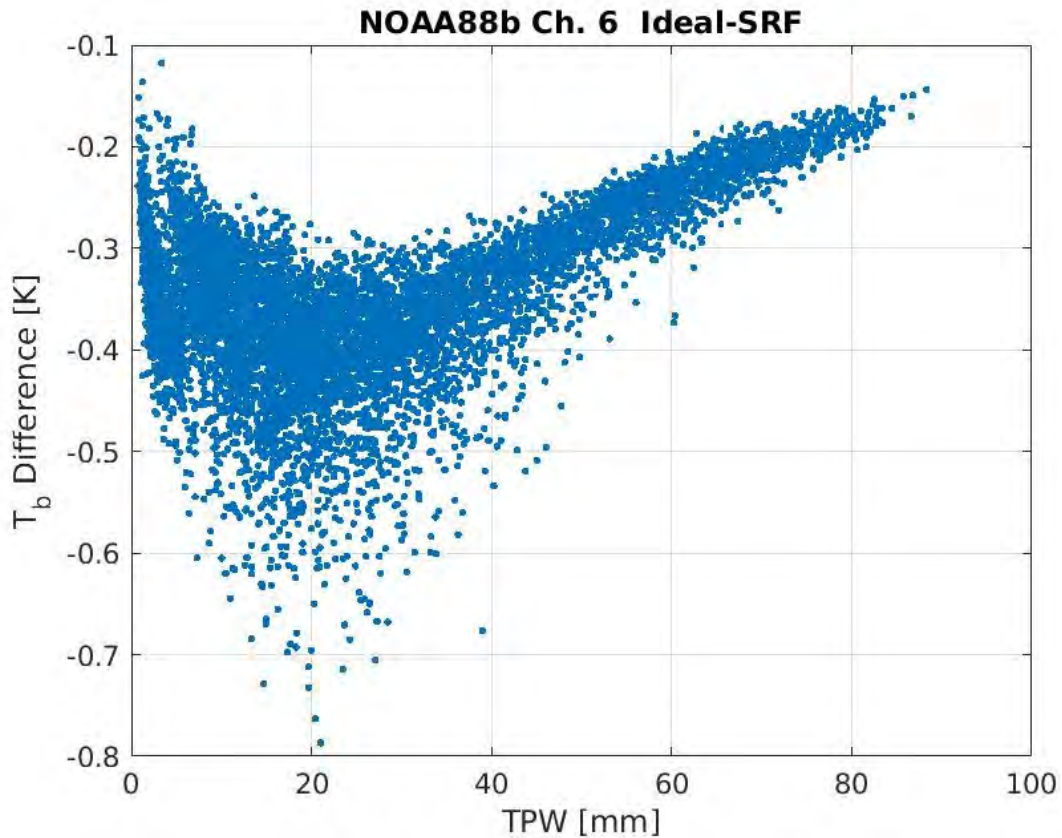


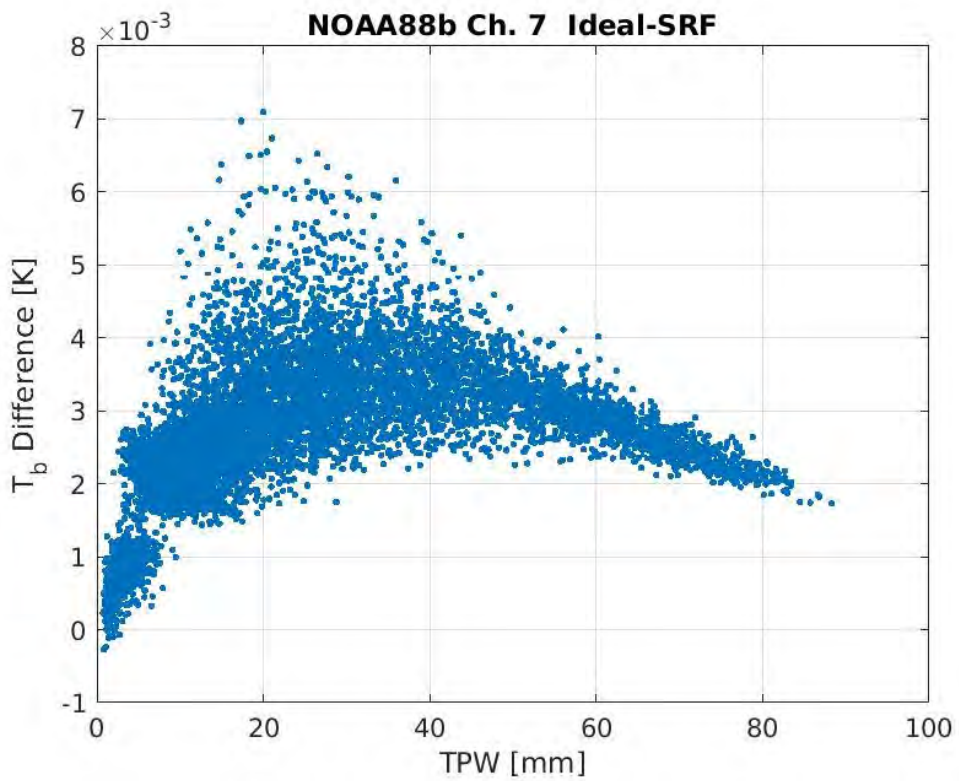
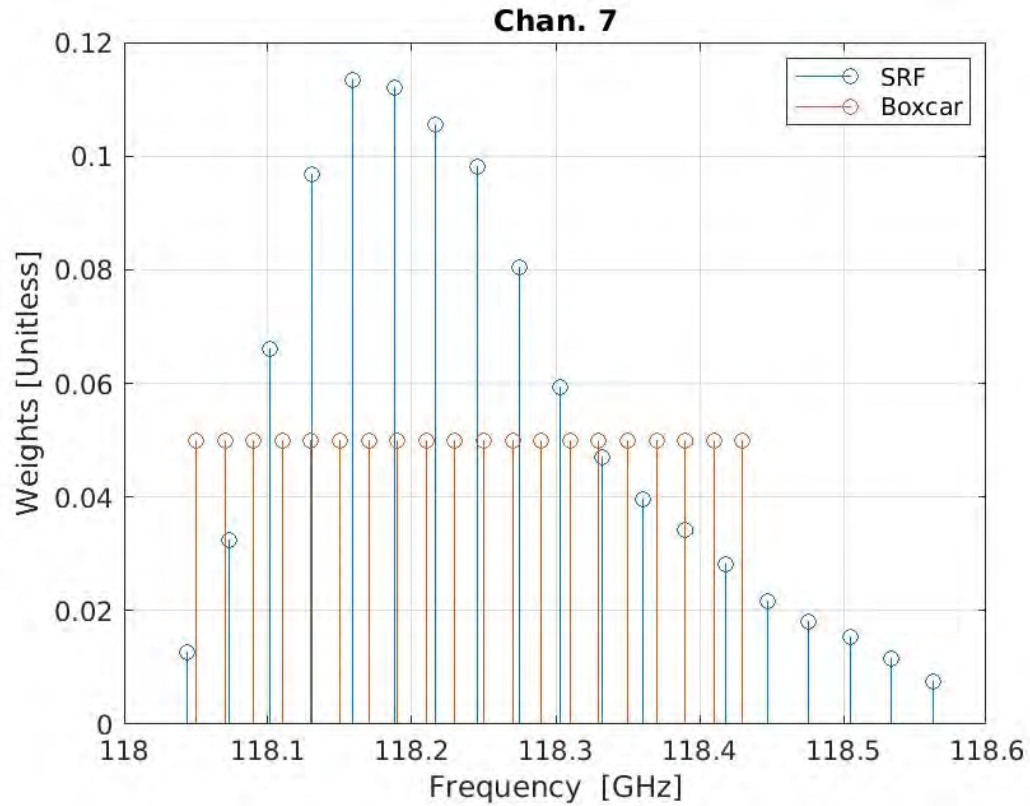


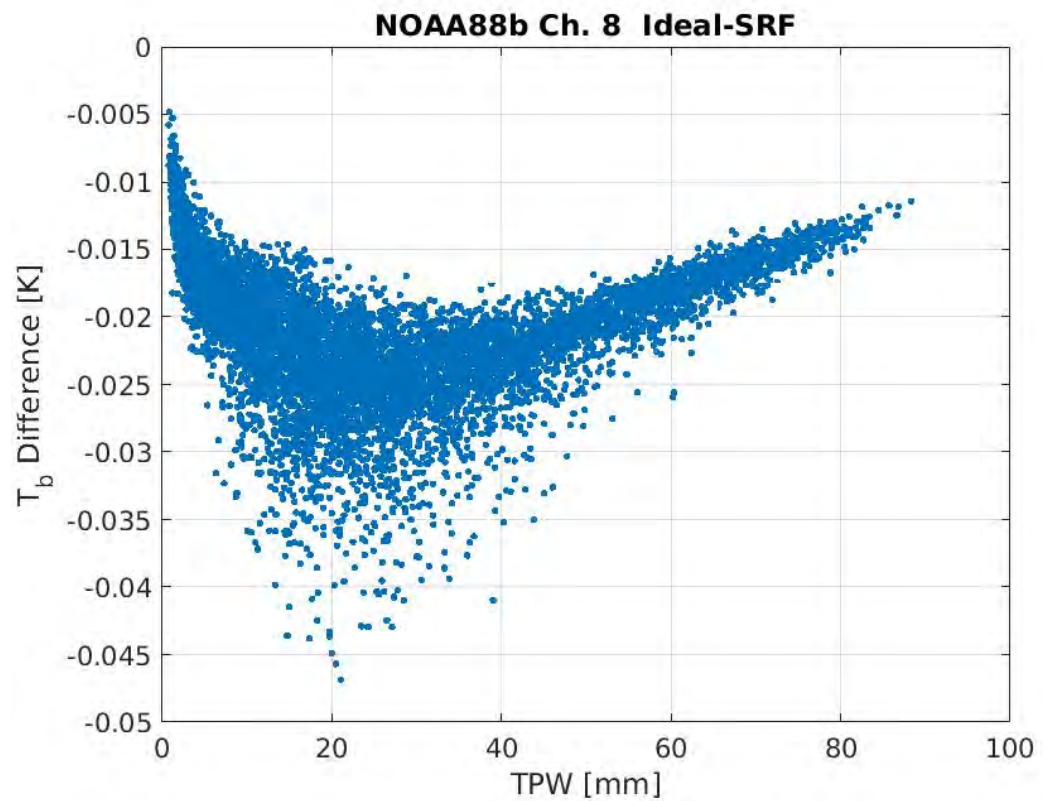
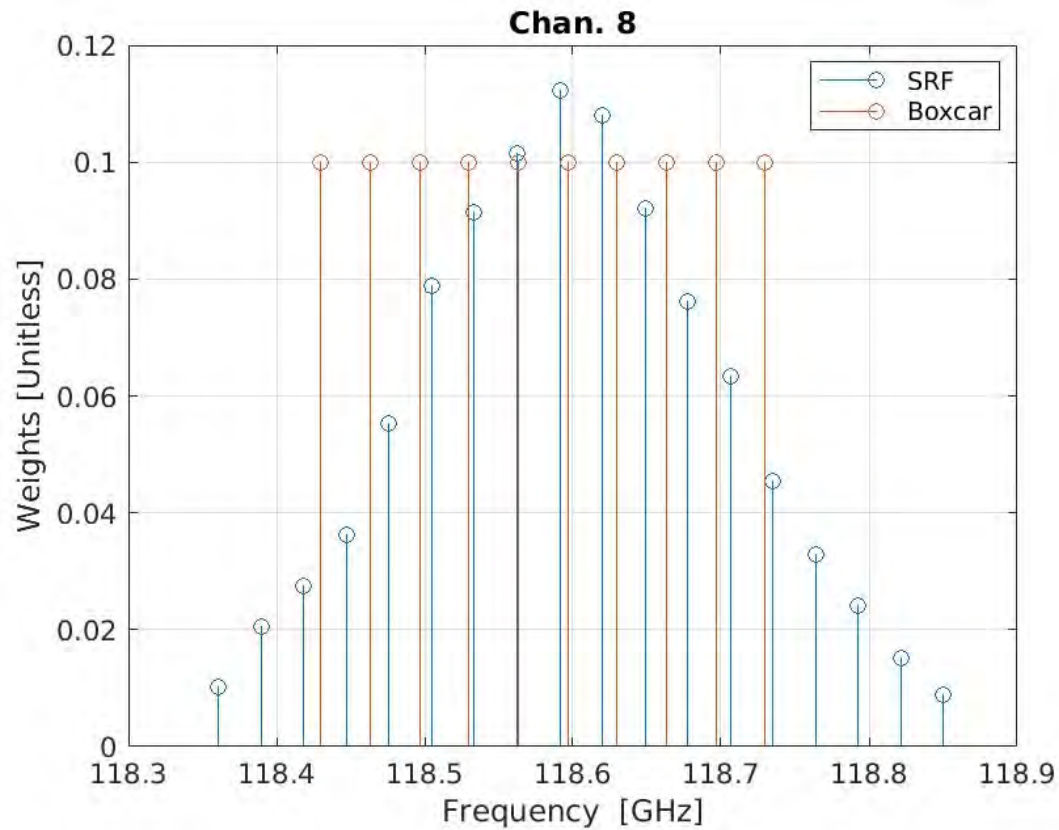


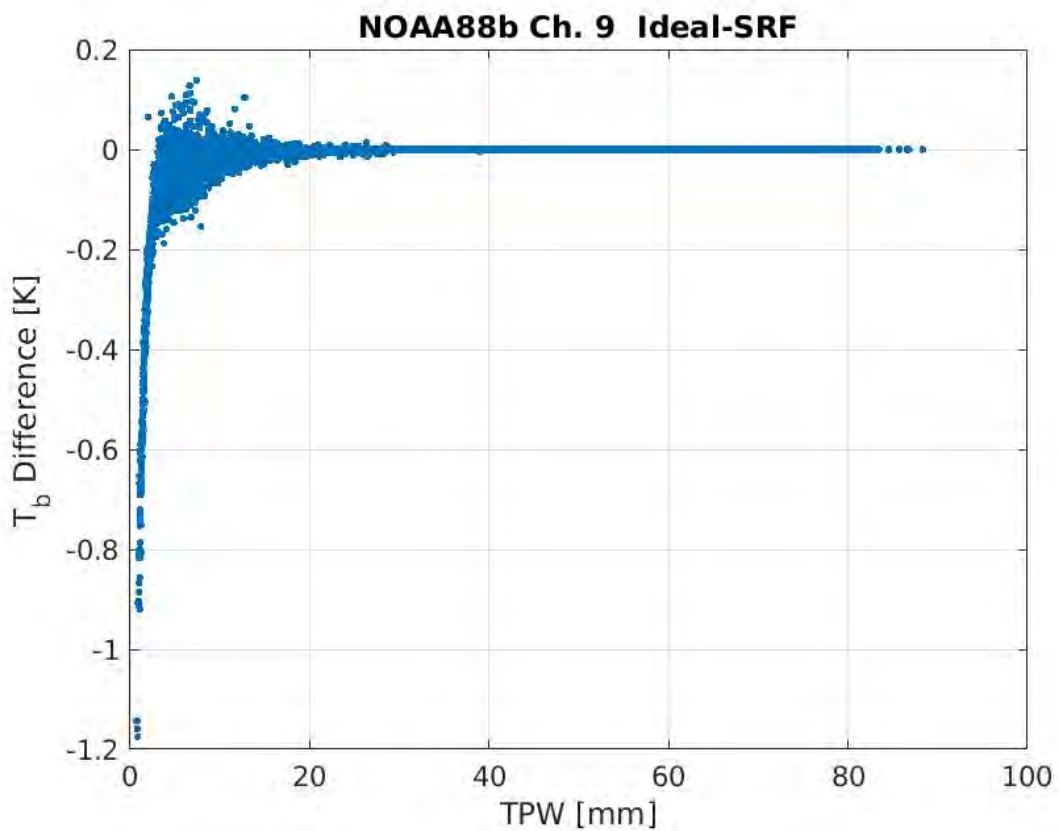
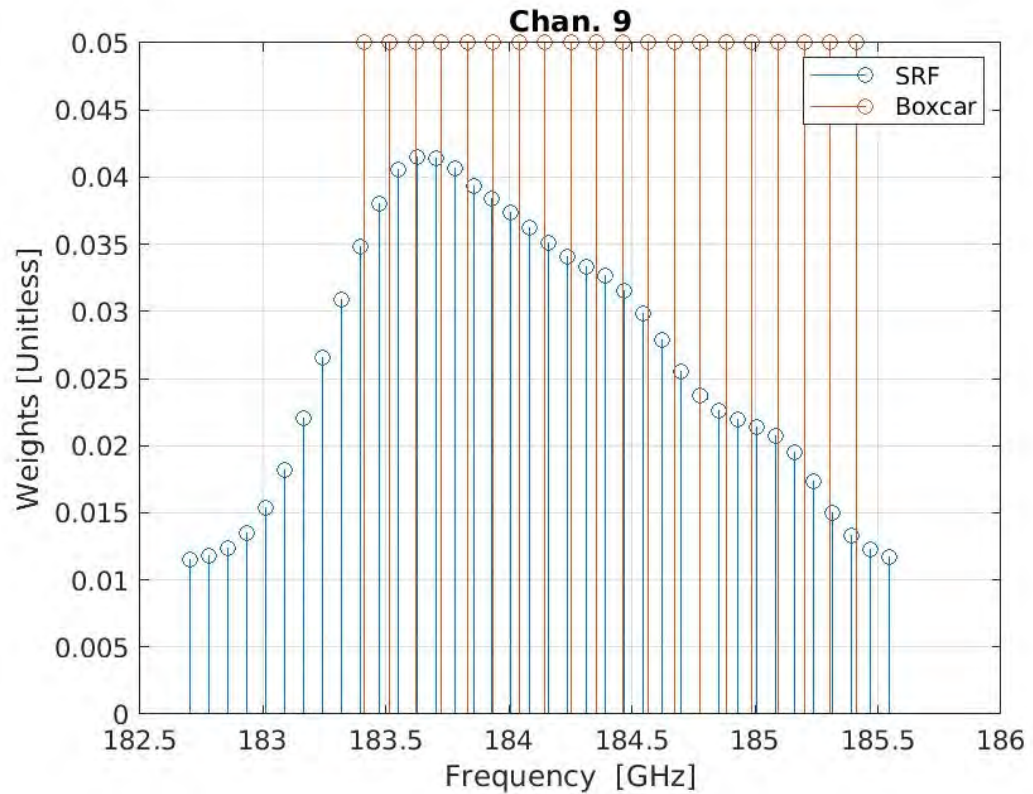


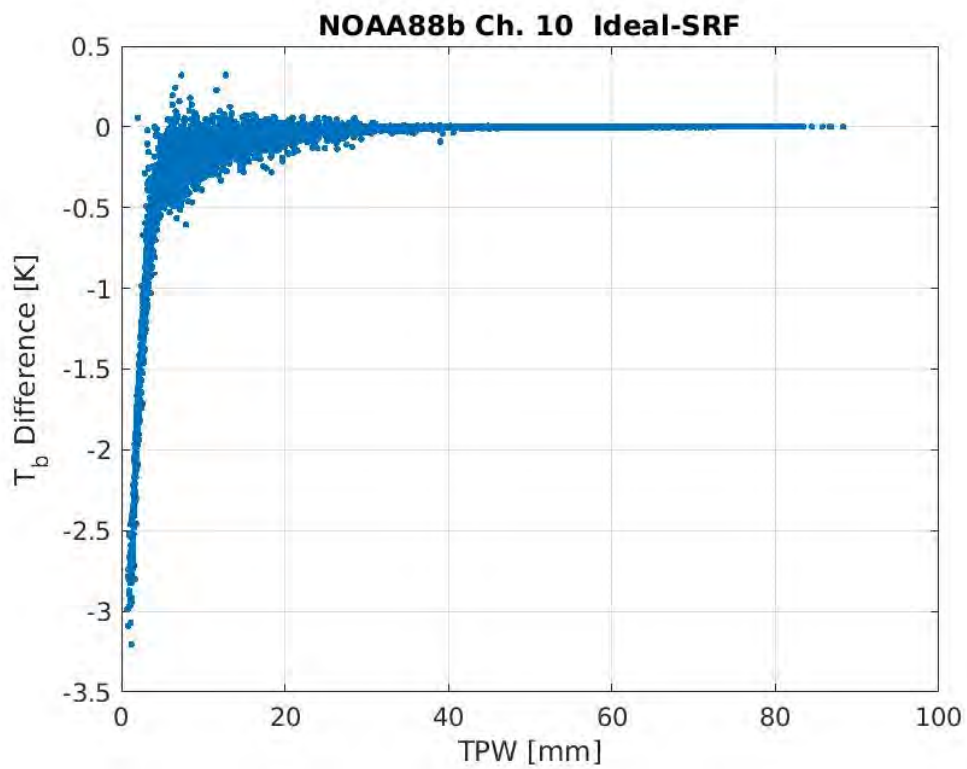
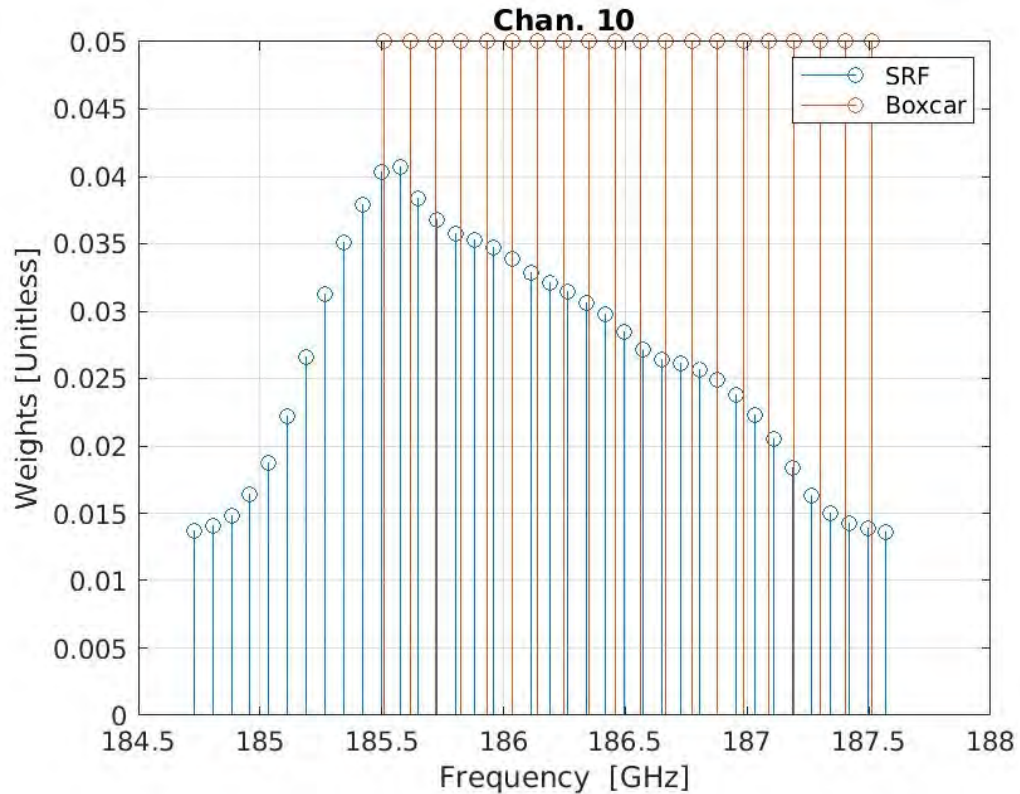


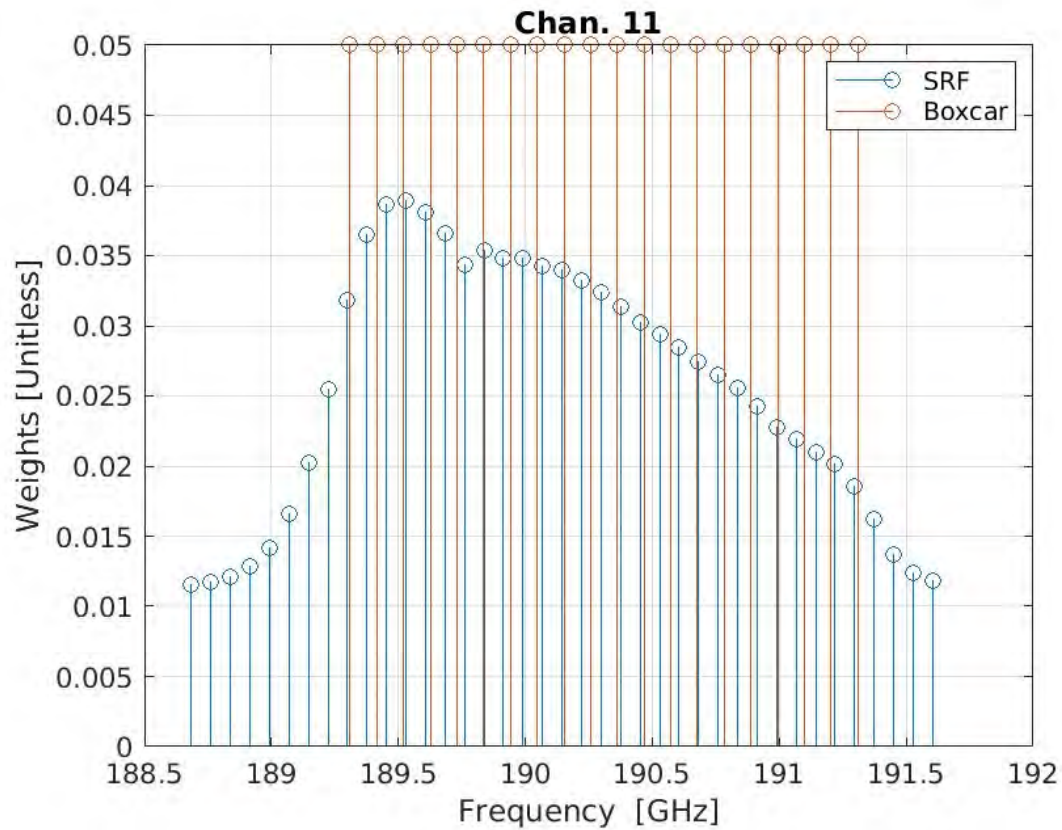


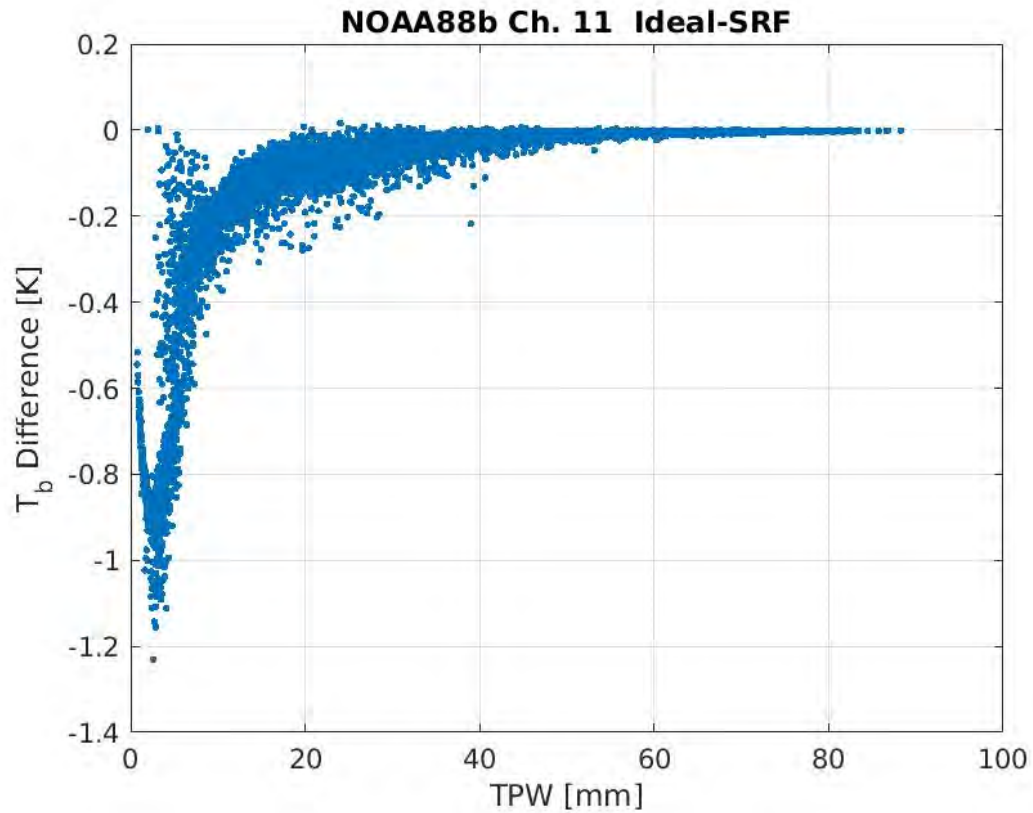


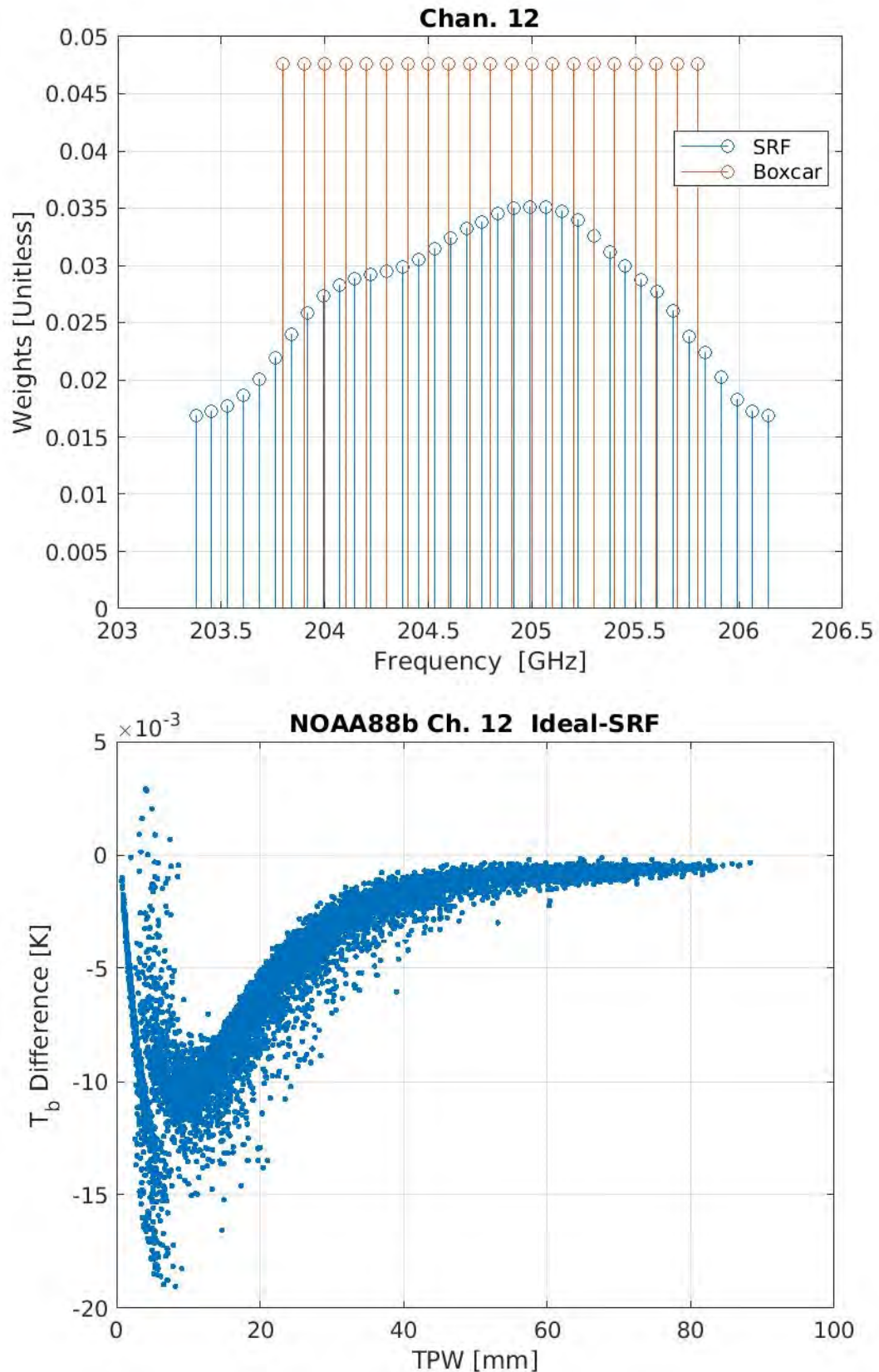












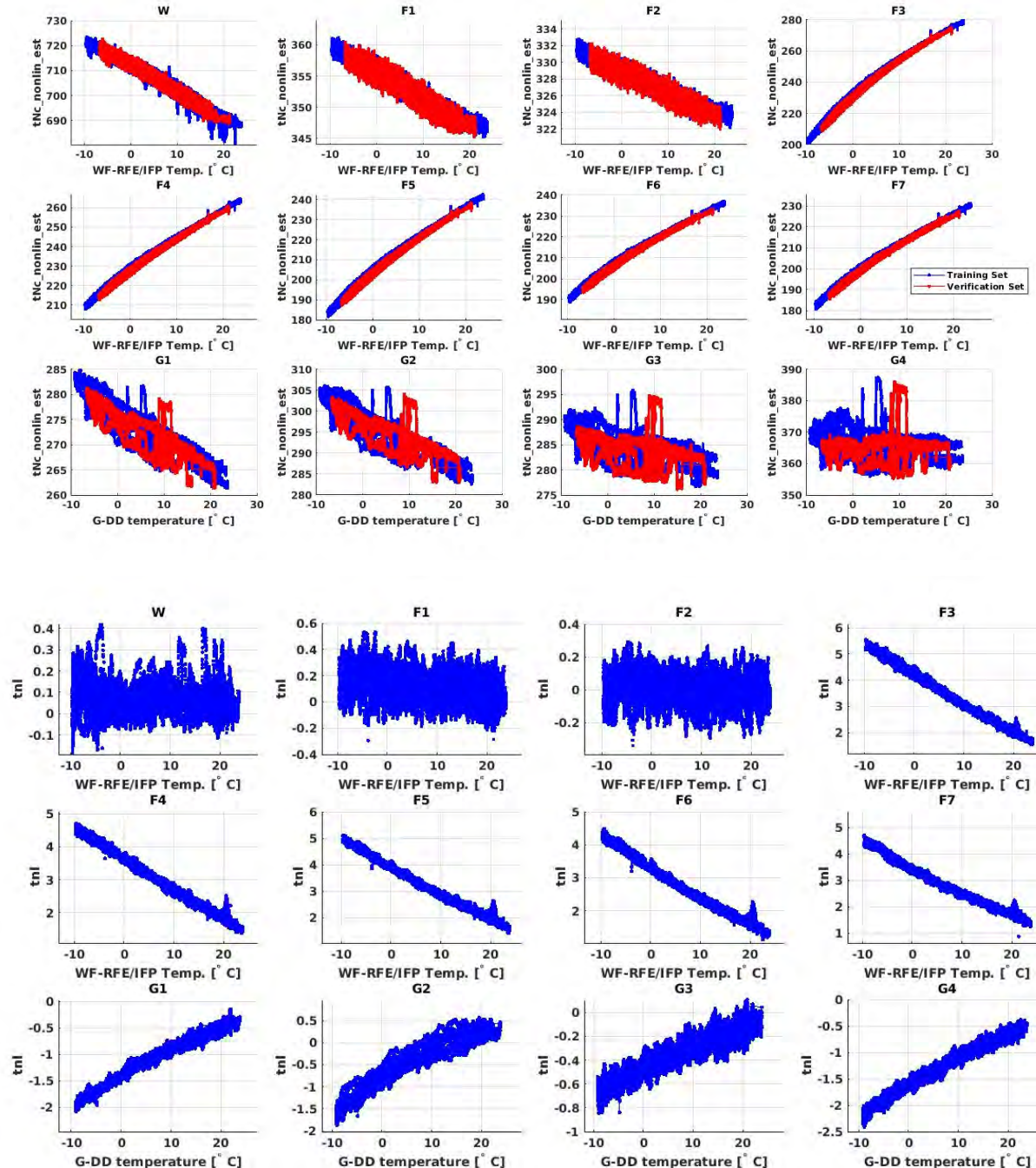
Appendix F: TROPICS-01 (Pathfinder) Characterization

TROPICS-01, i.e., Pathfinder, is the qualification unit for the constellation SV (i.e., TROPICS-02 to TROPICS-07). This means it went through more testing than the constellation. In some cases, components with the best performance were saved for the constellation. The ND in the G-band receiver in TROPICS-01 behave very differently than the ND in the constellation. The G-band channels needed both the G-band receiver's physical temperature, but also the ND voltage difference from all channels.

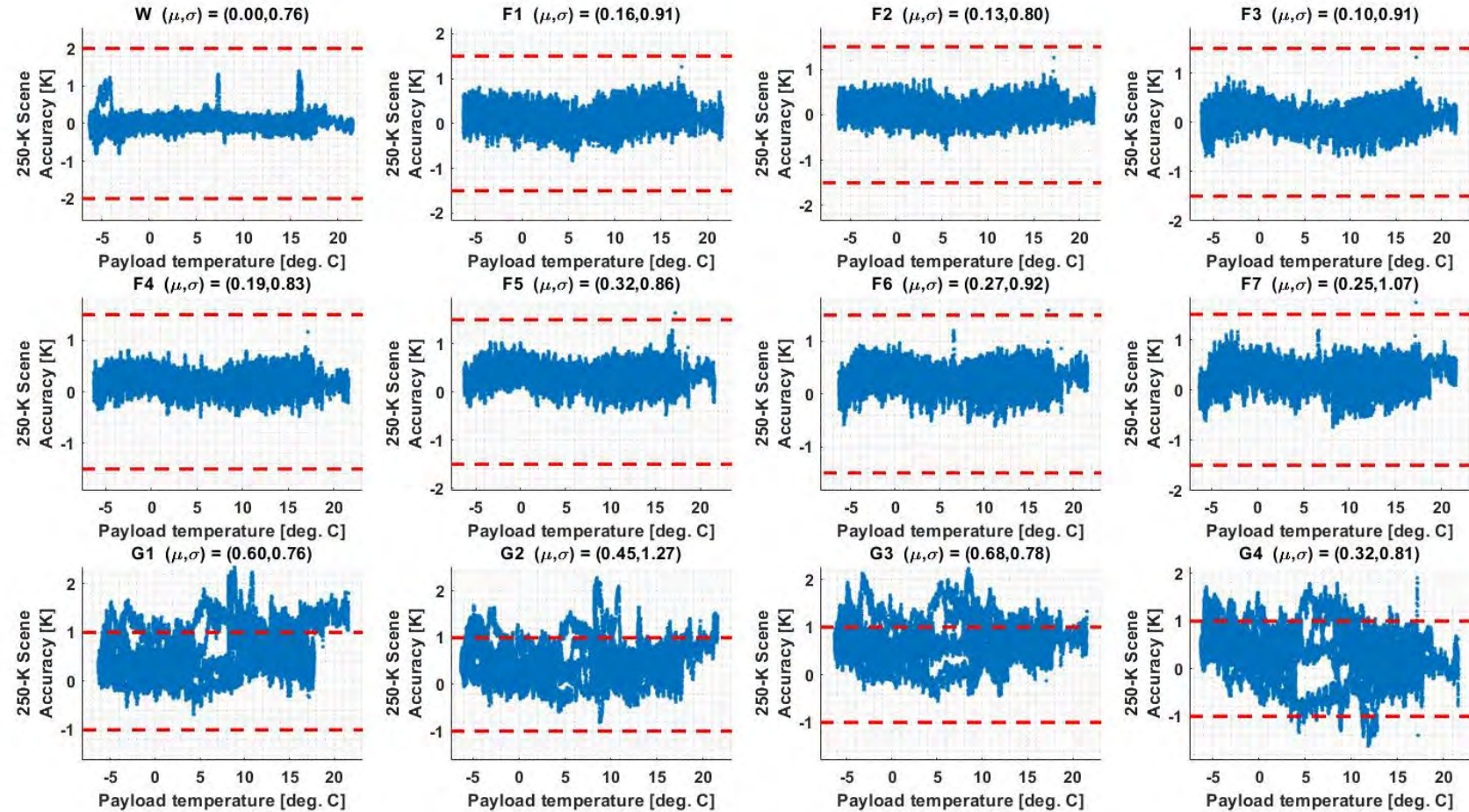
The table below has the general form of each TROPICS-01 channel's constant-coefficient linear regression (note there are still non-linear squared terms). The predictors are described for each channel. The regression's P values indicated each of the predictors were statistically significant with the exception of Ch. 4 with only F1 ND difference as statistically significant and Ch. 12 found G3 ND difference as not statistically significant. Section F.1 has the raw data for the ND characterization for two subsets of data: 1) training data used to calculate the regression coefficient (i.e., parameterization) and 2) data used in the verification. The data used in the verification is in operational mode and orbital thermal profile. The other data is the raw T_{NL} data that used to form a $T_{NL}(T_{instr}) = a_0 + a_1 \cdot T_{instr} + a_2 \cdot T_{instr}^2$ regression. Section F.2 is the verification results when using the parameterization for T_{ND} and T_{NL} in the table below and the on-orbit thermal profile. Section F.3 is the TROPICS-01 SRF and Section F.4 has plots of the antenna patterns.

Channel	T_{ND} Parameterization	Notes
1 (W)	$a_0 + a_1 \cdot X + a_2 \cdot X^2$ for temp. $< 0^\circ C$ and $b_0 + b_1 \cdot X + b_2 \cdot X^2$ for $> 0^\circ C$	X is the WF-RFE 1.8V telemetry, which is proportional to RFE temp.
2 (F1)	$a_0 + a_1 \cdot X + a_2 \cdot X^2$	
3 (F2)	$a_0 + a_1 \cdot X + a_2 \cdot X^2$	
4 (F3)		
5 (F4)		
6 (F5)		
7 (F6)		
8 (F7)		F1 is the voltage difference for the F1 channel with ND on and off; F2 is the voltage difference of F2
9 (G1)		
10 (G2)		
11 (G3)		
12 (G4)		G? is the voltage difference for the G? channel with ND on and off; T is the G-DD temp.; F1 & F2 are the same as above

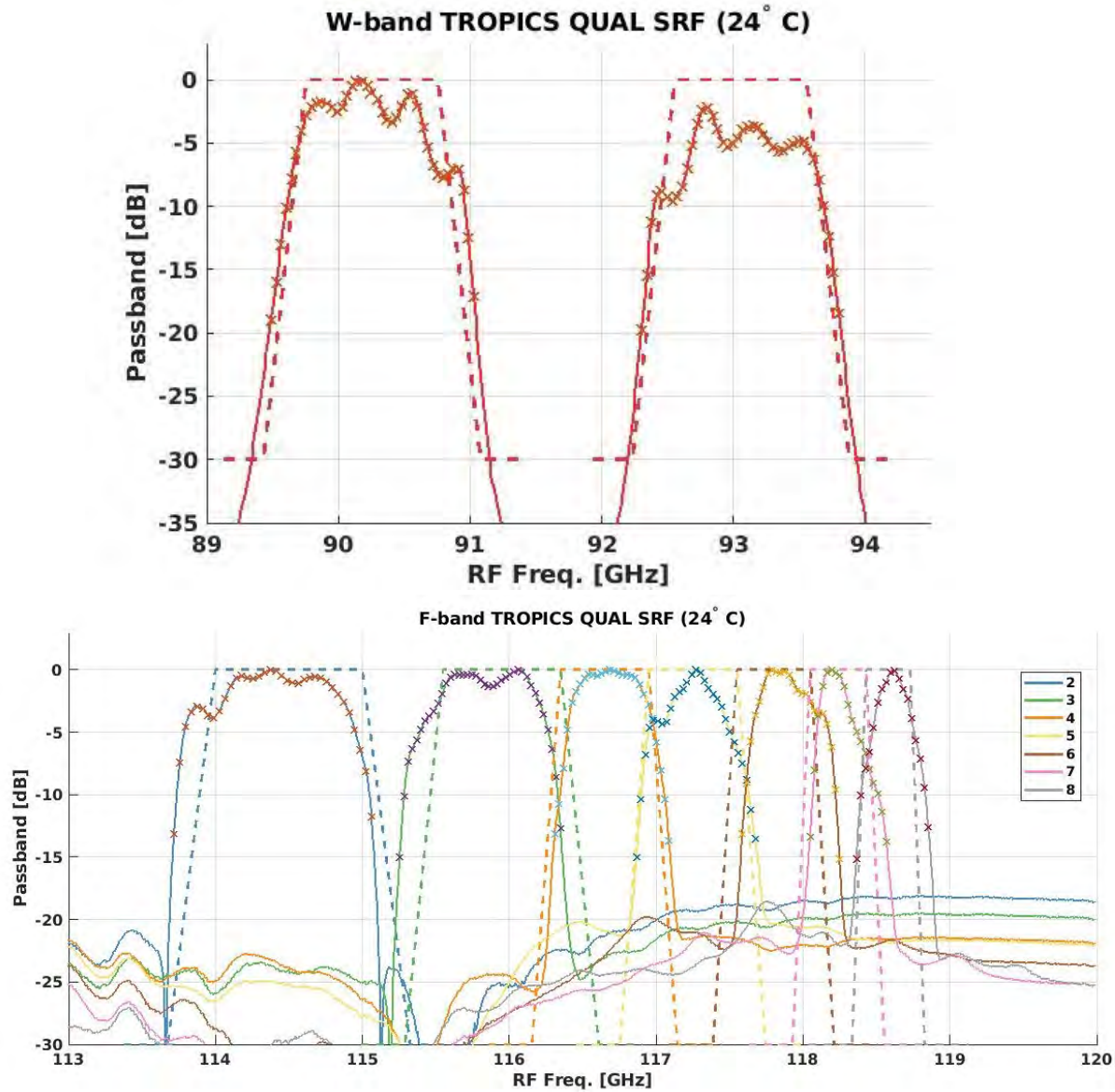
F.1 Calibration Characterization

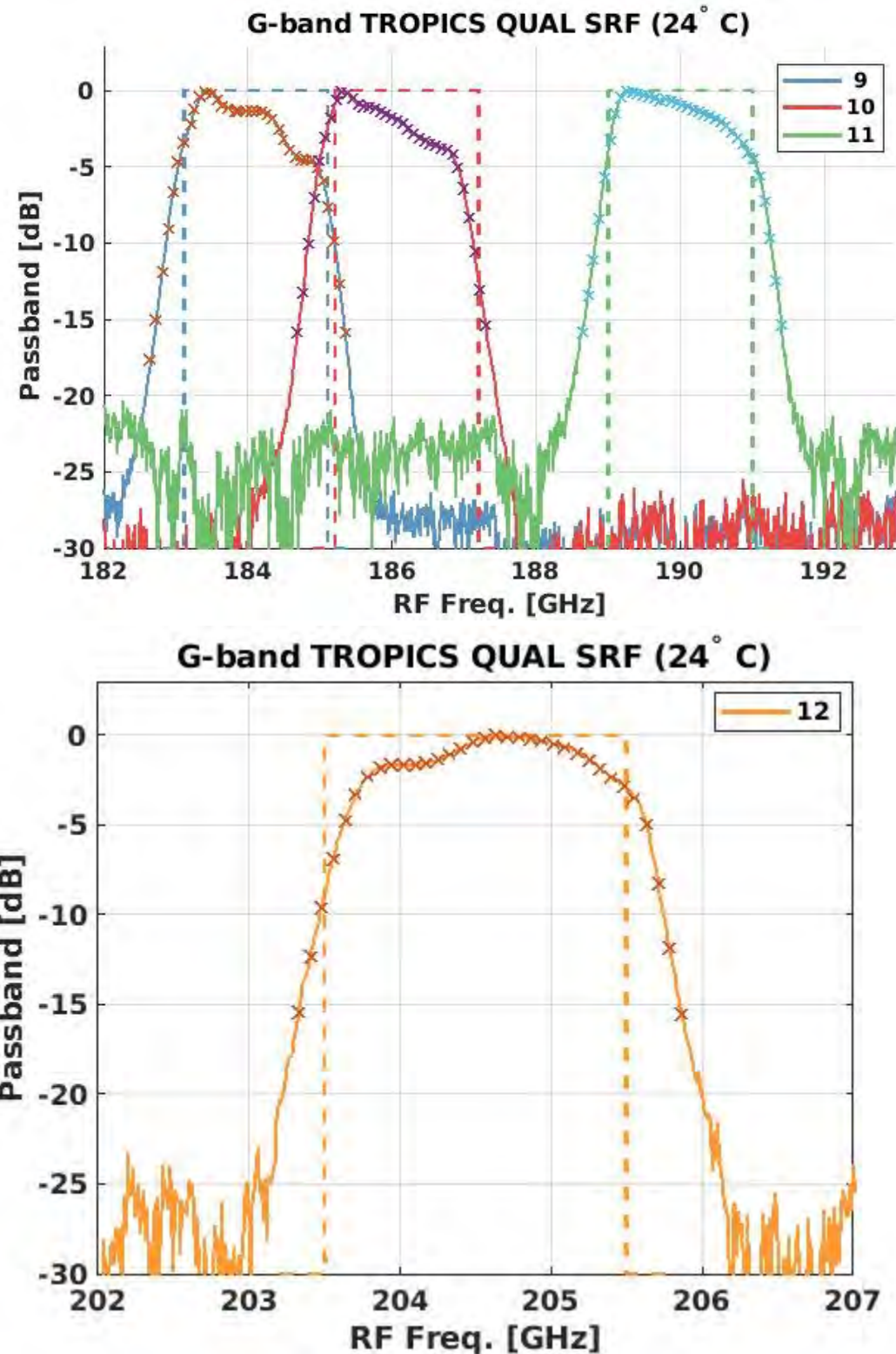


F.2 Calibration Verification



F.3 Spectral Response Functions





F.4 Antenna Patterns

